Comprehensive Study on the Behavior of Steel Girder Bridges

ALDOT Project Number: 930-939

Submitted to:
Alabama Department of Transportation
1409 Coliseum Boulevard
Montgomery, Alabama 36110

Prepared by:

Mohammad Javad Masoudi
Wei Song, Ph.D.

Department of Civil, Construction, and Environmental Engineering,
College of Engineering,
The University of Alabama

November 30, 2025

Technical Report Documentation Page

1. Report No. (FHWA/CA/OR-)	2. Government Accession No.	3. Recipient's Catalog No.
4. Title and Subtitle Comprehensive Study on the Behavior of Steel Girder Bridges		5. Report Date: November 30, 2025 6. Performing Organization Code
7. Author(s) Mohammad Javad Masoudi, Wei Song		8. Performing Organization Report No.
9. Performing Organization Name and Address Department of Civil, Construction and Environmental Engineering The University of Alabama 2021 H.M. Comer Hall 245 7th Avenue Tuscaloosa, AL 35487		10. Work Unit No. (TRAIS) 11. Contract or Grant No. ALDOT research Project No. 930-939 (GR 25905)
12. Sponsoring Agency Name and Address Alabama Department of Transportation 1409 Coliseum Boulevard Montgomery, Alabama 36110		13. Type of Report and Period Covered Final Report January 1, 2017 to September 30, 2025 14. Sponsoring Agency Code
15. Supplementary Notes		

16. Abstract

This research investigates the impact of cross-frame detailing on the behavior of horizontally curved and skewed steel I-girder bridges. An analysis procedure based on three-dimensional (3D) finite element (FE) method is developed to accurately capture the complex behavior of steel girder bridges with various cross-frame detailing methods. By following this procedure, a sophisticated FE model of a representative bridge is developed in Abaqus, utilizing its shell elements, and incorporating geometric and material nonlinearities, stress redistribution, and locked-in forces. The analyses assess three cross-frame detailing methods, No-Load Fit (NLF), Steel Dead Load Fit (SDLF), and Total Dead Load Fit (TDLF), with respect to girder deflections, cross-frame forces, layovers, and stress distributions. Findings demonstrate that detailing methods significantly affect cross-frame erection-stage initial forces and final locked-in forces, while having little impact on global deflections, layovers, or overall girder stresses. With the representative bridge, the TDLF method achieves the lowest locked-in forces but requires the largest erection efforts, the NLF method yields the opposite effects, and the SDLF method provides a balanced result between the two. The research provides a promising numerical procedure for analyzing cross-frame detailing to improve constructability and bridge performance, and can support the development of generalized criteria for selecting appropriate cross-frame fitting strategies as a function of bridge design.

17. Key Word(s)	18. Distribution Statement		
Horizontally curved steel I-girder bridges Skewed bridges, Cross-frame detailing methods, Locked-in forces, Finite-element modeling (FEM)			
19. Security Classif. (of this report)	**20. Security Classif. (of this page)**	**21. No. of Pages**	**22. Price**
Unclassified	Unclassified		

TABLE OF CONTENTS

List of Tables

List of Figures

Executive Summary

Modern highway interchanges increasingly rely on curved and skewed steel I-girder bridges to route traffic through urban and rural corridors with tight geometric constraints. In practice, these structures are sensitive to torsion, girder rotation, and cross-frame forces, and they can be difficult to construct. Current design specifications allow several detailing options for cross-frames, but provide little quantitative guidance on which approach is best for complex geometries. This project responds to this gap by providing ALDOT with a rational analysis procedure to support cross-frame detailing decisions on modern curved and skewed bridges.

This research investigates how different cross-frame fit methods, including No-Load Fit (NLF), Steel Dead Load Fit (SDLF), and Total Dead Load Fit (TDLF), influence the performance of a representative continuous, curved, and skewed steel I-girder (ICCS) bridge. The key engineering issues are: (i) how these detailing choices affect global behavior, such as vertical deflection, camber, and girder layover, and (ii) how they modify local demands in terms of cross-frame forces, girder stresses, and the magnitude of erection and fit-up forces required in the field. The overarching goal is to use this analysis to identify the trade-offs between constructability and long-term performance for modern interchange bridges.

To address these issues, an analysis procedure based on the three-dimensional (3D) finite element (FE) method is developed to accurately capture the complex behavior of steel girder bridges with various cross-frame detailing methods. By following this procedure, a detailed three-dimensional finite-element model of the representative bridge was developed using shell elements for both girders and cross-frames, incorporating nonlinear material properties, geometric imperfections, staged construction, and load application. The model was checked against design camber information, and then used to simulate NLF, SDLF, and TDLF conditions. For each detailing strategy, the study evaluated global responses (deflection profiles, camber, and girder layover) and local responses (cross-frame forces, major-axis and lateral bending stresses, and initial force-fitting demands during erection).

Overall, the analysis results for the representative bridge show that the choice of cross-frame fitting method has only a modest effect on global girder behavior: vertical deflections, camber, and girder layover are very similar for NLF, SDLF, and TDLF, and they are governed primarily by the bridge geometry and applied loads. In contrast, cross-frame forces and erection demands are highly sensitive to detailing: TDLF yields the lowest locked-in cross-frame forces under dead load but requires very large fit-up forces; SDLF provides intermediate reductions with still-substantial erection demands; and NLF produces the highest locked-in forces but is the simplest to fabricate and erect. The modeling framework developed in this project provides a rational analytical tool for agencies such as ALDOT as a means to quantify these trade-offs, which may lead to guidance for selecting cross-frame fit conditions in design and construction.

CHAPTER 1: INTRODUCTION

1.1. Background

Bridges are vital elements of a nation's transportation infrastructure, facilitating the efficient transit of individuals and commodities [1]. Nonetheless, they continue to be among the most susceptible components of any transportation network [2]. The swift growth of metropolitan regions in the United States has created intricate site restrictions, necessitating novel design solutions to ensure efficient traffic flow [3]. These constraints often lead to bridge projects with longer spans, sharper skew angles, tighter horizontal curvature, and more geometrically complex configurations [4]. In densely populated urban areas, such constraints render the construction of bridges with traditional straight alignments and standard geometry unfeasible [1]. Considering the elevated construction expenses and the substantial economic repercussions of service interruptions, enhancing the design and details of these bridges directly affects public safety, maintenance expenditures, and the efficacy of transportation systems.

In recent decades, the utilization of horizontally curved and skewed steel girder bridges has markedly risen, especially in urban settings where space is constrained and grade-separated interchanges are essential [5], [6]. These buildings are frequently utilized in scenarios where roadways or rivers connect at non-orthogonal angles, requiring skewed abutments to satisfy geometric and alignment specifications [7]. Curved steel bridges presently constitute over 25% of the nation's bridge inventory, with their prevalence anticipated to increase in the forthcoming years [8].

Historically, curved alignments were often approximated by connecting a series of straight girders at slight angles, forming a sequence of chords. This "chorded" method, although functional, led to inefficient utilization of short spans, created several production challenges, and elevated overall expenses. Improvements in analytical techniques and manufacturing technology have enabled the design and construction of genuinely curved girders that optimize structural performance and cost-efficiency while meeting intricate geometric specifications.

The current accessibility of sophisticated steel fabrication methods, such as precise Computer Numerical Control (CNC) cutting [9], cold and hot forming [10], and automated welding [11], has rendered the manufacturing of curved steel girders both feasible and cost-effective. In contrast to previous chorded designs, these contemporary girders diminish stress concentrations, enhance load distribution along the curved alignment, and offer a more aesthetically pleasing, natural appearance. The aesthetic quality is especially esteemed in multi-span designs, enhancing the visual allure of bridges while meeting stringent structural and geometric criteria (see Figure 1-1). As a result, curved and skewed steel girder bridges have emerged as some of the most efficient, cost-effective, and aesthetically pleasing solutions for tackling intricate geometry issues in densely populated metropolitan environments.

Figure 1-1. Curved steel I-girder bridge located in Tuscaloosa, Alabama, USA.

Notwithstanding its benefits, horizontally curved and skewed bridges pose significant analytical and structural difficulties [12], [13]. The intrinsic curvature of the girders generates torsional effects that complicate analysis and design [14]. Moreover, geometric flaws and asymmetry generate intricate internal force distributions, especially during multidirectional ground motions in seismic areas [15], [16]. These impacts necessitate sophisticated analytical techniques and a comprehensive comprehension of structure behavior to guarantee both safety and efficiency [2].

Conventional techniques, such as one-dimensional line-girder analysis and two-dimensional grid analysis, frequently prove insufficient for steel girder bridges characterized by intricate geometries, including skewed supports or curved alignments [17]. The American Association of State Highway and Transportation Officials (AASHTO) acknowledges these limitations in Article C6.7.2 of the LRFD Bridge Design Specifications [18], stating that "The erection and cambering of straight skewed bridges and horizontally curved bridges, with or without skewed supports, is a more complex problem than generally considered."

The construction of a steel bridge typically advances through five principal stages:

1. **Structural Analysis and Design**: Engineers assess load needs, analyze structural performance, and examine code stipulations, choosing suitable member dimensions, connection specifications, and bracing arrangements. For curved and skewed steel bridges, this phase frequently necessitates sophisticated three-dimensional modeling to precisely

account for the cumulative impacts of bending, torsion, warping, and load redistribution resulting from geometric abnormalities.

2. **Elaboration and Preparation of Fabrication Drawings**: The design is converted into comprehensive shop drawings and erection plans. Detailers must consider camber, sweep, cross-frame fit-up, and fabrication tolerances for intricate bridge geometries to ensure constructability and reduce locked-in loads during erection.
3. **Fabrication**: Steel girders, cross-frames, diaphragms, and additional components are produced in accordance with sanctioned shop drawings. Curved and skewed components frequently necessitate specialized procedures, such as CNC cutting [9], controlled cold or hot bending [10], and automated welding [11]. Rigorous quality-control protocols guarantee dimensional precision and appropriate alignment.
4. **Erection**: The steel superstructure is constructed and interconnected on-site. Curved and skewed bridges exhibit three-dimensional geometry that generates intricate load courses, alignment difficulties, and sequencing sensitivities. Temporary supports, erection towers, or adjustable shoring systems are frequently employed to preserve accurate geometry during assembly. Despite thorough preparation, field teams may face challenges like as misaligned bolt holes, difficulty in cross-frame fit-up, or unforeseen girder rotations necessitating on-site modifications.
5. **Deck Location and Accessories Installation**: The concrete deck is poured, parapets and railings are affixed, and utilities or other functional components are incorporated. In curved and skewed bridges, the sequence of deck pouring and the design of formwork must be meticulously managed to avert inadvertent torsional stress or deformation of the steel framework.

The three-dimensional (3D) response and geometric intricacy of curved and skewed steel bridges necessitate a high level of detail, rigorous compliance with erection tolerances, and tight collaboration among designers, detailers, fabricators, and construction teams. Inadequate management of these factors may lead to departures from the desired geometry, diminished serviceability, undesirable locked-in forces, or, in extreme instances, jeopardized structural integrity.

The bracing system, especially cross-frames in I-girder bridges, is a crucial determinant of the behavior of curved and skewed steel girder bridges [19]. These elements sustain girders, regulate deflections, preserve deck geometry during concrete laying, and establish load channels for lateral forces like wind [20]. Nonetheless, if inadequately conceived and specified, cross-frames may also produce unwanted secondary consequences [19].

The cross-frames shown in Figure 1-2 illustrate three prevalent configurations utilized in steel I-girder bridges, an X-braced frame, a K-braced frame, and a single-diagonal frame. The X-frame has superior in-plane stiffness owing to its symmetric bracing; the K-frame presents moderate stiffness with a decreased number of members; and the single-diagonal frame provides low stiffness, and is typically used where only limited lateral restraint is required.

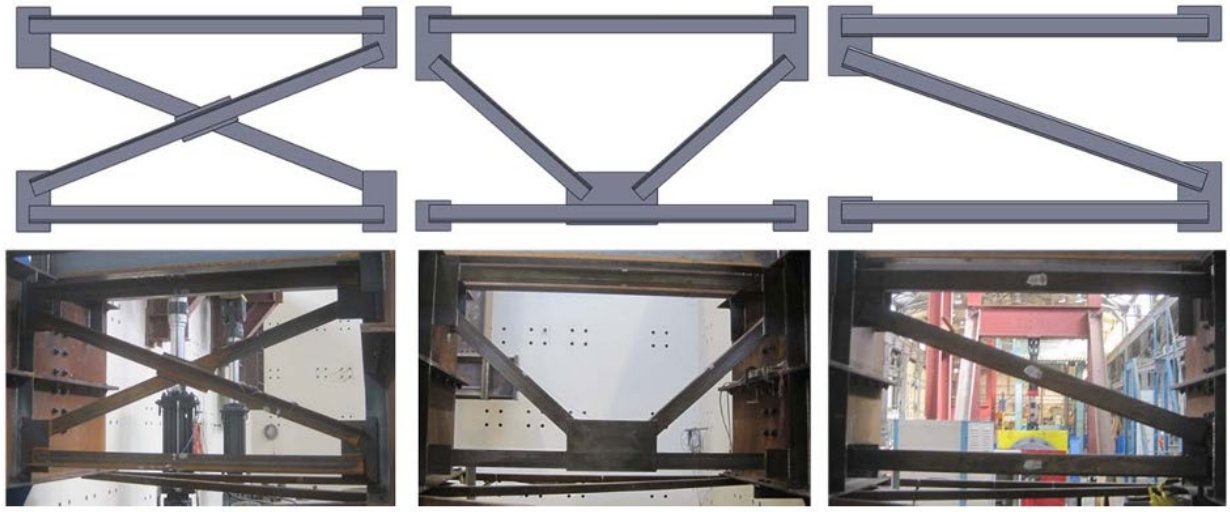

Figure 1-2. (a) X-Type Cross Frame, (b) K-Type Cross Frame, and (c) Z-Type Tube Cross Frame [21].

The bridge engineering profession recognizes the significance of cross-frames in horizontally curved steel girder bridges; nonetheless, limited research has focused on their particular behavior [22]. Despite significant advancements in the comprehension of worldwide curved bridge behavior, the analysis and design of cross-frames continue to present uncertainties, with numerous facets devoid of clear, well-defined rules [22].

When torsional deflections are considerable, cross-frames are typically designed to compensate ensuring that girder webs remain vertical under particular load situations. Engineers utilize diverse detailed techniques that specify the desired girder location under particular reference conditions: no-load, steel dead load, or total dead load [23].

Industry standards often adhere to three principal methodologies:

- **No-Load Fit (NLF)**: Cross-frames are detailed to align with the cambered geometry of the girders in their unloaded state, prior to the application of dead load. Under zero-load conditions, the girder webs remain plumb, and no initial stresses are introduced into the cross-frames.
- **Steel Dead Load Fit (SDLF)**: Considers girder deflection resulting from the self-weight of the steel. Cross-frames are meticulously designed to ensure that the girder webs attain vertical alignment solely upon the application of the steel dead load. Consequently, misalignment occurs in the no-load situation and under the total dead load, but appropriate geometry is achieved solely under the weight of the steel.
- **Total Dead Load Fit (TDLF**): Considers both the self-weight of steel and supplementary non-composite dead loads, including the concrete deck. Cross-frames are constructed to ensure that webs achieve vertical alignment only after the application of all non-composite dead loads.

Each approach generates a unique deformation pattern during erection. In SDLF and TDLF, the no-load state necessarily entails a misalignment between manufactured cross-frames and girders. This discrepancy generates locked-in forces even when components are assembled prior to the application of the expected dead loads.

Initial stresses are transient stresses that arise in cross-frames and girders during erection, when components are assembled and connected before the bridge reaches its intended dead-load state. The stresses during the erection phase largely diminish or redistribute once the permanent dead loads are imposed and the structure settles to its dead-load configuration. Conversely, locked-in stresses (or forces) are self-equilibrating internal actions that persist in the bridge after the erection phase, once the structure has reached equilibrium under its total dead load. They persist even after all temporary erection loads and supports have been removed, and the bridge bears solely its own weight. Locked-in force effects result from geometry disparities, fabrication and erection tolerances, and the specific cross-frame detailing and fit-up procedures adopted during construction.

The determination of when girders should be plumb—whether at no-load, steel dead load, or total dead load—continues to be a subject of contention among bridge engineers. Some individuals prioritize vertical alignment in the no-load condition to facilitate field assembly and prevent initial stresses, whilst others favor vertical alignment in the ultimate dead load state to enhance long-term operational performance. This decision influences global bridge behavior, internal force distribution, cross-frame requirements, and may impact the bridge's long-term durability and fatigue performance.

Various U.S. states adhere to distinct practices. Kansas generally employs the NLF approach, resulting in girders that are vertical under the theoretical no-load condition when linked to cross-frames. As dead loads are imposed, torsional deformations cause the webs to rotate out of alignment. Conversely, states like Alabama and Texas often employ the TDLF methodology, but SDLF is also implemented in specific areas. In SDLF and TDLF, cross-frames are deliberately constructed with starting geometry that does not align with girder connection points in the unloaded condition. Due to the simultaneous influence of dead loads and initial forces, the girders deform into positions where their webs are nearly vertical under the steel dead load for the SDLF scenario, and under the total dead load for the TDLF scenario (see Figure 1-3).

Current design specifications offer basic advice for curved and skewed steel girder bridges, although they frequently lack precise, performance-oriented criteria for cross-frame details under varying fit conditions. The consequent heterogeneity in state practices, coupled with the restricted availability of experimental and computational research, engenders uncertainty in forecasting cross-frame force demands, locked-in stresses, and their long-term effects on serviceability and fatigue life. Rectifying this deficiency is crucial for enhancing the reliability, cost-effectiveness, and feasibility of forthcoming bridge constructions.

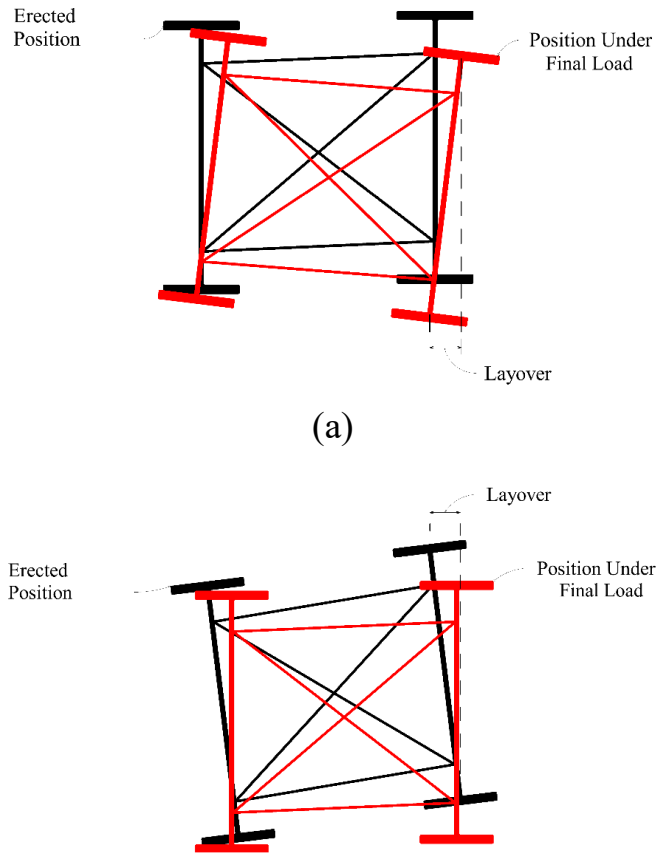

Figure 1-3. (a): No-Load Fit (NLF); (b): Total Dead Load Fit (TDLF).

1.2. Problem Statement

In the construction of steel I-girder bridges, ensuring appropriate fit-up, regulating internal stresses, and maintaining geometric control become progressively more difficult as span lengths increase and bridge shapes exhibit greater curvature or skew. Straight bridges with minor skew typically demonstrate predictable vertical displacements and restricted torsional effects, whereas curved and/or skewed bridges exhibit significantly more intricate structural characteristics [17]. Assessing such bridges necessitates the consideration of three-dimensional deformation patterns and force redistributions that are challenging to anticipate with traditional methods. The impact of assumptions and simplifications in previous experimental and numerical research on the dependability of projected structural responses is still inadequately comprehended [24].

In geometrically irregular bridges, significant torsional deformations can develop both in individual girders and across the entire cross-section. Torsional displacements induce differential deflections, cross-frame distortions, and warping stresses that must be meticulously considered during both design and construction. The deformation under gravitational loads is intrinsically three-dimensional, encompassing lateral rotations, out-of-plane bending, and warping stresses that

seldom arise in straight bridges. In certain instances, end rotations at girder supports may surpass bearing design limits, rendering the bridge non-constructible unless bearing pads are altered to handle these heightened rotations [17].

As girder webs can achieve perfect plumb alignment solely in one geometric arrangement, the judgments about cross-frame details are crucial. When webs are aligned in a no-load state, they generally become misaligned under the weight of the steel or total dead load [25]. Engineers utilize several detailed methods, No-Load Fit (NLF), Steel Dead Load Fit (SDLF), and Total Dead Load Fit (TDLF) to ensure vertical girder alignment at distinct load stages. Although these approaches seek to regulate torsional deformation, they may also induce locked-in stresses from lack of fit, potentially affecting fatigue life and long-term durability.

These bridges are especially vulnerable to second-order effects, including enhanced deformations, stress redistributions caused by warping, and the interplay between bending and torsion, which are frequently inadequately addressed by conventional design methodologies. This prompts a critical inquiry for designers: To what degree do cross-frame details affect the structural performance of curved and skewed I-girder bridges, and how should this impact be considered in the design process?

In NLF detailing, girders are interconnected without initial stresses in the unloaded condition; yet, they experience significant rotations under dead loads, especially near the bearings. SDLF and TDLF detailing methods minimize layover by addressing plumb geometry under particular load situations; however, this approach introduces locked-in forces that modify stress distribution and deformation patterns. The trade-off between diminished layover and heightened lock-in stress is inadequately defined.

The AASHTO LRFD Bridge Design Specifications [23] acknowledge the necessity of defining the intended plumb condition and load stage; nonetheless, they lack an analytical framework for assessing the structural consequences of various detailed techniques. Contemporary practice frequently presumes that:

- Girders are entirely vertical at the designated load phase;
- Flange lateral bending stresses are insignificant; and,
- Cross-frame locked-in stresses are absent.

Such assumptions overlook possible discrepancies during erection, indicating that the actual deformations, rotations, and stress states may diverge considerably from those anticipated in the design, and potentially result in erroneous short-term performance evaluations and an underappreciation of long-term fatigue requirements.

Recent improvements in three-dimensional finite element analysis (3D FEA) provide precise simulation of these effects, permitting engineers to duplicate experimental data and investigate detailed alternatives under realistic conditions. Utilizing these methods to methodically assess the impact of cross-frame detailing strategies on the performance of curved and skewed steel I-girder bridges can address a significant knowledge deficiency and result in more dependable, cost-

effective, and resilient bridge designs. Numerous prior investigations have utilized simplistic 3D finite element analysis models, wherein cross-frames were shown using truss elements, which overestimate their stiffness by roughly a factor of two [26]. This research models the entire bridge using precise S4R shell elements, explicitly incorporating both geometric and material nonlinearities, so offering a more realistic depiction of structural behavior.

1.3. Objectives and Scope of This Research

This research aims to develop a detailed finite-element framework to evaluate the impact of various cross-frame detailing techniques on the structural performance of horizontally curved and skewed steel I-girder bridges. The study employs advanced three-dimensional studies to quantify the impact of No-Load Fit (NLF), Steel Dead Load Fit (SDLF), and Total Dead Load Fit (TDLF) assumptions influence bridge performance during erection and under dead load conditions.

A detailed 3-D Abaqus model of the Corridor X–I-65 Interchange Bridge was used, incorporating geometric and material nonlinearities to simulate realistic deformation, stress redistribution, and locked-in forces. The study includes the subsequent critical response parameters for each detailing method:

- Vertical displacements,
- Girder stress distributions,
- Girder layovers and end rotations of girders,
- Initial forces in cross-frame, and
- locked-in forces in cross-frames.

The comparative results provide ALDOT with pragmatic guidance for choosing a suitable detailing method that balances constructability and long-term serviceability.

1.4. Organization of the Report

This report comprises six chapters, each designed to systematically elucidate the research problem, the employed technique, and the resultant findings regarding cross-frame details in skewed and curved highway bridges. The content is structured to guide the readers from a general context to specific conclusions and recommendations.

Chapter 1 establishes the groundwork of the study. It describes the context and motivation for the research, specifies the parameters, and outlines the specific objectives to be achieved. This chapter presents the technical difficulties specific to skewed-curved steel I-girder bridges, emphasizing the importance of meticulous cross-frame detailing in preserving structural performance and stability over the bridge's lifespan. It closes by describing the report's structure to assist the readers through subsequent chapters.

Chapter 2 defines and categorizes the essential geometric characteristics that influence the structural performance of curved and skewed I-girder bridges. It presents the primary plan and section parameters, including span configuration, curvature, and skew indices, and illustrates their impact on torsional demand, load path asymmetry, and erection stability. The chapter further

explains the process of selecting representative bridge configurations based on these geometric factors to ensure realistic and critical evaluation of different detailing methods in ensuing assessments.

Chapter 3 introduces and explains the analytical framework and practical procedures for cross-frame detailing methodologies. This research examines three detailed methods: No-Load Fit (NLF), Steel Dead Load Fit (SDLF), and Total Dead Load Fit (TDLF), outlining their theoretical foundations and practical applications. The chapter analyzes the impact of each method on girder alignment under different loading circumstances and investigates the potential consequences of detailed decisions on girder stability, erection forces, and service performance.

Chapter 4 describes the finite element modeling framework established for the research. It delineates the modeling assumptions, geometric definitions, boundary conditions, material attributes, and analytical instruments employed. The chapter outlines the sequential approach for executing each detailed condition within the model. The numerical model's validation is demonstrated by comparing its predictions to existing experimental data (of cross-frame only) or recognized analytical solutions, and thus confirming the reliability of the simulation results.

Chapter 5 presents, interprets, and synthesizes the finite-element simulation results obtained for the No-Load Fit (NLF), Steel Dead Load Fit (SDLF), and Total Dead Load Fit (TDLF) models. Key response parameters, such as vertical displacements, cross-frame forces, girder layovers, and stress distributions, are thoroughly examined to assess the impact of various detailing techniques on both global and local bridge performance. Comparative plots and deflection diagrams illustrate the impact of each detailing technique on locked-in forces, and overall service performance. The chapter concludes with an analysis of performance trends, implications for constructability, and suggests detailed methods based on these numerical results, establishing the technical basis for the concluding remarks and findings in Chapter 6.

Chapter 6 encapsulates the key findings of this research, highlighting the impact of geometric configuration and cross-frame detailing on the structural efficacy of curved and skewed steel I-girder bridges. It highlights the comparative advantages and limitations of NLF, SDLF, and TDLF approaches, identifies the governing behavioral mechanisms observed in the finite-element analyses, and offers pragmatic recommendations for design, detailing, and construction sequencing. The chapter concludes by addressing study limitations and proposing directions for future research, such as parametric expansion to other bridge types, and empirical validation of analytical predictions.

Collectively, these chapters establish a coherent and rational narrative, progressing from problem identification to literature context, methodological advancement, comprehensive analysis, and culminating in pragmatic insights for design and construction practices.

CHAPTER 2: SELECTION OF GEOMETRIC FACTORS

2.1. Overview

Geometric factors represent the primary plan and section dimensions and layout characteristics of a bridge, including arc-span length, deck width, horizontal curvature, bearing-line skew and pattern, and span type. These parameters determine the global load paths, the allocation of dead and live loads to supports, and the overall stiffness and stability of the girder-deck system. Fundamentally, geometry dictates the performance of a bridge during both its construction and operational phases.

For curved and skewed I-girder bridges, even minor alterations in parameters can lead to substantial variations in torsional demands, uplift tendencies at bearings, deflections, and interactions among adjacent spans. Due to this sensitivity and interaction effects, geometric factors serve as the key organizing variables in parametric and analytical studies. By systematically altering arc span, width, curvature, skew, and span type, researchers can evaluate how design assumptions and simplified analytical approaches perform across realistic bridge configurations.

Studying geometric factors also helps define practical design limits, such as the maximum permissible skew or curvature that could raise stability or constructability concerns. It additionally specifies which geometric combinations require special detailing, bracing, or field controls during erection.

In conclusion, choosing and modifying geometric parameters enables engineers to evaluate analytical precision, and formulate dependable recommendations that are reliable for typical as well as extreme yet practical bridge geometries. In this chapter, geometric factors are treated both as descriptors of bridge configuration. The subsequent sections delineate each principal geometric factor, explain its mechanical and practical significance, and outline the chosen ranges and representative levels used in the study.

2.2. Span Configuration Types

This study categorizes bridge superstructure geometry based on span configuration type, utilizing a concise code describing three independent yet interacting features of a span unit: whether it is simple or continuous in the longitudinal direction, whether its plan form is straight or curved, and the orientation of its bearing lines as either non-skewed or skewed. The seven configuration types employed in the parametric investigation are:

- **ISSN:** Simple-span, straight, with non-skewed supports
- **ISSS:** Simple-span, straight, with skewed supports
- **ISCR:** Simple-span, curved, with radial supports
- **ISCS:** Simple-span, curved, with skewed supports
- **ICSS:** Continuous-span, straight, with skewed supports
- **ICCR:** Continuous-span, curved, with radial supports
- **ICCS:** Continuous-span, curved, with skewed supports

Each configuration isolates distinct structural characteristics and construction requirements. This classification renders the parametric results explicit, systematic, and readily compared. Simple-span cases highlight positive bending at mid-span and larger vertical deflections under load, making them more susceptible to erection staging and temporary loading conditions. Continuous-span cases introduce negative bending over supports and create interactions among adjacent spans through moment redistribution, coupled torsion, warping, and cross-frame force transfer. These differences are essential as continuity modifies both the intensity and distribution of flexural and torsional forces.

The distinction between straight and curved configurations governs the importance of torsion and out-of-plane behavior. Straight-span cases (ISSN, ISSS, ICSS) offer fundamental comparisons for classical beam theory and isolate the influence of skew. Curved-span cases (ISCR, ICCR, ISCS, ICCS) encompass torsion generated by curvature, lateral load paths, and the influence of radial or skewed bearings on span length and load distribution. Curved, radially supported spans (ISCR, ICCR) have bearing lines that point toward the center of curvature. This makes reactions less skewed and more torsionally coupled. Curved, skewed spans (ISCS, ICCS) represent common field geometries where bearing lines are not radial, resulting in asymmetrical span lengths and larger localized torsional and warping requirements.

Among all bridge types, the ICCS system (continuous, curved, and skewed) is the most crucial. This combination of continuity, horizontal curvature, and skewed supports produces the most robust interaction between torsion and bending. The coupling of curvature-induced torsion and skew-induced eccentricity results in intricate stress distributions, elevated warping requirements, and substantial cross-frame forces near the supports. Continuity amplifies these effects by linking spans across the piers, facilitating the passage of torsional distortion and negative bending forces between them. ICCS bridges, therefore, represent the most challenging configuration for analysis and construction, establishing the upper limit of geometric sensitivity in curved I-girder bridge behavior.

2.3. Skew Index

The skew index is a geometric parameter developed to quantify the impact of skew on the global behavior of bridges. It offers a uniform measure that combines the effects of span configuration, skew angle, and deck geometry into a single dimensionless form. In steel I-girder bridges, where skewed supports frequently arise from roadway alignment or site limitations, the skew index facilitates systematic comparison among different configurations and helps evaluate the impact of skew on performance, load distribution, and constructability.

The skew index is developed based on the geometric relationship between the skew angle of the bearing lines and the overall bridge layout. It reflects how the orientation of supports deviates from a perpendicular alignment with the bridge centerline. The index increases as the skew angle becomes larger or as the deck plan departs from a rectangular configuration. In the limiting case of a straight, non-skewed bridge, the skew index approaches zero, indicating symmetrical load distribution and uniform girder response.

The skew index I_s proposed by Sanchez [19] provides a quantitative means of the overall geometric skew within a bridge system:

$$I_s = \frac{(n_g - 1) \cdot s \cdot \tan(\theta)}{L_s} \tag{2.1}$$

where n_g denotes the quantity of girders, s is the transverse spacing between adjacent girders, θ is the skew angle of the supports relative to the bridge centerline (considered as the angle between the girder's perpendicular at the support and the bearing line, thus $\theta = 0$ indicates no skew), and L_s is the span length measured along the bridge centerline (arc length in curved bridges). This dimensionless metric accurately reflects how skewed geometry alters the relative alignment of girders and supports. As the skew angle or girder spacing increases, I_s also increases, indicating a higher degree of geometric distortion and probable torsional interaction in the superstructure. Conversely, I_s approaches zero for straight, orthogonal bridges, indicating uniform load distribution and symmetrical behavior. Sanchez's formulation allows comparison among bridges of different sizes and configurations, linking geometric layout directly to structural response characteristics. According to Sanchez [19], bridges with $I_s < 0.3$ exhibit minimal skew effects, whereas for $I_s > 0.65$ skew can significantly affect girder major-axis bending stresses and vertical displacements. Figure 2-1 illustrates the plan view of a skewed bridge and the skew angle θ.

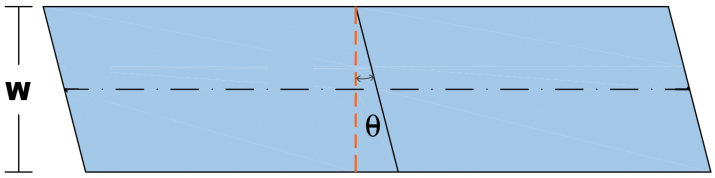

Figure 2-1. Plan view of a skewed bridge.

The skew index functions as a useful indicator of the structural and analytical complexity introduced by skew. Elevated skew values can induce considerable interaction between bending and torsion, leading to nonuniform force distribution and increased cross-frame demand. The skew angle affects the direction of the bearing line, which in turn impacts the alignment of the girder during erection and deck installation. These geometric effects can alter live-load distribution, cause lateral girder deflection, and complicate cross-frame fit-up, particularly in continuous or curved spans. By expressing skew quantitatively, the skew index helps identify these influences early in design and incorporate them into analytical or parametric studies.

2.4. Curvature Index

The curvature index, defined as the ratio L_s/R, offers a non-dimensional assessment of the degree of horizontal curvature in a bridge span. Here, L_s represents the arc-span length along the bridge centerline and R denotes the radius of curvature. This parameter effectively reflects the geometric severity of curvature and has been widely acknowledged as a critical variable influencing the structural behavior of horizontally curved I-girder bridges. Figure 2-2 illustrates the curvature index in the plan view of a curved bridge.

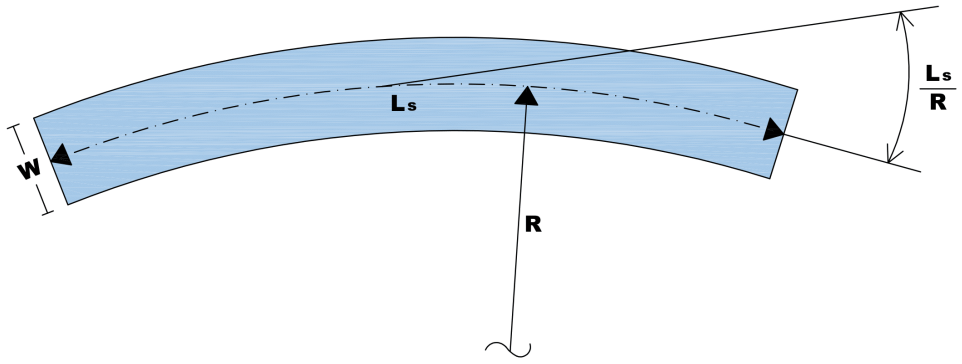

Figure 2-2. Plan view of a horizontally curved bridge.

A bigger L_s/R ratio indicates a tighter curvature, leading to greater torsional demand, higher lateral bending stresses, and an increased potential for uplift at bearings adjacent to the inner edge of the curve. In contrast, smaller L_s/R ratios are associated with flatter configurations, wherein the bridge behavior more closely resembles that of a straight bridge. For curved I-girder systems, the impact of L_s/R affects to the distribution of internal forces, deformation patterns, and stability during both erection and service phases. Bridges with large L_s/R ratios tend to demonstrate increased warping, larger differential deflections between interior and exterior girders, and heightened sensitivity to geometric imperfections.

High L_s/R ratios can induce structural instability during erection due to significant eccentricities of self-weight, while very low ratios result in negligible curvature effects and may inadequately characterize the behavior of curved bridges. Narrower bridges can tolerate higher curvature (larger L_s/R) without excessive overturning, whereas wider bridges must sustain smaller L_s/R ratios to avert uplift or imbalanced reactions at the bearings.

2.5. Bridge Selection

To evaluate the influence of different detailing methods on bridge performance, a representative bridge must be selected for detailed finite element analysis. This section evaluates five possible bridges based on geometric parameters previously addressed, including span configuration, curvature index, and skew index, to identify the most suitable structure for this study. A total of five candidate bridges were provided by ALDOT for consideration. These bridges are:

- Corridor X–Railroad
- Greenbrier
- Outer Loop Interchange I-85
- Galleria I-459/US-31
- Corridor X–I-65

Each bridge displays unique geometric attributes and varying degrees of complexity, facilitating a comprehensive study of the interactions among curvature, skew, and continuity in practical designs.

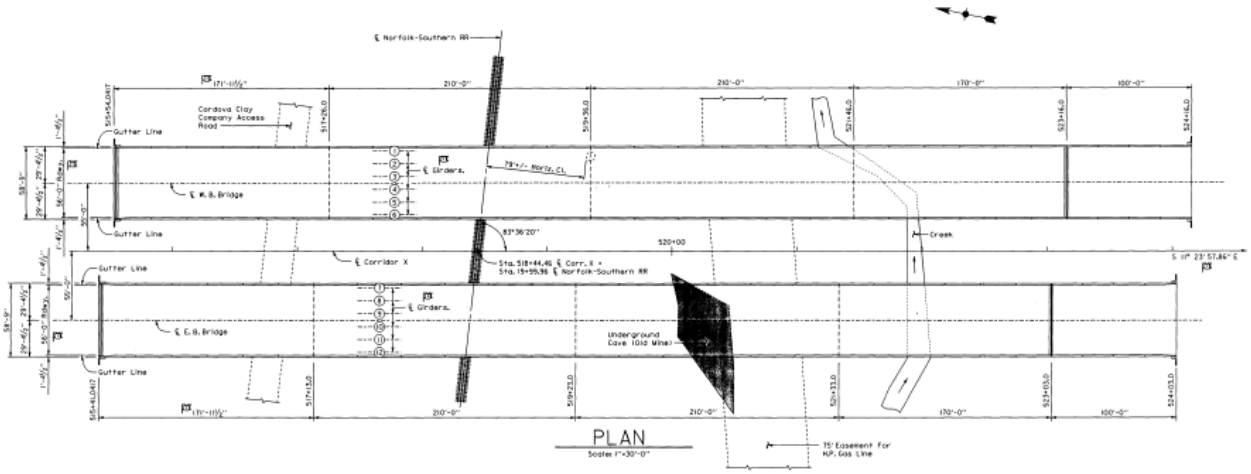

Figure 2-3. Corridor X–Railroad Bridge (ICSN type, straight and non-skewed configuration).

Figure 2-3 shows the Corridor X–Railroad Bridge, located in Walker County, Alabama. The project comprises two independent, adjacent bridges, one designated for the westbound lane (WBL) and the other for the eastbound lane (EBL). The bridge includes five spans with a total length of 861.95 ft and a deck width of 58.75 ft, supported by six girders. The superstructure integrates continuous welded steel plate girders in the main spans and simple prestressed concrete girders in the end spans. The alignment is straight, exhibiting no curvature or distortion, and the bridge is categorized as an ICSN-type (continuous, straight, non-skewed). Owing to its simple geometry, it represents a baseline configuration with negligible torsional interaction and is hence not deemed significant for detailing assessment.

The Greenbrier Bridge, shown in Figure 2-4, is a three-span continuous steel plate girder bridge situated in Limestone County, Alabama, where Greenbrier Road crosses I-565. It has a total length of 300 ft and a deck width of 54 ft, supported by eight girders. The bridge features four skewed supports exhibiting a skew angle of 25.42° and a skew index of 0.079. The skew adds slight geometric complexity, and the small span, along with the lack of curvature, leads to small torsional

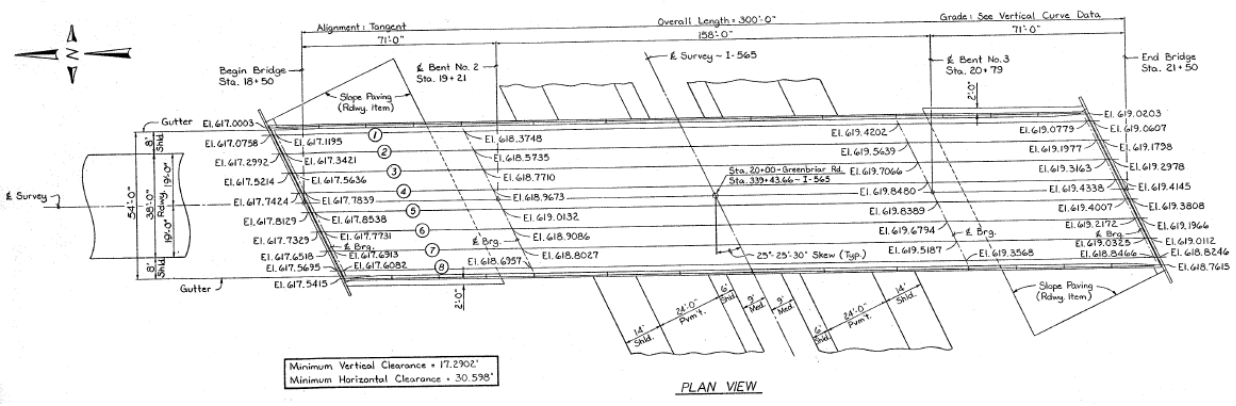

Figure 2-4. Greenbrier Bridge (ICSS type, straight and skewed three-span steel plate girder bridge).

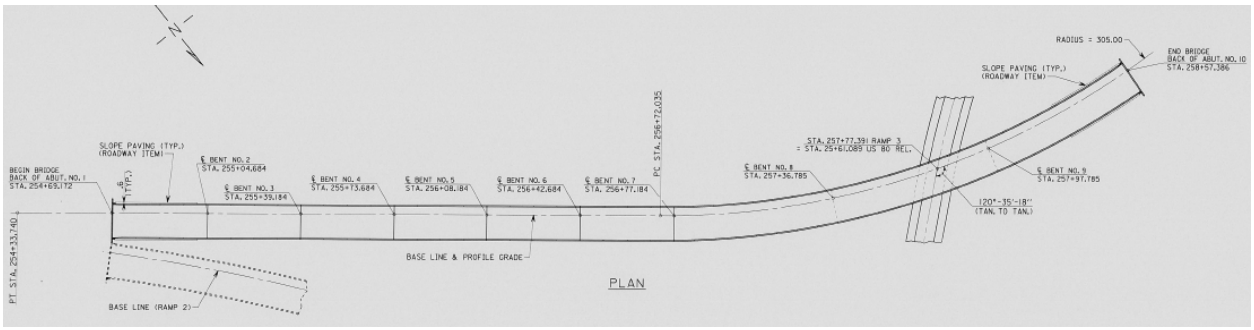

Figure 2-5. Outer Loop Interchange I-85 Bridge (ICCR type, curved and radial continuous steel plate girder bridge).

coupling. The bridge predominantly exemplifies ICSS-type geometry (continuous, straight, skewed).

Depicted in Figure 2-5, the Outer Loop Interchange I-85 Bridge is a multi-span, horizontally curved steel plate girder bridge. The curved segment of the superstructure has an arc length of 591.2 ft, a radius of 1000.66 ft, and consists of five girders with a deck width of 42.12 ft. The bridge has no skewed supports and is categorized as an ICCR-type (continuous, curved, radial). This bridge, with a curvature index of 0.5908, demonstrates significant curvature effects; nevertheless, the absence of skew diminishes the interaction between torsion and bending. It offers essential data for separating curvature effects independent of skew influence.

Figure 2-6 illustrates the Galleria I-459/US-31 Bridge, a four-span continuous steel plate girder bridge located in Jefferson County, Alabama. The structure measures 919.7 ft in total length, features five girders, and a deck width of 40.16 ft. The bridge features four radial and one skewed support, with a radius of 765.42 ft and a skew angle of 56.42°. The curvature and skew indices are 1.214 and 0.053, respectively, and the maximum girder spacing is 8.12 ft. The interplay of curvature and skew generates considerable coupling and localized warping near the supports. The bridge type is ICCS (continuous, curved, skewed), representing a moderately complex configuration with both curvature-induced and skew-induced effects.

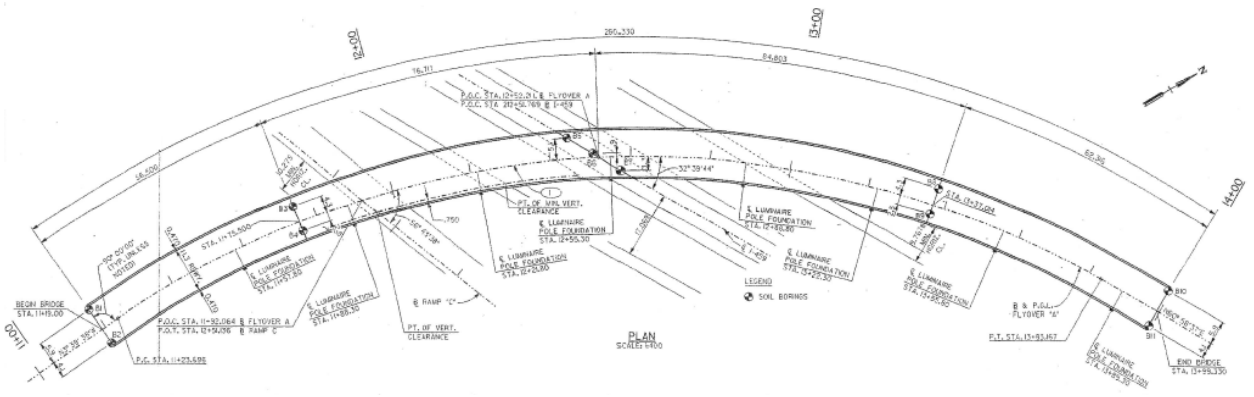

Figure 2-6. Galleria I-459/US-31 Bridge (ICCS type, curved and skewed four-span continuous bridge).

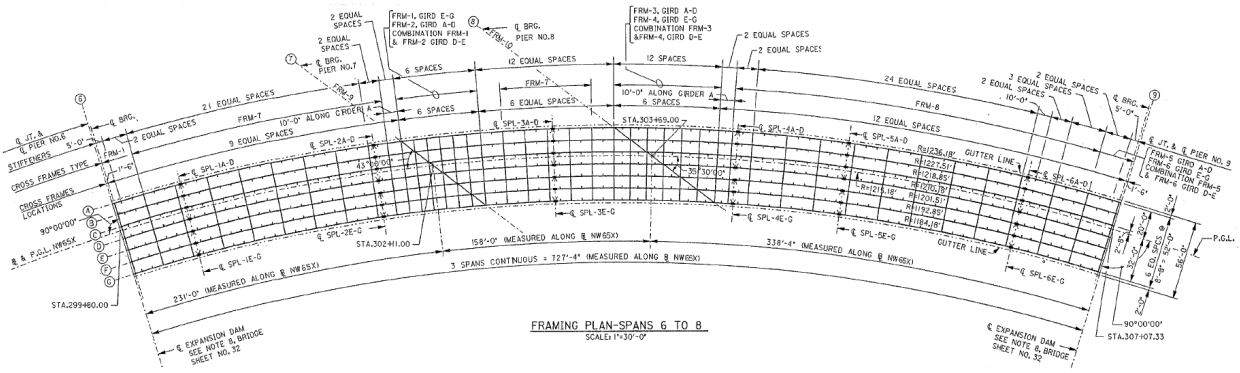

Figure 2-7. Corridor X–I-65 Bridge (ICCS type, curved and skewed three-span continuous bridge—selected for this study).

The Corridor X–I-65 Bridge, shown in Figure 2-7, is a three-span continuous steel plate girder bridge featuring four supports (bents). Two bents are radial, and the other two are skewed. Each pier supports seven girders at slightly varying elevations. The bridge has a total centerline length of 731.88 ft, a centerline radius of 1,210.18 ft, and a deck width of 58 ft. The curvature index and skew index are 0.5982 and 0.1, respectively, showing a mix of curvature and skewness. The maximum span length of 373.5 ft exceeds that of the Galleria Bridge (278.2 ft), enhancing flexibility and amplifying differential girder behavior. The maximum girder spacing is 8.66 ft, which further contributes to cross-frame demand and out-of-plane distortion.

The combination of significant skew and moderate curvature creates a crucial interaction area around the bents, where major-axis bending is tightly coupled with torsional rotations. This relationship, together with the extended free span, renders the bridge susceptible detailing assumptions, locked-in stresses, and erection sequencing.

While both the Galleria I-459/US-31 and Corridor X–I-65 bridges are classified as ICCS-type structures and exhibit complex interactions arising from the combined effects of curvature and skew, the Corridor X–I-65 Bridge was selected as the reference structure for this study. It exhibits:

- The highest skew index,
- A larger span length, leading to greater flexibility and secondary torsional effects,
- Noticeable curvature–skew coupling in critical regions near the supports,
- A realistic configuration representative of modern highway interchanges in Alabama,
- More skewed supports.

This combination of geometric attributes guarantees that the impacts of different detailing methods (NLF, SDLF, and TDLF) can be well evaluated under the most demanding conditions. The selected bridge thus provides a robust and representative platform for analyzing the sensitivity of curved and skewed steel I-girder bridges to cross-frame detailing assumptions. Table 2-1 summarizes the essential geometric factors of the analyzed bridges, establishing a clear foundation for comparison.

Table 2-1. Summary of geometric factors for candidate bridges.

Bridge ID	Type	L_s	W	R (ft)	n_g	s	θ	L_s/R	I_s
CorridorX-Railroad	ICSN	-	58.75	-	6	10.25	-	-	-
Greenbrier	ICSS	-	54	-	8	7.16	25.42	-	0.079
OuterLoopInterchange_I85	ICCR	591.2	42.12	1000.7	5	8.59	-	0.5908	-
Galleria_I459-US31	ICCS	919.71	40.16	765.42	5	8.12	56.42	1.214	0.053
CorridorX-I65	ICCS	731.88	58	1210.18	7	8.66	54.5	0.5982	0.1

L_s: Span length measured along the bridge centerline (ft); W: Width (ft); R: Radius (ft); n_g: Number of girders; s: Transverse spacing between adjacent girders (ft); θ: Skew angle; L_s/R: Curvature index; I_s: Skew index.

CHAPTER 3: METHODS FOR CROSS-FRAME DETAILING

3.1. Overview

In steel bridges, cross-frames fulfill several essential roles: they offer lateral load resistance, allocate traffic loads across girders, and diminish the effective buckling length of compression flanges. During construction, before the hardening of the concrete deck, cross-frames are crucial for bracing steel girders, preserving geometric integrity, and providing lateral stability against wind and other temporary stresses [27].

In horizontally curved steel I-girder bridges, the structural role of cross-frames becomes even more pronounced [28]. The curvature produces radial forces in the upper and lower flanges, which subsequently cause torsional rotations along the longitudinal axis. The combination of bending and torsion results in a complicated three-dimensional structural response, positioning cross-frames as primary load-bearing elements rather than merely secondary bracing. They counteract forces resulting from torsion, differential girder deflections, and live-load distribution, which are essential to maintaining the bridge's overall stability, geometric control, and serviceability.

In addition to offering lateral stability to individual girders throughout construction and service, cross-frames also maintain the intended geometric form of the superstructure, regulate distortion, and enable load transfer between adjacent girders. Due to these significant contributions, cross-frames in curved and skewed bridges must be considered and designed as key structural elements, with the same level of rigor in analysis, detailing, and manufacture as the main girders.

The American Association of State Highway and Transportation Officials (AASHTO) identifies three principal detailing methods employed for curved and skewed I-girder bridges to attain vertical girder webs under a specified dead load condition: No-Load Fit (NLF), Steel Dead Load Fit (SDLF), and Total Dead Load Fit (TDLF) [29]. Every technique possesses unique advantages and constraints, and its efficacy is contingent upon the type of bridge, span design, and geometric layout. These descriptions are provided from the perspective of structural analysis and behavior. In practice, detailers and fabricators do not conduct structural analysis independently [17].

In bridges designed using a SDLF or TDLF method, the cross-frames are constructed to align with the theoretical final vertical geometry of the girders at the designated stage. This target geometry addresses and mitigates differential vertical displacements and rotations caused by dead loads, with the objective of attaining a plumb web alignment under such situations.

3.2. No-Load Fit (NLF) Detailing

The No-Load Fit (NLF) approach specifies that cross-frames or diaphragms are designed to ensure their connection points align accurately with those on the girders in their no-load, completely cambered configuration, hence eliminating the need for force-fitting during installation [23]. The system is designed for an initial stress-free fit, with both girders and cross-frames vertically aligned under no-load conditions. As dead loads are imposed, the girders experience deflection and rotation

from their initial vertical alignment into a non-vertical arrangement [25]. This technique is occasionally termed “fully-cambered fit detailing” [23].

Fabricators of NLF bridges generally employ one of two methodologies for the construction of intermediate cross-frames [25]:

a) Adjust the drop of the cross-frames along the bridge length to correspond with elevation discrepancies between girders (Figure 3-1a).
b) Employ uniform cross-frame proportions consistently and modify the connection plate details to account for camber discrepancies (Figure 3-1b).

In practice, variations in cross-frame drop often occur due to changes in cross-slope and superelevation. These can be incorporated during manufacture by modifying one side of the jig utilized for assembling the cross-frames [23]. This method guarantees superior geometric alignment, reduces field modifications, and is simple to execute; therefore, the initial approach of altering the drop is the predominant choice in the industry [25].

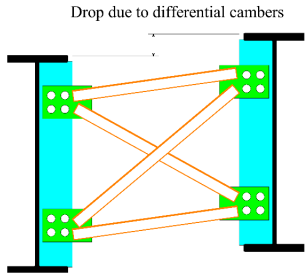

(a)

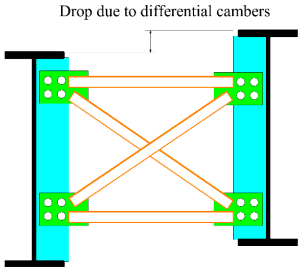

(b)

Figure 3-1. Illustrating two different approaches in the NLF method.

Figure 3-2 depicts the standard No-Load Fit (NLF) detailing and installation procedure [29]:

1. **Fabrication and Installation**: Girders are manufactured with camber that corresponds to the Total Dead Load (TDL). Cross-frames are constructed to accommodate these girders in their unloaded, plumb configuration. The girders are positioned in their estimated no-load state utilizing temporary shoring or appropriate supports (Figure 3-2a).

2. **Cross-Frame Installation**: Cross-frames are utilized to interconnect the girders, hence constituting the assembled system. The installation is stress-free, requiring no force-fitting, as both girders and cross-frames are in a no-load state (Figure 3-2b).

3. **Implementation of Total Dead Load**: Upon the application of total dead load, girders deform to their designated elevations. However, torsional distortion causes the webs to rotate, misaligning the girders in the final condition (Figure 3-2c).

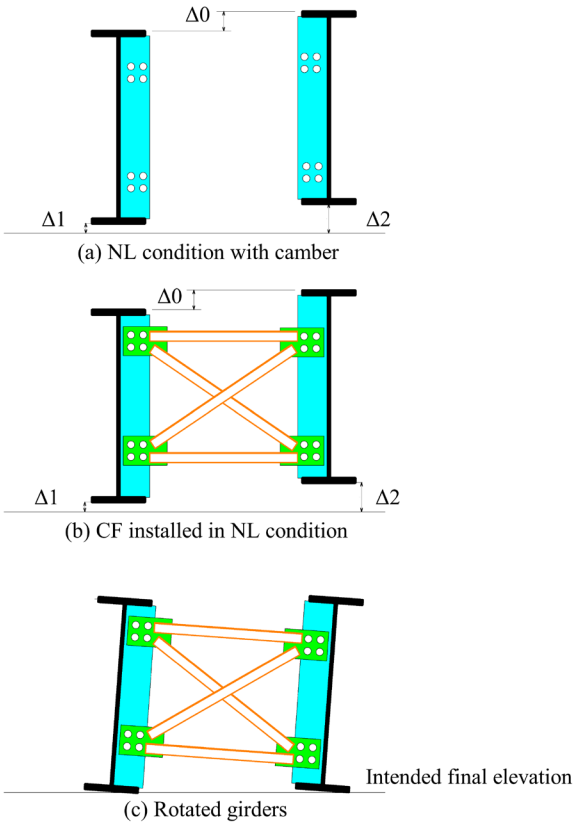

Figure 3-2. Illustration of the behavior associated with NLF detailing at intermediate cross-frames.

3.3. Total Dead Load Fit (TDLF) Detailing

The Total Dead Load Fit (TDLF) method entails specifying the cross-frames or diaphragms to ensure their connection points coincide with those on the girders, considering the vertical deflections and major-axis rotations induced by the total dead load (TDL) [23]. This method involves fabricating the intermediate cross-frames to conform to the final plumb geometry under full dead load, implying they will not align with the girders in their no-load configuration. The inherent stiffness of the cross-frames in their respective planes [25] results in a lack of fit during installation under no-load conditions, necessitating resolution during erection.

When the cross-frames are force-fitted in situ, internal forces are engendered. These forces generate torsion in the comparatively pliable girders, opposing the direction of their inherent

torsional displacements under the total dead load. Depending on the bridge geometry, the impacts of the dead load and the locked-in forces may either partially offset each other, resulting in little net torsional stress, or compound, hence elevating internal stress levels [17]. This method is also known as “final-fit detailing” [23].

Figure 3-3 illustrates the Total Dead Load Fit (TDLF) process [27]:

1. **Fabrication and Initial Positioning**: The girders are manufactured with a camber that aligns with the total dead load. Cross-frames are constructed to conform to the girders in their ultimate plumb configuration, presuming this state will be attained under the complete dead load. Initially, during erection, the girders are positioned in a near no-load state (Figure 3-3a).

2. **Partial Cross-Frame Attachment**: In the no-load condition, the cross-frames are first affixed to one girder. A lack-of-fit is evident with the second girder due to the discrepancy between the manufactured geometry and the unloaded girder location. (Figure 3-3b).

3. **Complete Cross-Frame Installation**: Installation forces are applied to connect the cross-frames to the second girder, closing the gap and overcoming the lack-of-fit. This procedure generates a pre-twist (cross-sectional rotation) in the girders to mitigate the expected rotation from the total dead load (Figure 3-3c).

4. **Application of Total Dead Load**: Upon applying the total dead load, the girders should ideally attain vertical webs and their designated final elevations, provided there is no coupling between cross-sectional rotation and vertical deflection. Curved girders demonstrate coupling, leading to positive elevation deviations and webs that are not entirely vertical. (Figure 3-3d).

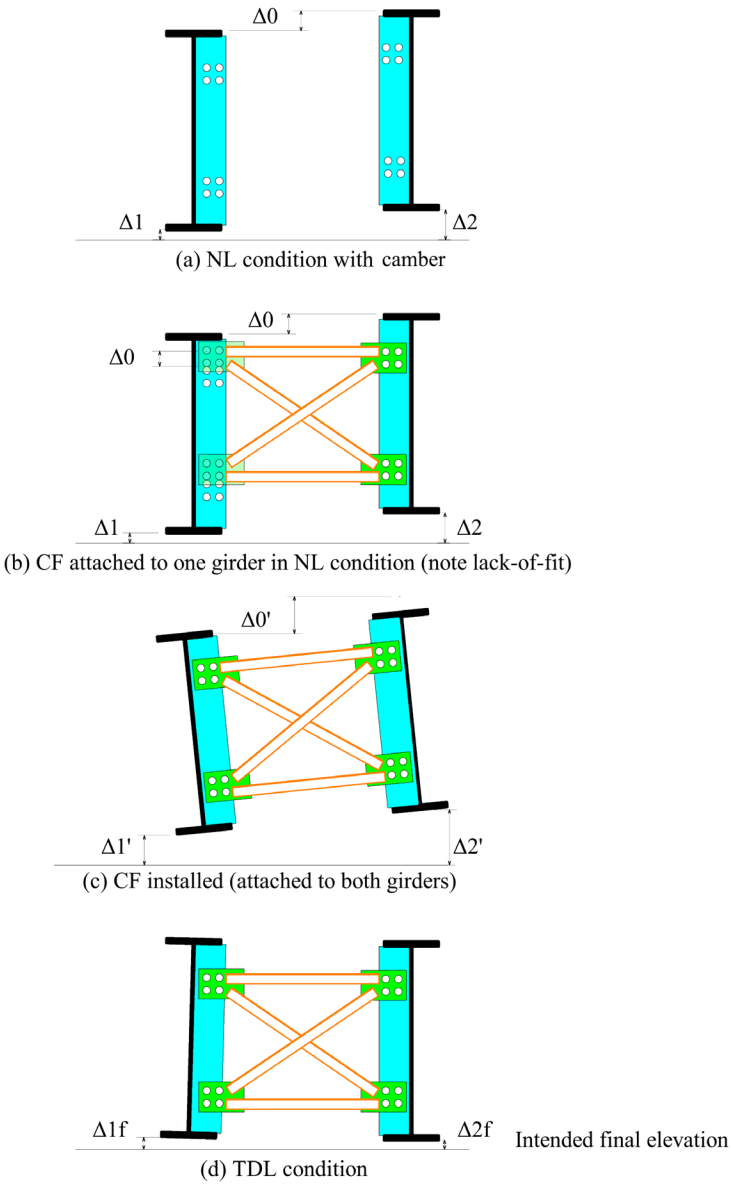

Figure 3-3. Illustration of the behavior associated with TDLF detailing at intermediate cross-frames.

3.4. Steel Dead Load Fit (SDLF) Detailing

The Steel Dead Load Fit (SDLF) approach specifies the cross-frames or diaphragms to ensure their connection points line with those on the girders, considering the vertical deflections and major-axis rotations induced by the steel dead load (SDL) [23]. The intermediate cross-frames are constructed according to the girder geometry under the steel dead load condition, indicating they will not align with the girder positions in the no-load state. Similar to TDLF, the cross-frames exhibit considerable rigidity in their respective planes and withstand deformation during installation [25]. The pressures confined during installation create torsion in the flexible girders against their inherent torsional displacement under the steel dead load. This pre-twist aligns the

webs to be almost vertical at the conclusion of steel erection. Similar to TDLF, the interplay between loads and locked-in forces can either counterbalance, diminishing net stresses, or be cumulative, elevating internal stresses [17]. This method is sometimes referred to as “erected-fit detailing” [23].

Figure 3-4 illustrates the step-by-step procedure for detailing and installing cross-frames using the Steel Dead Load Fit (SDLF) method [29]:

1. **Fabrication and Initial Positioning**: The girders are manufactured with a camber that aligns with the total dead load. Cross-frames are specified for the geometry presumed when the girders are vertical under the steel dead load condition. During erection, the girders are positioned in a nearly no-load state (Figure 3-4a).
2. **Partial Cross-Frame Attachment**: Cross-frames are first affixed to a single girder. The difference between the constructed geometry and the no-load girder location results in a misalignment with the second girder (Figure 3-4b).
3. **Complete Cross-Frame Installation**: Installation forces are exerted to eliminate the gap, linking the cross-frames to the secondary girder. This creates a pre-twist in the girders designed to counteract the rotation induced by the steel dead load (Figure 3-4c).
4. **Application of Steel Dead Load**: Upon the application of the steel dead load, and presuming no interdependence between rotation and vertical displacement, the girders ought to achieve their designated vertical displacement (total dead load camber minus steel dead load deflection) and maintain vertical alignment. Curved girders demonstrate coupling in practice, resulting in positive elevation deviations and non-vertical webs (Figure 3-4d).
5. **Application of Concrete Dead Load (to reach total dead load)**: As the concrete load is applied, resulting in the complete total dead load condition, further cross-sectional rotation transpires. The girders frequently exhibit positive elevation deviations from the steel dead load stage, while the webs stay marginally out of plumb due to the combined effects of load-induced deformation and locked-in stresses (Figure 3-4e).

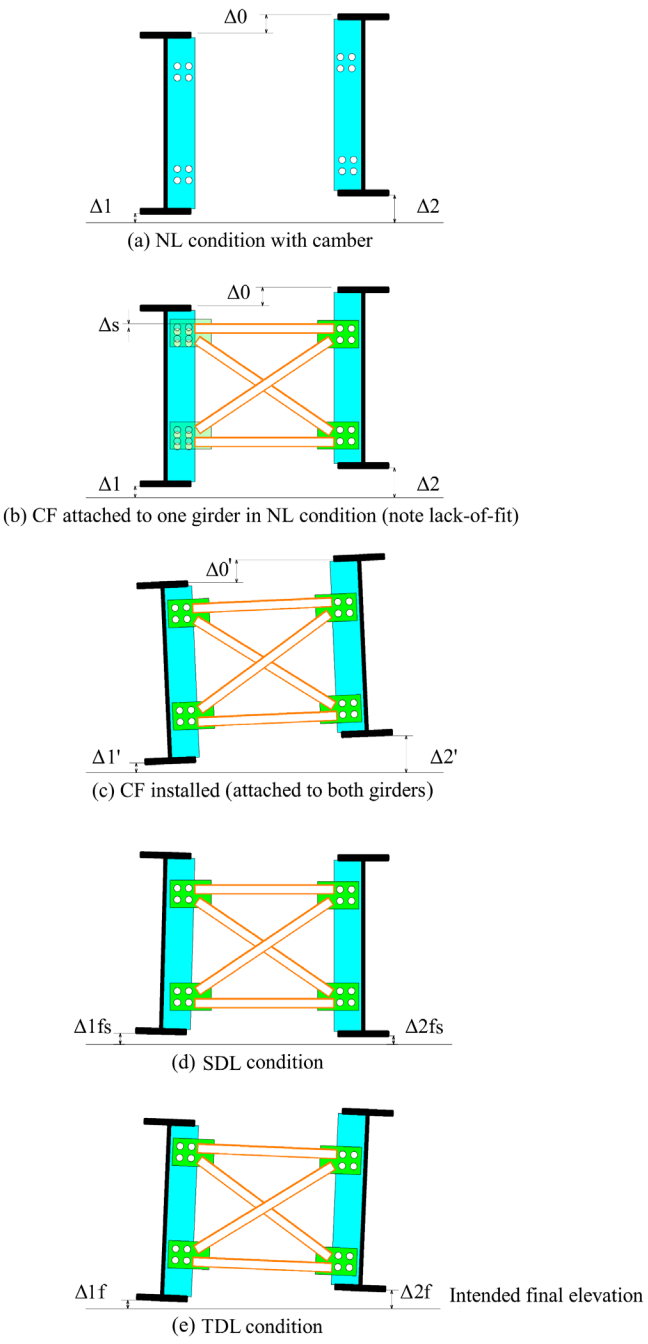

Figure 3-4. Illustration of the behavior associated with SDLF detailing at intermediate cross-frames.

3.5. Locked-In Forces

Locked-in forces are the self-equilibrating internal forces that remain within a bridge after the erection phase, when the structure reaches equilibrium under its total dead load. In contrast to initial forces, which are the temporary erection forces necessary for establishing connections during construction, locked-in forces remain within the structure after all external erection loads

are removed, and the bridge begins to carry its own weight. Locked-in forces arise due to geometric discrepancies, fabrication tolerances, and the specific cross-frame detailing method adopted during construction.

In horizontally curved and skewed I-girder bridges, locked-in forces are significantly affected by the fabrication of cross-frames in relation to the anticipated girder deflections under dead load. When detailing methods such as the Steel Dead Load Fit (SDLF) or Total Dead Load Fit (TDLF) are used, the fabricated geometry often differs from the as-erected geometry. Thus, the girders and cross-frames must undergo modest deformation as the dead load is applied to achieve the desired ultimate configuration. These deformations induce residual internal forces that remain "locked-in" once the bridge settles under the total dead load, notwithstanding the removal of external erection forces [23]. Cross-frame forces can be determined from the axial stresses and corresponding axial forces in the upper and lower chords, as well as in the diagonals of the cross-frames.

The intensity and distribution of locked-in stresses are influenced by curvature, skew, span configuration, and the detailing technique. Among common practices, TDLF generally produces the least locked-in stresses under total dead load, as cross-frames are constructed to match the final deflected geometry; upon the application of dead load, the structure aligns closely with its fabrication assumptions, resulting in small residual mismatch. SDLF (designed just for the self-weight of steel) generally generates modest locked-in strains under the total dead load. Conversely, NLF (designed for the as-erected, no-load geometry) often results in the largest locked-in stresses once dead load is applied. Locked-in stresses physically denote the strain energy retained in the bridge as its components adjust to achieve compatibility under the total dead load, and are especially significant near highly skewed bents and regions of pronounced curvature, where differential girder rotations are most prominent.

The interaction between dead load effects and locked-in stresses can either diminish or enhance the total internal forces within the bridge, depending on the detailing method and geometry. In some cases, the two effects counteract each other, leading to small net torsion, whereas in other scenarios, they act in the same direction, intensifying cross-frame and girder stresses. This amplification is especially critical for curved or skewed configurations, where cross-frames significantly influence overall stiffness and stability [17].

Locked-in stresses are assessed from the internal force state following the assembly of the bridge, application of the total dead load, and system equilibrium. Incorporating locked-in stresses, typically overlooked in simplified bridge calculations, enhances the accuracy of the actual structural condition, thereby improving estimates of girder rotations, layovers, and cross-frame force demands.

3.6. Definition of Layovers

Girder layover refers to the lateral displacement between the upper and lower flanges of an I-girder, measured at a bearing or cross-frame location. This displacement is primarily caused by the torsional rotation of the girder, and in skewed or curved bridges, it additionally results from the coupling between the girder's major-axis bending and torsional rotations. Layover quantifies

the extent to which a girder twists or shifts out of its vertical alignment, often expressed as the horizontal offset between the centroids of the flanges at a specific location. Figure 3-5 shows the layover, denoted as Δ_x.

This study generated layover diagrams for the three analyzed methods, No-Load Fit (NLF), Steel Dead Load Fit (SDLF), and Total Dead Load Fit (TDLF) to enable a direct comparison of their effects on cross-frame layover behavior. These data offer vital details about how varying girder deflections, resulting from construction sequence and design choices, influence girder rotations across the bridge span. The main objective of utilizing the SDLF and TDLF detailing methods in skewed and curved steel girder bridges is to minimize girder layover under targeted dead load conditions. Comparing these detailing methods is crucial, as it demonstrates their effectiveness in attaining plumb girders under the specified dead loads, and the resulting locked-in forces.

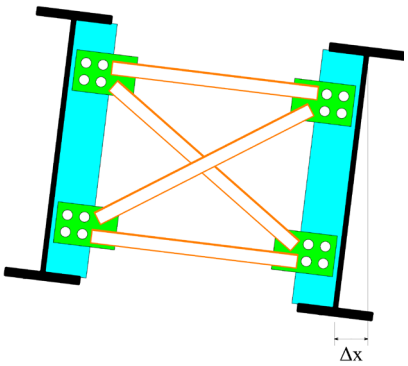

Figure 3-5. Definition of the cross-frame layover (Δ_x).

CHAPTER 4: FINITE ELEMENT MODELING FRAMEWORK

4.1. Overview

The finite element method (FEM) is a prevalent methodology utilized across various engineering disciplines for conducting sophisticated numerical computations. It is based on continuum mechanics, which addresses the equilibrium, motion, and deformation of solid bodies. In the Finite Element Method (FEM), a continuous system (or continuum) is shown through a discrete model wherein the structure is segmented into numerous smaller components referred to as elements. The elements are interconnected at nodes, and the entire system is depicted as a mesh. Each element contains special functions (so called "shape functions") that characterize its behavior, and the nodal values are compiled to estimate the overall reaction of the system. The precision of this approximation typically enhances with an increase in the number of nodes.

The element functions are integrated into a comprehensive system of equations that includes both material qualities and geometric attributes. External forces are applied via load vectors at the nodes. As the system assembles, the matrices increase in size and computational complexity, necessitating substantial processing resources for resolution. The principal outcomes derived from resolving these equations are the nodal displacements, which can subsequently be utilized to compute strains, stresses, and other response metrics.

Finite element simulations were performed in this work utilizing the commercial program ABAQUS/CAE. Both industry and academia extensively use this software to address a wide range of issues, from basic linear analyses to intricate nonlinear simulations. ABAQUS/CAE facilitates the modeling process by enabling users to create geometry, assign physical and material properties, specify loads, and implement boundary conditions [30]. It is considered a robust FEM platform for the analysis of three-dimensional issues across various engineering disciplines. This study utilized Abaqus 2025 [31] to simulate Plan Set 2 of the Corridor X–I65 & I-65 Interchange, based on the design drawings obtained from ALDOT and developed by Volkert and Associates, Inc., Consulting Engineers. All material and geometric properties used in the finite element models were taken directly from these drawings. The subsequent sections depict the geometric models, materials, mesh, boundary conditions, and loading configurations used in the numerical analyses. The chapter finishes with a description of the numerical modeling techniques for the detailing methods and the subsequent post-processing analysis procedures.

4.2. Geometry

The case study bridge is a three-span, continuous, curved steel–concrete composite I-girder structure measuring 736.29 ft in total length, with a maximum plan curvature radius of 1236.18 ft and a deck width of 58 ft (see Figure 4-1). It consists of seven principal girders and 264 X-shaped cross-frames constructed in 10 dimensional variations. The bridge is sustained by two radial abutments at each end and two skewed middle piers, collectively sustaining the seven longitudinal girders. The girder stiffeners are arranged asymmetrically: girders A, B, and C contain stiffeners on the inner side, whereas girders D, E, F, and G contain them on the outer side. Figure 4-2 presents a perspective view of the bridge model, with distinct colors used to differentiate the various input components. In the finite element model, each girder was divided into three segments to facilitate accurate application of boundary conditions.

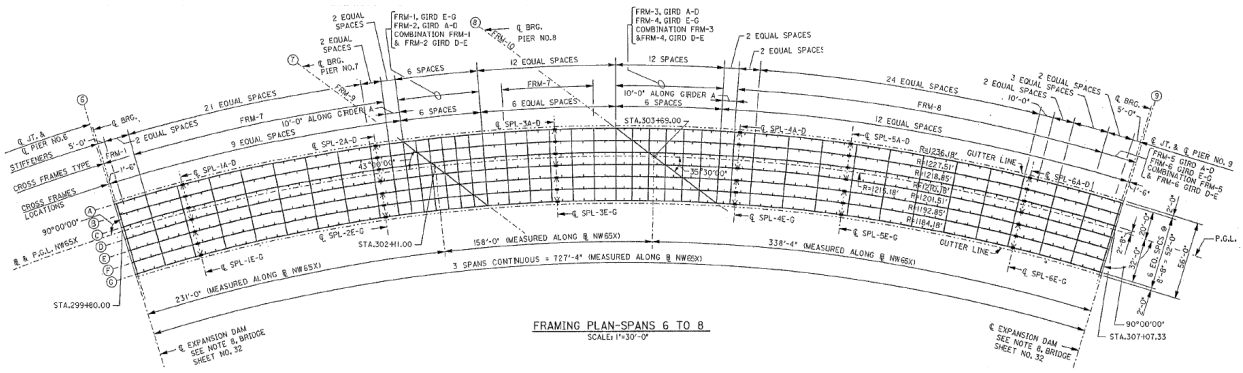

Figure 4-1. Plan view of the Corridor X Bridge showing the span layout and principal dimensions.

For a deeper understanding of the Corridor X Bridge, the plan view with critical dimensions is provided in Figure 4-1. An overview of fundamental geometric properties, including girder span length in elevation (L), plan arc length (L_s), and curvature radius (R) is presented in Table 4-1. The girder span length in elevation (L) represents the straight-line distance between the bearing lines of a girder as viewed in elevation (see Figure 4-3), distinguishing it from the plan arc length (L_s), which follows the bridge's horizontal curvature and can be calculated using Eq. (4.1).

$$L_s = 2R\ sin^{-1}\left(\frac{L}{2R}\right) \tag{4.1}$$

The bearings are positioned at varying elevation levels along the bridge. Table 4-2 enumerates the elevation levels of each bearing. Figure 4-4 illustrates the plan view of Bent No. 6, serving as an example of how bearing elevation magnitudes are represented in the design drawings.

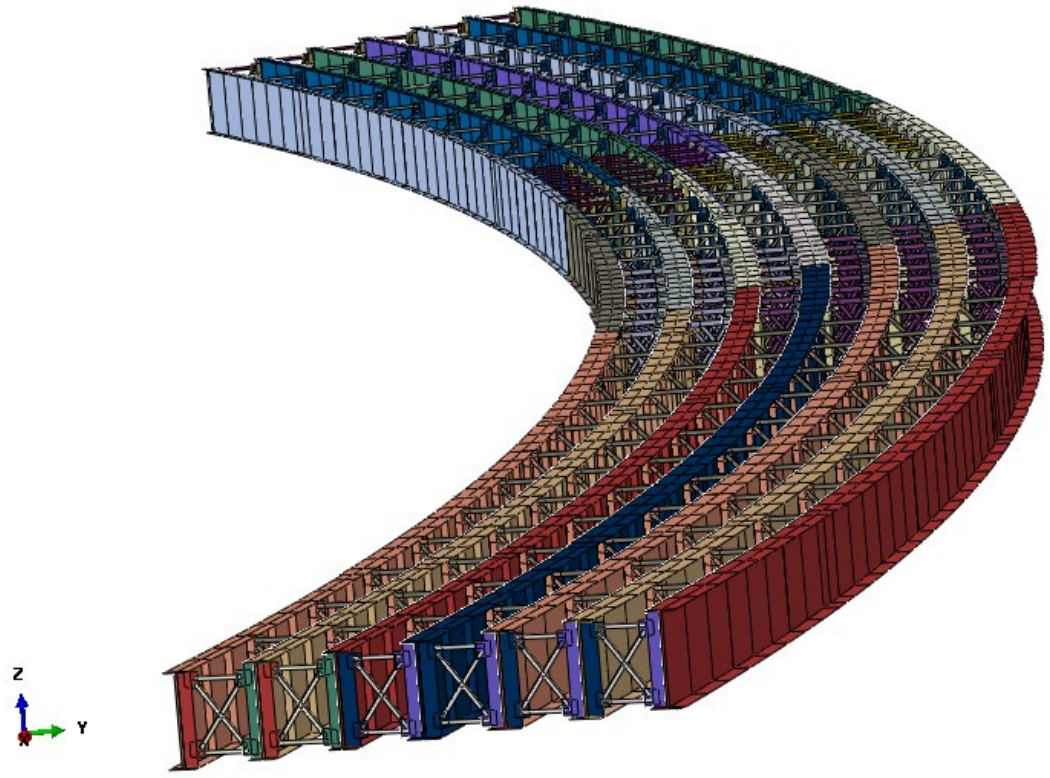

Figure 4-2. Perspective view of the three-span curved steel–concrete composite I-girder bridge model.

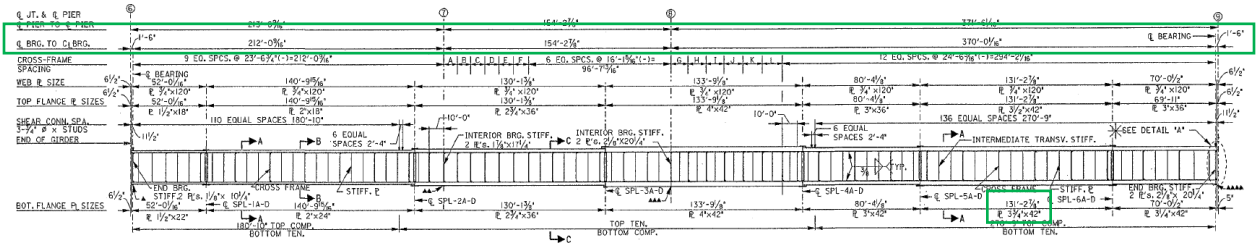

Figure 4-3. Elevation view showing the girder span length L between bearing lines.

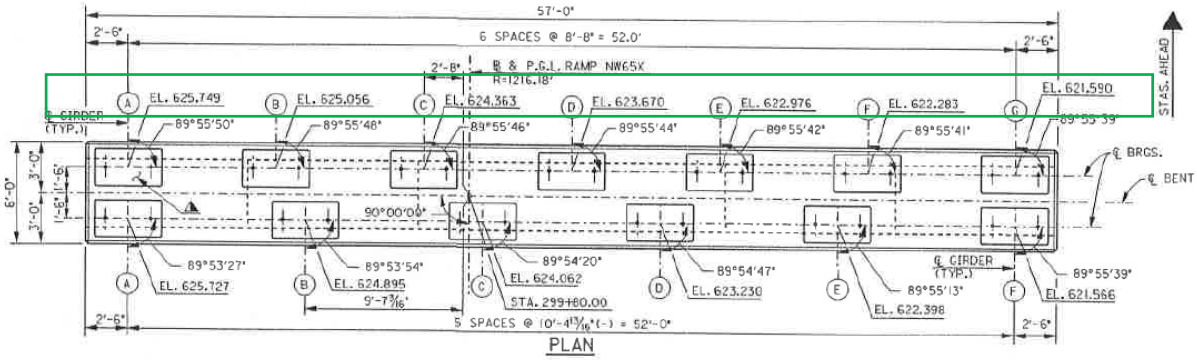

Figure 4-4. Plan view of Bent No. 6 illustrating bearing elevation levels.

Figure 4-5 illustrates the intermediate cross-frame located in Span 8 (Type FRM 8), together with its corresponding finite-element representation. The figure provides a representative example of the geometric characteristics adopted for the cross-frames in the analysis. This configuration is one of the ten distinct cross-frame dimensional types used throughout the bridge. In the numerical model, intermediate stiffeners were omitted, and the diagonal members were interconnected using *tie constraints* to reduce computational cost while preserving the intended force transfer mechanism.

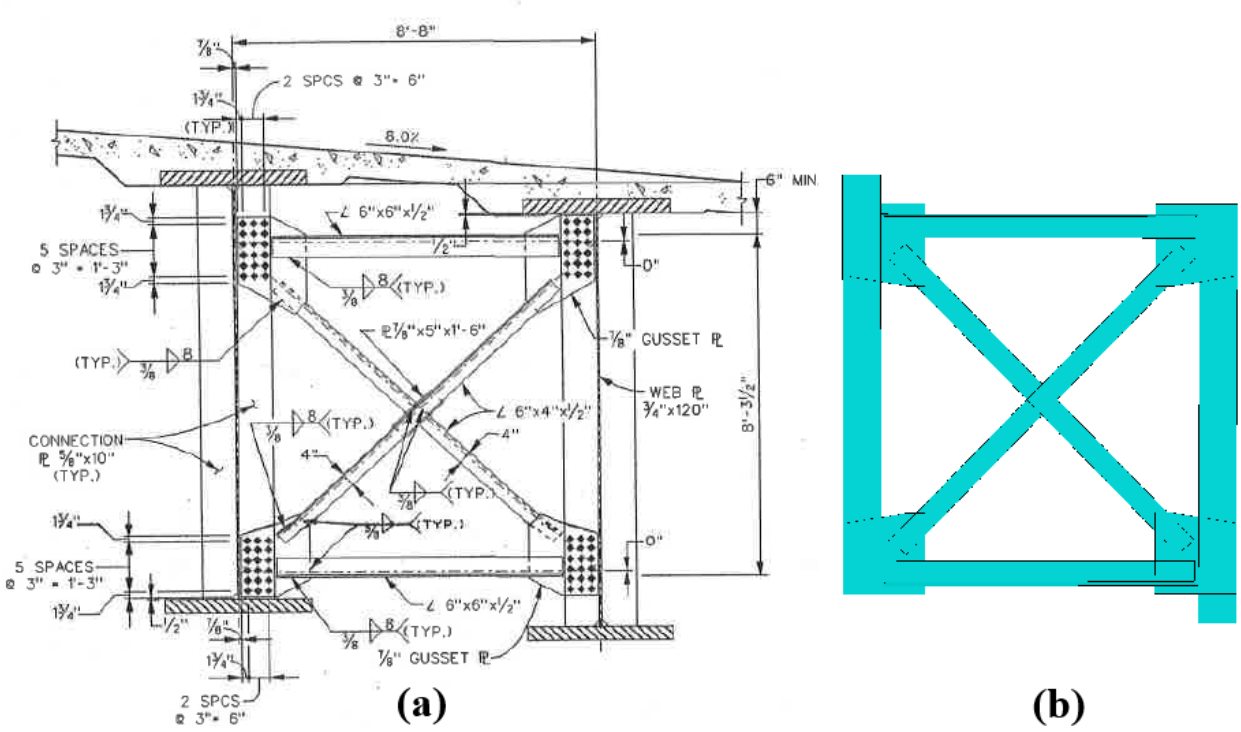

Figure 4-5. Intermediate cross-frame in Span 8 (Type FRM 8) and its corresponding finite-element model.

The length of each span is presented in Table 4-3, where Span X–Y denotes the segment of the bridge located between Bents X and Y. The grade angle for each span is calculated using,

$$\alpha = \tan^{-1}\left(\frac{\Delta h}{L}\right) \tag{4.2}$$

where Δh denotes the elevation difference between the two bearings of a span, and L represents the span length. The resulting grade line angles are summarized in Table 4-4. α_1 represents the grade angle of Span 6–7 (between Bents 6 and 7), α_2 corresponds to Span 7–8, and α_3 corresponds to Span 8–9. The grade line diagram for Girder A with the corresponding angle for each span is depicted in Figure 4-6 as an example.

Table 4-1. Essential geometric characteristics of the bridge girders (ft).

Girder	A	B	C	D	E	F	G
Span Length (L)	736.29	731.10	725.93	720.74	715.56	710.38	705.19
Arc Length (L_s)	747.63	742.38	737.13	731.88	726.63	721.38	716.12
Radius (R)	1236.18	1226.85	1217.51	1208.18	1198.85	1189.51	1180.18

Table 4-2. Elevation levels of bridge bearings along each girder (ft).

Girder	A	B	C	D	E	F	G
Bent 6	625.749	525.056	624.363	623.670	622.976	622.283	621.590
Bent 7	628.390	627.770	627.150	626.530	625.971	625.348	624.724
Bent 8	629.266	628.617	627.968	627.321	626.779	626.134	625.491
Bent 9	630.250	629.557	628.863	628.170	627.540	626.846	626.153

Table 4-3. Span lengths measured between consecutive bents (ft).

Girder	A	B	C	D	E	F	G
Span 6-7	212.047	219.563	227.151	234.813	242.557	250.380	258.292
Span 7-8	154.240	155.813	157.474	159.219	161.068	163.026	165.104
Span 8-9	370.005	355.729	341.302	326.708	311.932	296.969	281.792

Table 4-4. Calculated grade line angles for individual spans (degrees).

Girder	A	B	C	D	E	F	G
$\boldsymbol{\alpha_1}$	0.7099	0.7082	0.7029	0.6978	0.7074	0.7013	0.6951
$\boldsymbol{\alpha_2}$	0.3257	0.3114	0.2976	0.2846	0.2874	0.2762	0.2661
$\boldsymbol{\alpha_3}$	0.1519	0.1514	0.1502	0.1489	0.1397	0.1373	0.1346

Table 4-5. Modeling parameters expressed in U.S. customary units adopted for the numerical simulations.

Quantity	Length	Force	Mass	Stress	Density	Energy	Time
US Customary Unit	ft	lbf	slug	lbf/ft^2	$slug/ft^3$	lbf·ft	s

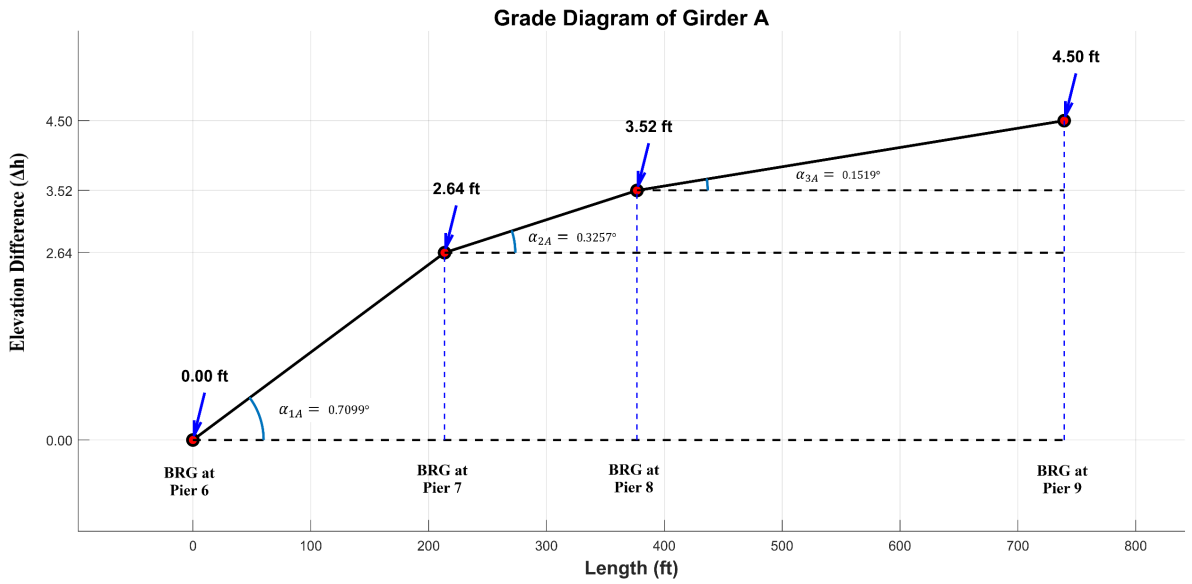

Figure 4-6. Grade diagram of Girder A showing elevation differences (Δh) and grade angles (α) between adjacent bearing lines.

4.3. Material

In Abaqus, material behavior is defined independently of the model geometry to allow consistent assignment across multiple components. This study established a singular inelastic material model to represent all structural steel components, including girders, cross-frames, plates, and stiffeners. The material specification included mass density (ρ), elastic parameters such as the modulus of elasticity (E) and Poisson's ratio, and a true stress–true strain curve obtained from material testing to represent yielding, strain hardening, and other nonlinear properties of AASHTO M270 Grade 50 steel. The material was assigned to shell sections, which were then applied to the girder and cross-frame regions. This method guarantees consistent material characterization across the finite element model and efficiently reflects the nonlinear mechanical behavior of the bridge components.

The steel components employ a weight density of 490 lb/ft³, a modulus of elasticity of 4.27×10^9 psf, and a Poisson's ratio of 0.3. The concrete deck was not explicitly modeled using solid elements; instead, its contribution was represented as a uniformly distributed pressure load applied to the top flange of each girder based on the effective tributary slab area. A concrete unit weight of 150 lb/ft³ was utilized to calculate this load.

The design specifications for the Corridor X–I65 bridge mandate the utilization of AASHTO M270 Grade 50 steel for all principal structural elements. Grade 50 is the predominant structural steel employed in contemporary bridge building, attributed to its elevated yield strength, excellent weldability, and consistent performance under both elastic and inelastic loading circumstances [32]. These properties make it well suited for accurately capturing the nonlinear behavior required in the numerical simulation of curved and skewed steel I-girder bridges.

In Abaqus, the material model for steel must be defined using true stress and true plastic strain to ensure an accurate representation of nonlinear response. Accordingly, the engineering stress–strain data for Grade 50 steel were converted to true stress and true strain utilizing Equations (4.3) and (4.4). The elastic strain component was subsequently eliminated using Eq. (4.5) to derive the true plastic strain, which was then associated with the appropriate true stress values and incorporated into the Plastic material specification in Abaqus.

$$\sigma_{true} = \sigma_{eng} \times (1 + \varepsilon_{eng}) \tag{4.3}$$

$$\varepsilon_{true} = \ln (1 + \varepsilon_{eng}) \tag{4.4}$$

$$\varepsilon_p = \varepsilon_{true} - \frac{\sigma_{true}}{E} \tag{4.5}$$

In these equations, σ_{eng} and ε_{eng} are the engineering stress and strain, σ_{true} and ε_{true} are the true stress and strain, ε_p is the true plastic strain, and E is Young's modulus.

Table 4-6. Data points representing the multi-linear stress–strain behavior of steel members.

Point	True Strain (%)	True Stress (ksi)
Yielding	0.17	50
Onset of strain hardening	1.12	50.38
Intermediate strain hardening	3.84	66.31
Ultimate strength	11.65	79.56

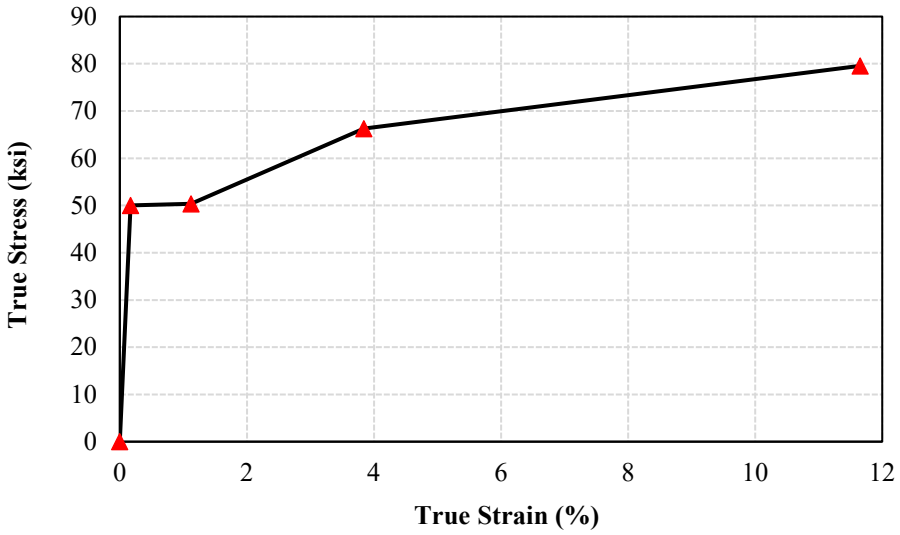

Figure 4-7. True stress–strain behavior of Grade 50 structural steel.

A multi-linear model was utilized to characterize the stress-strain behavior of the steel, enabling precise capture of the material response during various deformation stages. The curve is defined using several key anchor points. The first point at 50 ksi represents the yield strength and marks the onset of plastic deformation. A second anchor point is selected at the beginning of the strain-hardening region, where the steel begins to gain additional strength beyond yield. A third point is generally positioned within the strain-hardening region to depict the nonlinear curvature of the response more accurately. The final point represents the ultimate stress and its corresponding strain, indicating the material's maximal strength. This method offers a dependable and comprehensive depiction of the true stress–strain relationship necessary for nonlinear finite-element analysis. The stress–strain curve for AASHTO M270 Grade 50 steel, sourced from Cagri (2011) [25], is illustrated in Figure 4-7, and the corresponding numerical values are listed in Table 4-6.

4.4. Boundary Conditions

The Corridor X–I-65 Bridge is a continuous, three-span bridge with four bents (piers), as shown in Figure 4-8. This figure illustrates the locations of the bearings used in the numerical model based on the official drawings. Bents 6 and 9 are radial, while bents 7 and 8 are skewed. Each pier supports seven bearings, one for each girder, at different elevations.

Each girder is modeled using three segments corresponding to the three spans. For example, Girder A is divided into segments A1, A2, and A3. A reference point (RP) is established at the end of each girder segment, and a coupling constraint encompassing six degrees of freedom is implemented to link the RP with the respective girder end. This method facilitates the convenient assignment of boundary conditions by identifying the relevant reference point and confining the corresponding degrees of freedom.

In intermediate bearings, the ends of neighboring girders within a span are connected to a shared reference point, enabling them to function as a continuous girder. Boundary conditions are subsequently imposed directly on this RP, guaranteeing accurate force transfer and compatibility over the span. This modeling technique offers flexibility in establishing support conditions and facilitates modifications to the boundary configuration, which is especially advantageous in multi-span bridge assessments where various support types (pinned, roller, or fixed) may be included.

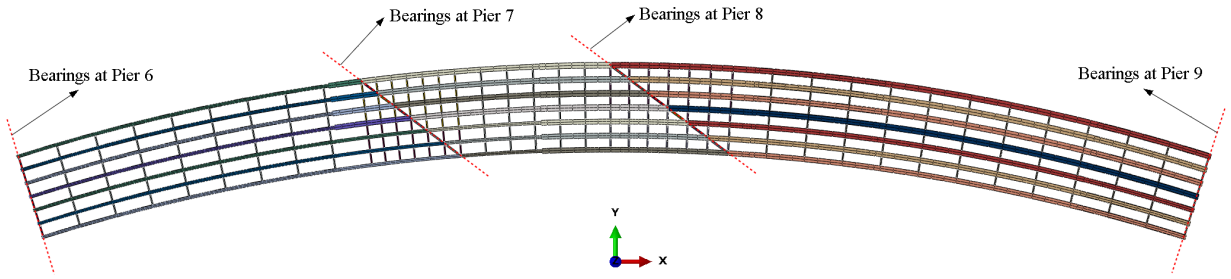

Figure 4-8. Representation of bearing positions in the numerical model.

4.5. Interactions

As depicted in Figure 4-9, each cross-frame in the numerical model is segmented into three discrete components: the left section, the central section, and the right section. The left and right components mainly comprise stiffeners and gusset plates, which impart rigidity and facilitate force transfer between the cross-frame members and the girders. The central component comprises the structural elements that constitute the load-bearing system, specifically the upper and lower chords in conjunction with the diagonal braces. To ensure accurate structural behavior, the three components are connected using *tie constraints*, which enforce displacement and rotational compatibility at the shared interfaces.

A total of ten distinct types of cross-frames were integrated into the finite element model, mirroring the differences outlined in the design drawings obtained from ALDOT. This degree of detail helps ensure that the numerical model accurately reflects the constructed bridge arrangement. Each cross-frame is connected to the adjacent girders utilizing *tie constraints*. This ensures complete compatibility between the displacements of the cross-frame members and the girder flanges, enabling a realistic representation of load transfer. By enforcing these compatibility conditions, the cross-frames act integrally with the girders, contributing to lateral stability and appropriate load distribution consistent with the actual behavior of the bridge.

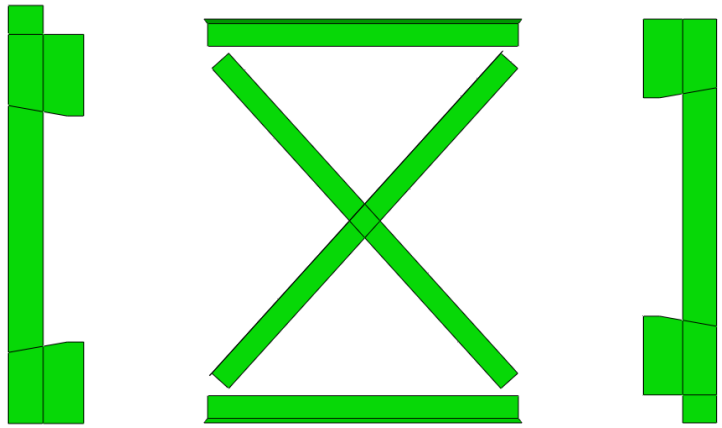

Figure 4-9. (a) Left-side part, (b) middle part, and (c) right-side part of the cross-frames.

4.6. Mesh

The complete bridge system, comprising girders, cross-frames, plates, and stiffeners, was simulated utilizing S4R shell elements. These four-node, reduced-integration, finite-membrane-strain shell elements offer an optimal balance between precision and computing efficiency for extensive structural systems. Shell-section characteristics with five integration points across the thickness were designated to accurately capture bending loads and local stress gradients in thin-walled components. All plates, stiffeners, and cross-frame members were precisely modeled, enabling the shell formulation to accurately depict their axial, bending, and shear responses.

A structured meshing approach was applied to the cross-frames to ensure uniform element distribution and proper alignment of diagonal, horizontal, and gusset plate regions. A sweep-meshing approach was employed for the horizontally curved girders to accurately express the elongated geometry and ensure smooth element placement along the curvature. The mesh density along the girder length and within the cross-frames was optimized to ensure that the resulting shell elements attained aspect ratios near unity, hence enhancing element quality and numerical stability. The final reference model contained 1,215,691 elements.

Shell elements were chosen due to their ability to accurately represent plate bending, local buckling phenomena, out-of-plane deformation, and the stiffness contribution of gusset plates-effects that are essential for reliable cross-frame modeling. Simplified cross-frame models employing truss elements consider solely axial deformation and disregard other deformation modes, resulting in an overestimation of cross-frame stiffness. Beam-element models introduce a different set of inaccuracies, as they typically omit gusset plates and stiffeners and connect members at web–flange junctions, artificially increasing the effective member lengths and altering the load-transfer mechanism. Such simplifications lead beam models to underestimate cross-frame stiffness and misrepresent internal force distribution. The utilization of S4R shell elements overcomes these limitations and enables the model to accurately depict the three-dimensional structural behavior of cross-frames.

Figures 4-10 and 4-11 illustrate the resulting finite-element mesh for the girders and cross-frames. The mesh density in the girder flanges and cross-frame connection regions was intentionally increased to capture localized stress concentrations and deformation patterns that are critical for evaluating cross-frame forces and girder layover behavior under dead load induced rotations.

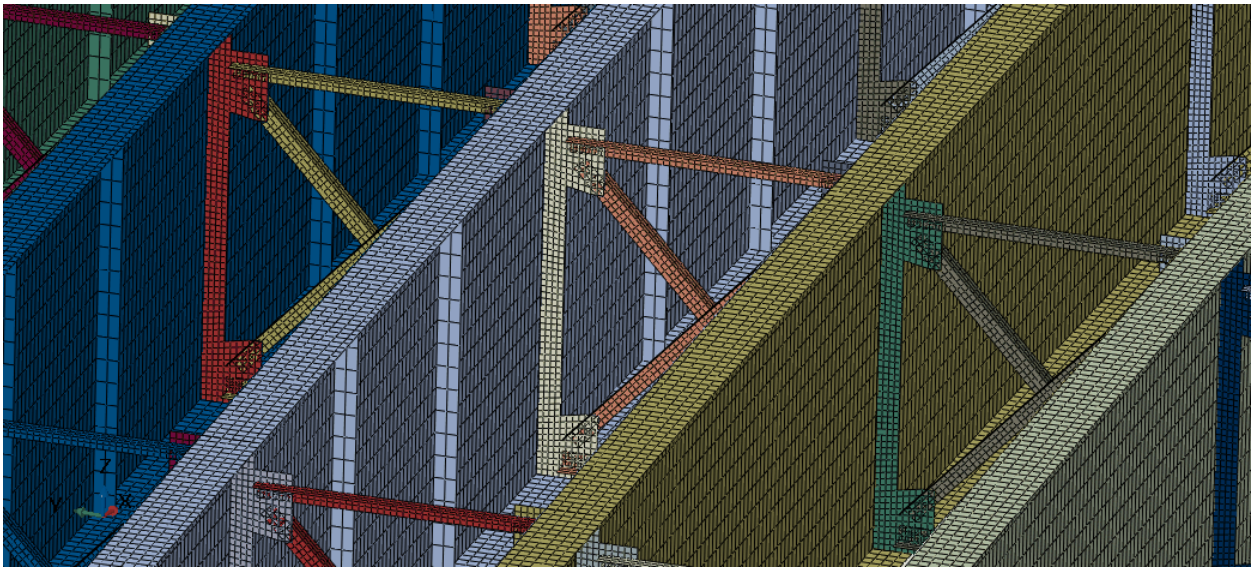

Figure 4-10. Perspective view of the finite element mesh for girders and cross-frames.

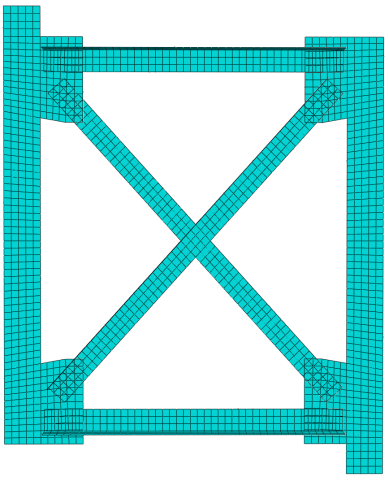

Figure 4-11. Sample cross-frame model with S4R mesh.

4.7. Loading

This study analyzes all bridge models under the dead load from the self-weight of the steel, the weight of the fresh concrete deck, and additional construction-stage loads affecting the non-composite bridge. The structural behavior during construction is of special interest; thus, the steel girders are presumed to support the wet concrete load alongside their own self-weight, the weight of slab reinforcement, formwork, and temporary construction equipment.

In the finite element model, gravity was implemented with the Gravity load option in Abaqus, which incorporates the self-weight of the steel components as distributed body forces. The precision of this loading relies on the accurate specification of the material density. If the weight density (lb/ft³) is indicated in the material properties, the gravitational coefficient must be established at 1 ft/s². However, when mass density (slugs/ft³) is employed, the gravitational coefficient must be designated as 32.174 ft/s² to precisely reflect gravitational acceleration.

The concrete dead load was calculated according to the elevation and section specifications provided in the design drawings obtained from ALDOT. Each longitudinal girder comprises seven beam segments, each characterized by unique flange widths and lengths (see Figure 4-3). To evaluate the concrete load acting on each girder, the total concrete weight of the deck portion supported by each beam segment was initially calculated and subsequently applied to the top flange surface as a uniform pressure, represented by σ_c:

$$\sigma_c = \frac{P}{A_f} \tag{4.6}$$

where P is the total concrete load supported by the beam segment and A_f is the flange top surface area. Figure 4-12 presents Section B–B at Bent 7, illustrating the slab thickness and effective width corresponding to each girder. The slab thickness varies slightly along the bridge length, both

between adjacent girders and over the flanges. The total concrete load P for each segment was obtained as:

$$P = V_e \times \rho \tag{4.7}$$

$$V_e = A_e \times t_c \tag{4.8}$$

$$A_e = W_e \times L \tag{4.9}$$

where V_e is the effective slab volume, ρ is the concrete density (150 lb/ft³), A_e is the effective slab area supported by the girder, t_c is the slab thickness, W_e is the effective slab width (10.401 ft), and L is the length of the beam segment. This approach yielded the distributed concrete load utilized in the finite element model to depict the deck's self-weight exerted on each girder. Figure 4-13 provides a three-dimensional visualization of the concrete dead load applied across the numerical bridge models, showing the uniform distribution of deck and parapet loads along the girder flanges.

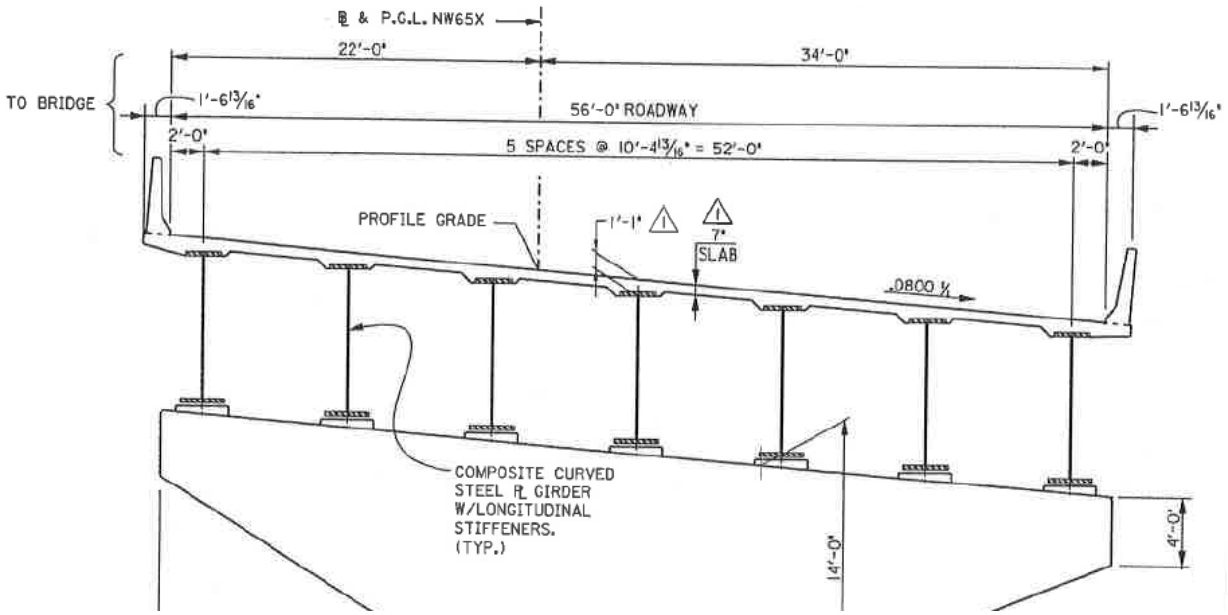

Figure 4-12. Section B–B at Bent 7, showing the slab thickness profile and the effective slab width assigned to each girder.

Besides dead loads, the model accounts for the influence of barriers (overhang brackets), which uphold the wet concrete and formwork at the fascia girders. These barriers exert torsional forces on the fascia girders. The barrier weight was computed and applied to Girders A and G to account for this effect. The barriers were presumed to integrate into the girder webs at the web-flange connections. To replicate the resultant torsion, two equal and opposing radial forces were exerted on the edges of the upper and lower flanges, thereby generating a uniformly distributed torque along the fascia girders. The magnitude of the torque is derived from the weight of the barrier and its eccentricity relative to the girder web (see Figure 4-14). The whole barrier weight, represented

as a concentrated downward force F_1 at the centroid of the barrier, and d as the horizontal distance from this centroid to the girder web, allows the torque M to be articulated as:

$$M = F_1 \times d \tag{4.10}$$

By dividing this torque by the web height, h, the equivalent pair of radial flange forces, F_2, can be obtained as:

$$F_2 = \frac{M}{h} \tag{4.11}$$

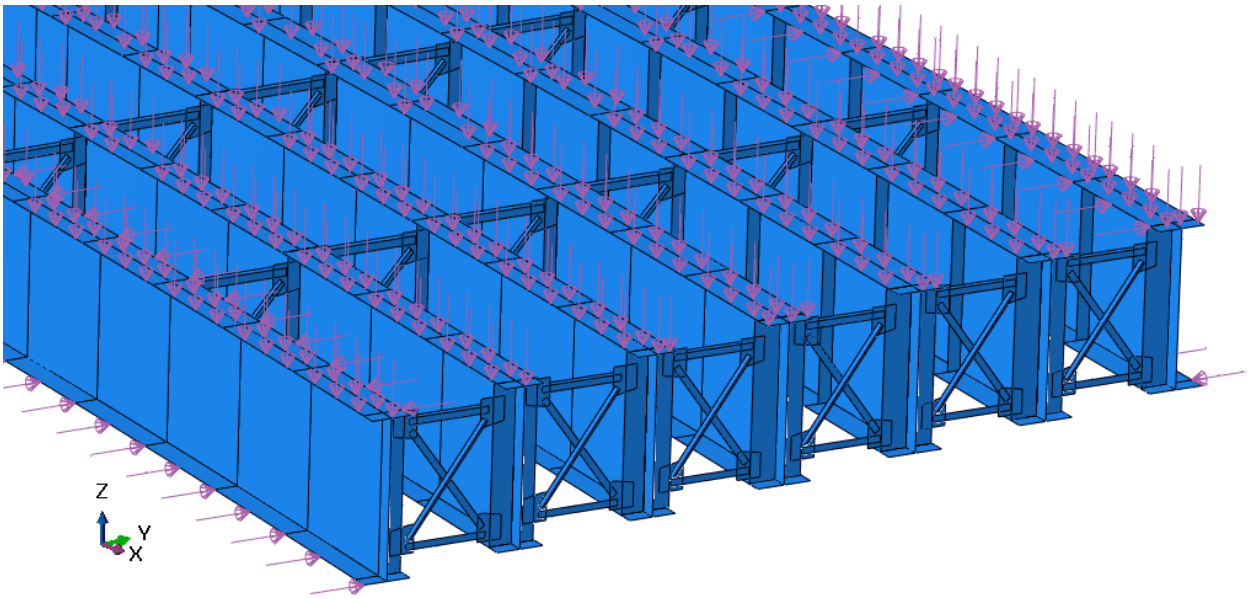

Figure 4-13. Three-dimensional view of the applied concrete loads on the numerical models.

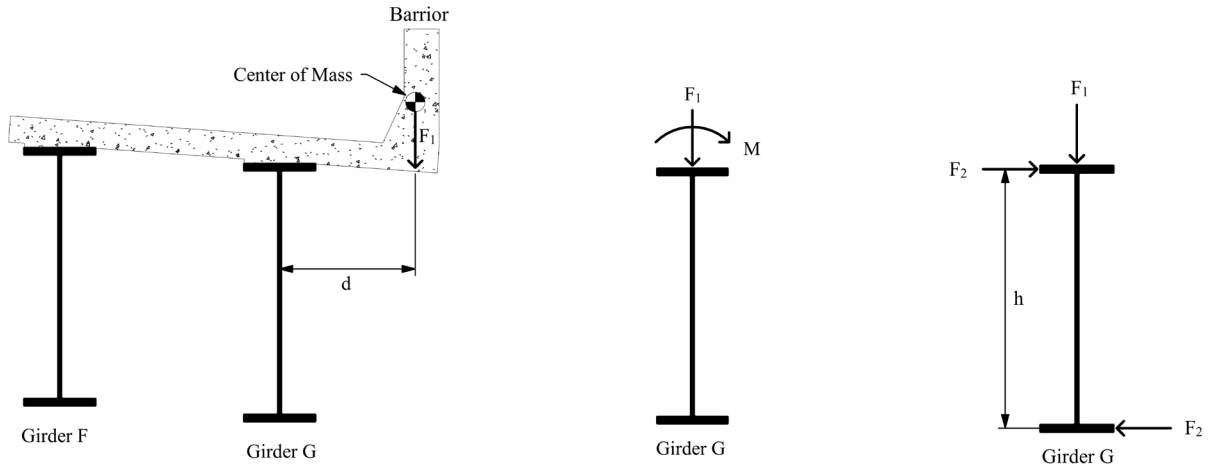

Figure 4-14. Schematic illustration of (a) barrier load, (b) barrier load effects on girder G, and (c) moment decomposed into a force couple, representing the equivalent torsional effect on the fascia girder.

4.8. Verification of Cross-Frame Modeling

The experimental program undertaken by Battistini et al. [26] was utilized as a benchmark to validate the numerical simulation of cross-frame modeling. The study conducted extensive stiffness testing on various cross-frame types to measure their real stiffness and compare it with analytical forecasts. Additionally, a comprehensive comparison of the drawing-based and FEM-based camber diagrams is provided in Section 5.2.

The experimental setup consisted of three hydraulic tension–compression actuators and three reaction struts, with the schematic illustration provided in Figure 4-15. The actuators, denoted by arrows labeled F, applied the test loads, while the reaction struts, indicated by arrows labeled R, supplied the requisite restraints. The actuators and struts were affixed to a pair of W30×90 beams, which functioned to replicate the rigid cross sections of two contiguous girders linked by the cross-frame. To minimize deformation in the loading beams, stiffeners were welded at the cross-frame connection points, therefore establishing a suitably rigid load frame and confining the deformations to the cross-frame components. Each cross-frame specimen was affixed on either side to a WT9×35.5 member having a thickness of 0.5 inches. Figure 4-16 illustrates the nominal geometry of the evaluated cross-frames.

The in-plane stiffness of the cross-frame system, functioning as a torsional brace for the girders, can be determined by dividing the torsional restraining moment, M, by the associated girder rotation at the brace, θ, as specified in Eq. (4.12).

$$\beta_b = \frac{M}{\theta} = \frac{F.h_b}{\theta} \tag{4.12}$$

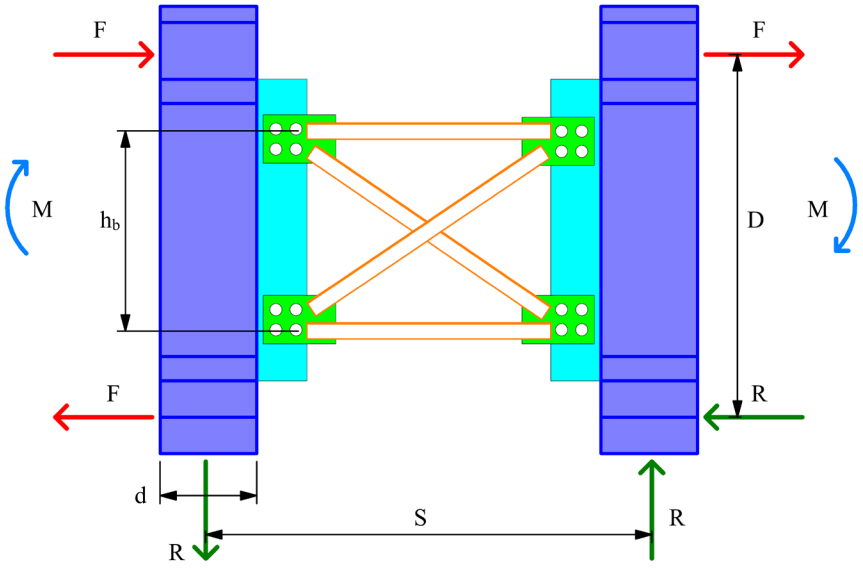

Figure 4-15. Free-body diagram of the test setup used by Battistini et al. [24].

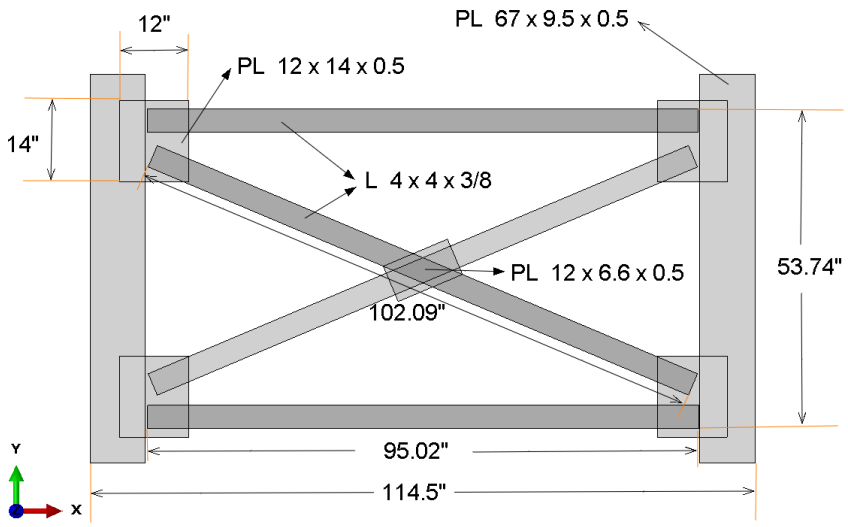

Figure 4-16. Geometry and dimensions of the single-angle X-frame specimen used for verification.

The cross-frame specimens were numerically modeled by following the modeling procedure of the Corridor X–I65 bridge. Each cross-frame was discretized with S4R shell elements, employing a refined mesh with two elements per angle to precisely represent the angular geometry. The plate situated between the two diagonals was connected to them by a *tie constraint*, a method that accurately simulates the welded connections found in the physical specimens. The top and bottom chords, along with the diagonals, were connected to the gusset plates by a *tie constraint*, which was merged with the stiffeners to create a unified, continuous component. Each stiffener was additionally linked to the neighboring girders by a coupling constraint to replicate the actual attachment and load distribution.

Boundary conditions were implemented to represent the laboratory testing configuration (see Figure 4-17 for the positions of constraints). To prevent out-of-plane deformations of the model and depict the connection to the girders, the upper and lower surfaces of the load beams were restricted in the Z direction. A pin support was modeled by restricting the left beam bottom from translating in both the X and Y axes, whereas a roller support was modeled by limiting the right beam bottom just in the Y axis. Two side load beams were simulated using B31 beam elements and were connected to the outer edges of the stiffeners to replicate the laboratory load frame. Concentrated forces, F, in accordance with the laboratory loading protocol, were exerted on these load beams.

A three-dimensional, linear elastic analysis was conducted to determine the brace rotation, and the associated stiffness was computed using Eq. (4.12).The calculated stiffness values and their comparisons with experimental and analytical data are displayed in Table 4-7. Percentage errors are expressed in relation to the experimentally determined stiffness from Battistini et al. [26]. The numerical model accurately replicated the measured stiffness, exhibiting a discrepancy of around 1% from the experimental values. Figure 4-18 presents the deformed shape of the shell-element model used for verification. As shown, the cross-frame exhibits out-of-plane buckling.

Table 4-7. Comparison of experimental and numerical in-plane cross-frame stiffness (kN.m/rad).

Cross-frame type	Experimental	Numerical	Error (%)
Single Angle X Frame	98520	99515.5	1.01

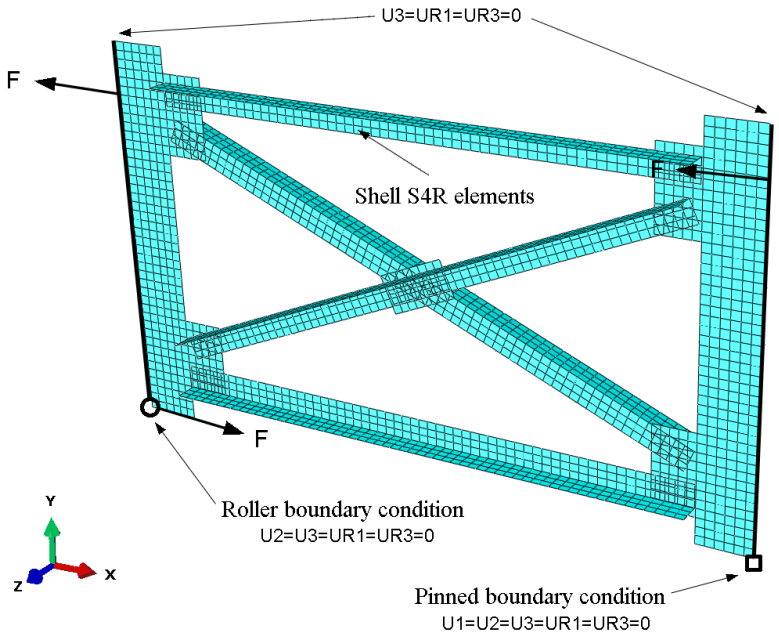

Figure 4-17. Three-dimensional shell-element model of the cross-frame used in numerical analysis.

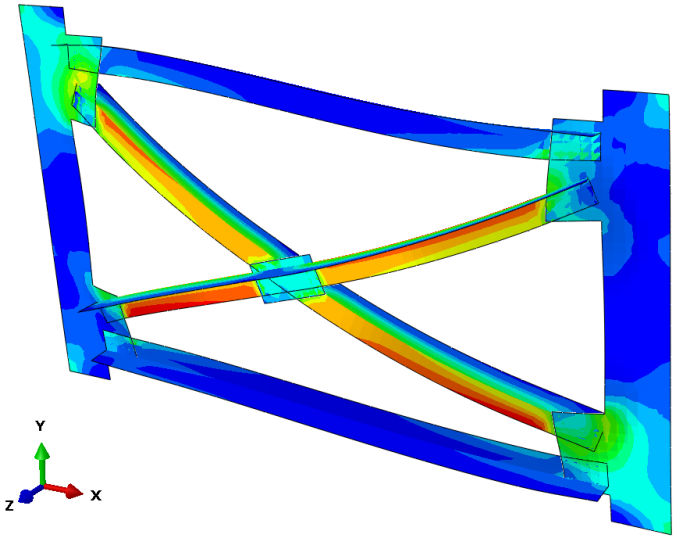

Figure 4-18. Deformed shape (200× magnified) of the shell-element model used for verification.

The second phase of verification involved comparing the camber diagrams from the design drawings with those derived from the comprehensive FEM model of Corridor X–I65. This comparison further validated that the continuous girders and boundary conditions were accurately predicted. A minor mismatch was noted between the FEM-predicted cambers and those depicted in the drawings, attributable to variations in modeling methodologies. The detail for this comparison is described in Section 5.2.

4.9. Numerical Simulation of Detailing Methods

A reference finite-element model was created to depict the ultimate plumb-and-level arrangement of the bridge superstructure, featuring all girders vertically aligned and all cross-frames completely interconnected in their final position desired in the design drawing. Utilizing the modeling approach outlined in this chapter, this model was employed to simulate the NLF, SDLF, and TDLF detailing methods. It additionally served to determine the geometric camber and to establish the initial cross-frame stress state necessary for the SDLF and TDLF simulations.

Prior to the development of the three primary simulation models (NLF, SDLF, and TDLF), it was essential to establish the initial conditions. Since girders are fabricated with a camber designed to match the total dead load, an initial camber profile must be assigned in each model to realistically simulate the construction sequence. In addition, the TDLF and SDLF models require initial stresses to represent the lack-of-fit effects under total dead load and steel dead load, respectively. To obtain these initial stresses and camber values, three preliminary analysis models, U1, U2, and C1, were developed and executed to derive the initial stresses and camber values prior to developing the main detailing models.

4.9.1. Model U1

To ascertain the required camber for achieving the intended as-built geometry, the total dead load was applied in the reverse (upward) direction to the girders, producing an upward deflection. This setup is designated as model U1. The resulting displacement at the web–flange junction represents the girder's vertical curvature and the magnitude of the final camber. The camber magnitude was determined to ensure that, under the full non-composite dead load (prior to deck slab casting), the bridge deck remained almost level. This model is also used to calculate the lack-of-fit stresses in cross-frames for TDLF model.

Figure 4-19 presents the stress contour of the U1 model at its final state under the reverse (upward) total dead load. In this model, the stresses developed in the cross-frames represent the lack-of-fit effects among interconnected components, then utilized as the initial stress input for the TDLF model (see Figure 3-3c).

4.9.2. Model U2

Another configuration, designated to as model U2, was developed similarly to U1 but subjected only to the steel self-weight. The stresses in the cross-frames of model U2, indicative the lack-of-

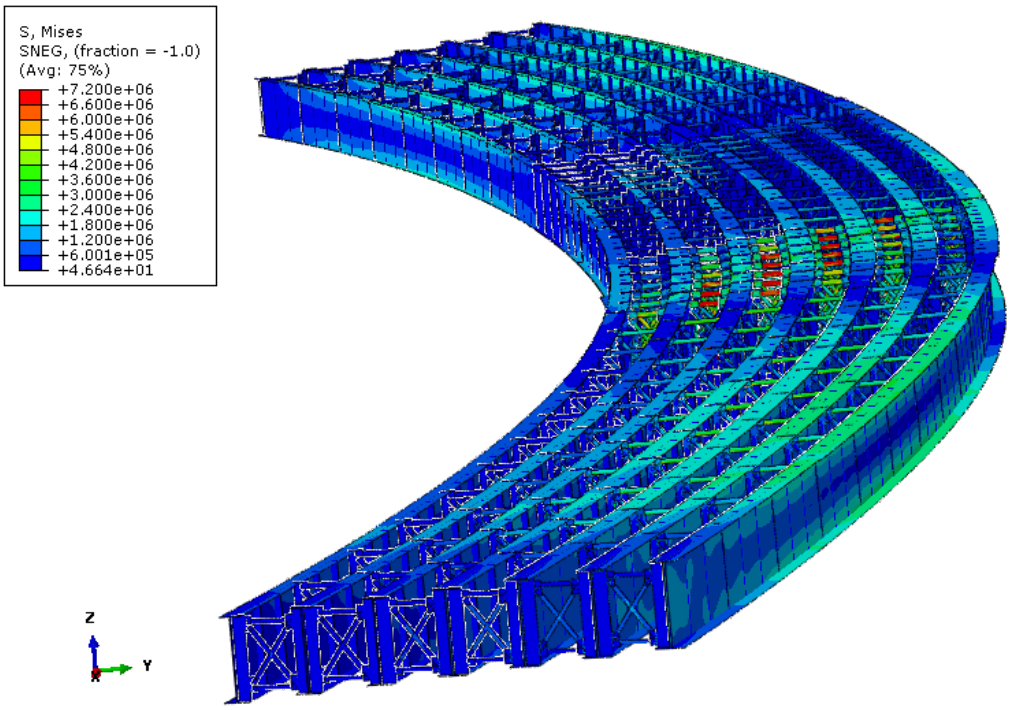

Figure 4-19. Final-stage stress distribution of the U1 model under the reverse total dead load.

fit under the steel dead load, served as the initial stress state for the SDLF model (refer to Figure 3-4c).

4.9.3. Model C1

The girders are manufactured with a camber that aligns with the total dead load, necessitating an initial camber profile for each model to accurately reflect the building process. Since girders are fabricated in a plumb condition, displacement-controlled analysis was conducted to determine the predicted camber profile corresponding to the deflection observed at the web–upper flange junction in model U1. This displacement-controlled model is designated as model C1. During this analysis, the lateral and radial degrees of freedom of the girders were restrained to prevent any out-of-plane movement, and a prescribed vertical displacement equivalent to the deflection obtained from model U1 was applied. This procedure produced the desired camber while maintaining plumb girder webs, consistent with the vertical alignment of cambered girders in the actual bridge. Figure 4-20 and Figure 4-21 illustrate the magnified deflected shapes of the U1 and C1 models, respectively, at their final states under the reverse total dead load condition.

The resultant nodal displacements form the dead load camber, representing the geometric imperfection used to simulate camber conditions. The camber profile was integrated into the girder models via the Abaqus *IMPERFECTION* input, enabling subsequent analyses to begin with the cambered geometry.

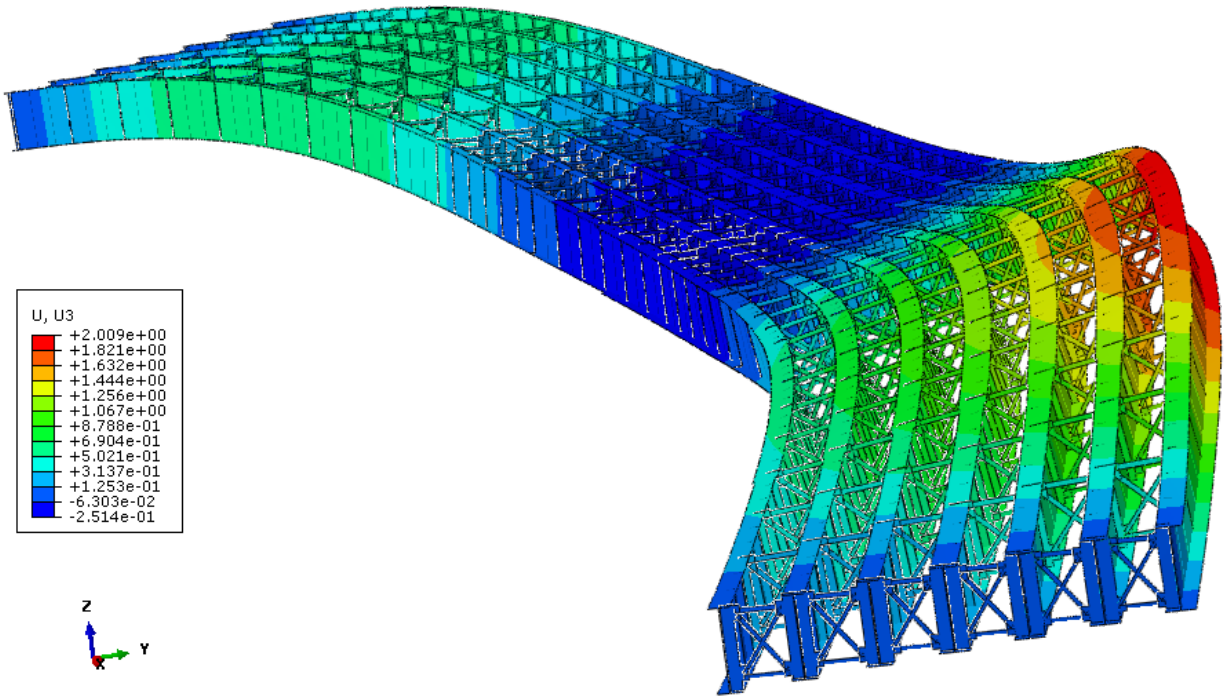

Figure 4-20. Magnified deflected shape (10×) of the U1 model under reverse total dead load.

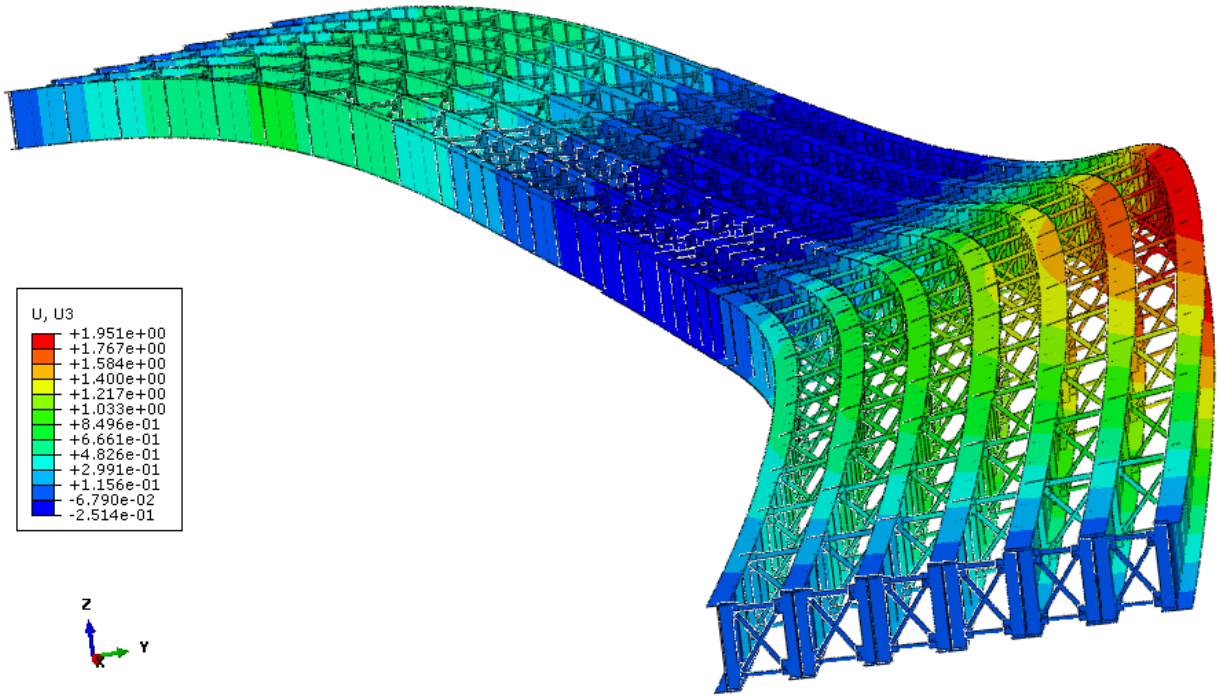

Figure 4-21. Magnified deflected shape (10×) of the C1 model with plumb webs under reverse total dead load.

In summary, model C1 defines the geometric camber utilized in all NLF, SDLF, and TDLF analyses. The cross-frame stresses from model U1 were assigned as the initial stresses for the TDLF model, whilst those from model U2 were assigned to the SDLF model.

The automation of stress field transfer was accomplished by Abaqus Python scripting, which extracted the required data and applied them as initial conditions in the corresponding analyses. This technique guaranteed uniform and replicable camber and stress settings that reflect the related lack-of-fit issues encountered in practice. The pre-analysis models U1, U2, and C1 are summarized in Table 4-8 for comparison.

During the numerical modeling phase, three principal bridge models were created from the reference model to depict the No-Load Fit (NLF), Steel Dead Load Fit (SDLF), and Total Dead Load Fit (TDLF) detailing conditions. All models had identical geometry, boundary conditions, mesh density, and material definitions, and each began with the initial camber profile derived from the reference C1 model to ensure a consistent starting configuration. The primary difference between these models is the handling of initial stresses and the conditions of lack of fit attributed to the cross-frames.

Table 4-8. Summary of Pre-Analysis Models (U1, U2, and C1)

Model ID	Loading Type	Purpose / Exported Output	Lateral DOF Condition	Loading Method	Description / Application
U1	Reverse of Total Dead Load (TDL)	Initial stress field for TDLF model	Unrestrained	Force-controlled	Simulates the reverse total dead load to obtain cross-frame stresses representing lack-of-fit effects under full dead load.
U2	Reverse of Steel Dead Load (SDL)	Initial stress field for SDLF model	Unrestrained	Force-controlled	Similar to U1 but includes only the steel self-weight; provides the initial stress field corresponding to steel dead load conditions.
C1	Reverse of Total Dead Load (TDL)	Initial geometric camber for all models	Restrained	Displacement-controlled	Determines the camber profile based on displacements from U1, with lateral and radial DOFs restrained to prevent out-of-plane movement.

4.9.4. Model NLF

The No-Load-Fit (NLF) model begins with the camber profile derived from the C1 model (refer to Figure 3-2a at no-load condition with camber). This model is analyzed without any pre-existing internal stresses, representing a system fabricated and erected without intentional lack-of-fit between the girders and cross-frames (see Figure 3-2b). This configuration establishes a baseline situation wherein all cross-frames are presumed to be stress-free before the imposition of any loads.

The dead load effects were implemented in two consecutive stages. First, the steel dead load (SDL) was applied, reflecting the self-weight of the steel girders, cross-frames, and associated components. The corresponding stresses and deformations under the SDL condition were exported. This phase captures the initial deformation, torsional rotation, and stress redistribution that transpire prior to the installation of the concrete deck. After the structure stabilized under the SDL, the TDL was applied, including both the steel self-weight and the additional weight of the concrete deck and parapets. The stresses and deformations at the TDL stage were then exported (refer to Figure 3-2c). Figure 4-22 and Figure 4-23 depict the magnified deflected configurations of the NLF bridge model under the SDL and TDL, respectively.

4.9.5. Model TDLF

The Total Dead Load Fit (TDLF) model also initiates with the camber profile obtained from the C1 model (see Figure 3-3a). In this model, initial stresses exported from the U1 analysis are applied to the cross-frames. These stresses represent the lack-of-fit that develops when the structure deforms under the total dead load (see Figure 3-3b). Figure 4-24 illustrates the stress distribution of the TDLF model immediately after the application of the initial stresses, during which the girders remain predominantly stress-free. The stresses in the cross-frames at this stage correspond exactly to the cross-frame stresses at the final state of the U1 model shown in Figure 4-19.

Upon the model's release, the structure attains a new equilibrium configuration that corresponds to the geometry shown in Figure 3-3c. At this stage, the stresses in the cross-frames diminish while the stresses in the girders escalate, indicating the redistribution caused by the imposed lack of fit. Figure 4-25 shows the magnified deformed shape of the Corridor X–I65 bridge at its equilibrium state. Upon establishing this initial condition, the steel dead load was implemented, and the resultant stresses and deformations were exported. In the final step, the total dead load was applied by adding the concrete load onto the girders, and the corresponding stresses and deformations were subsequently exported (see Figure 3-3d).

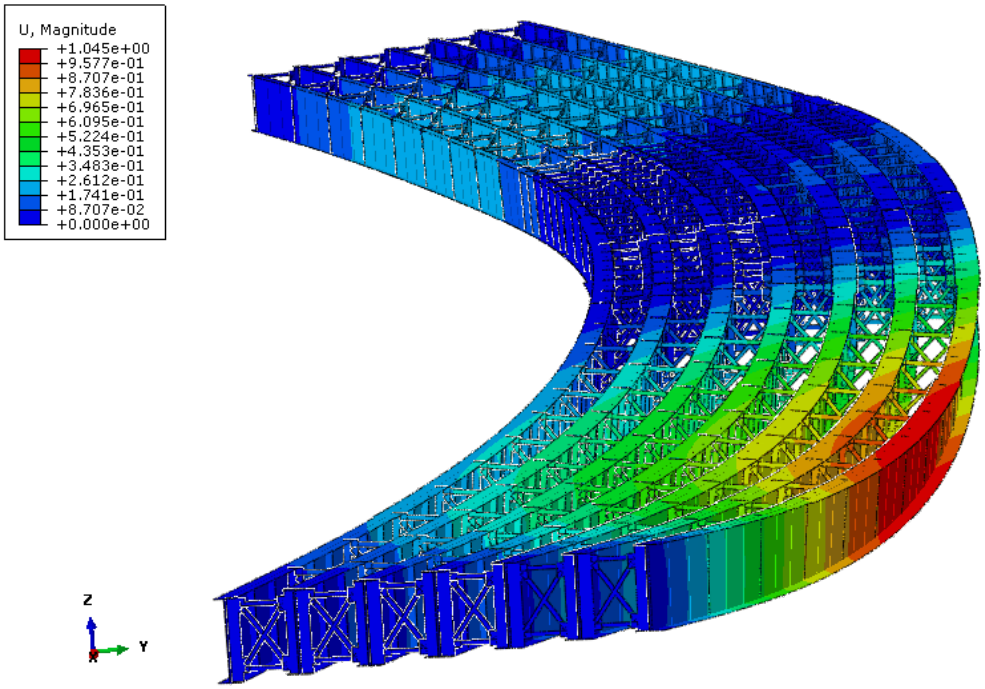

Figure 4-22. Deflection shape (10× magnified) of the NLF bridge model under steel dead load.

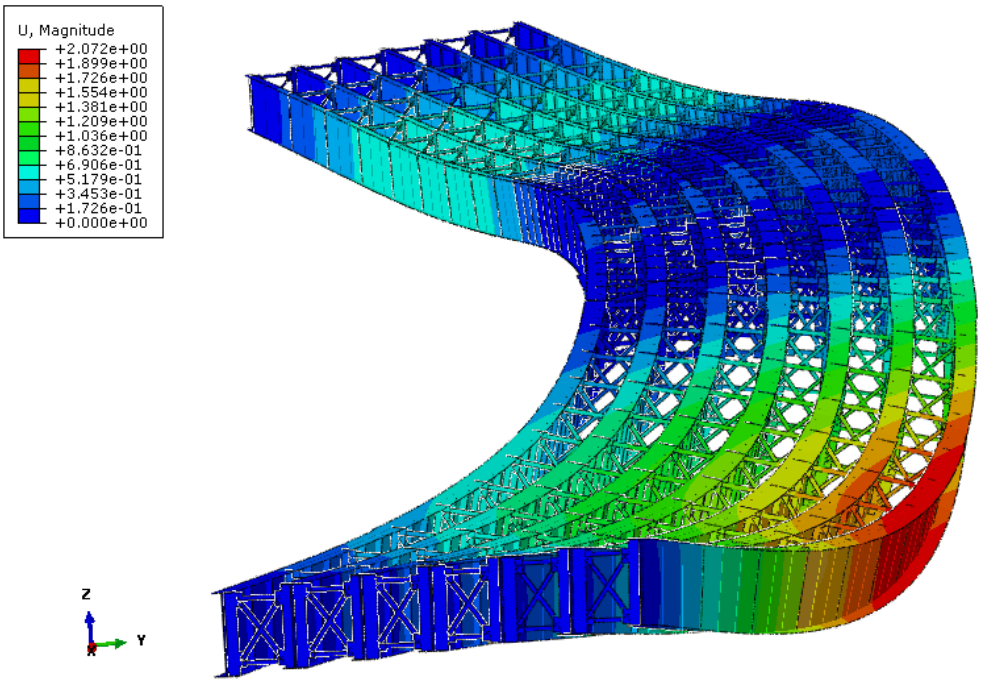

Figure 4-23. Deflection shape (10× magnified) of the NLF bridge model under total dead load.

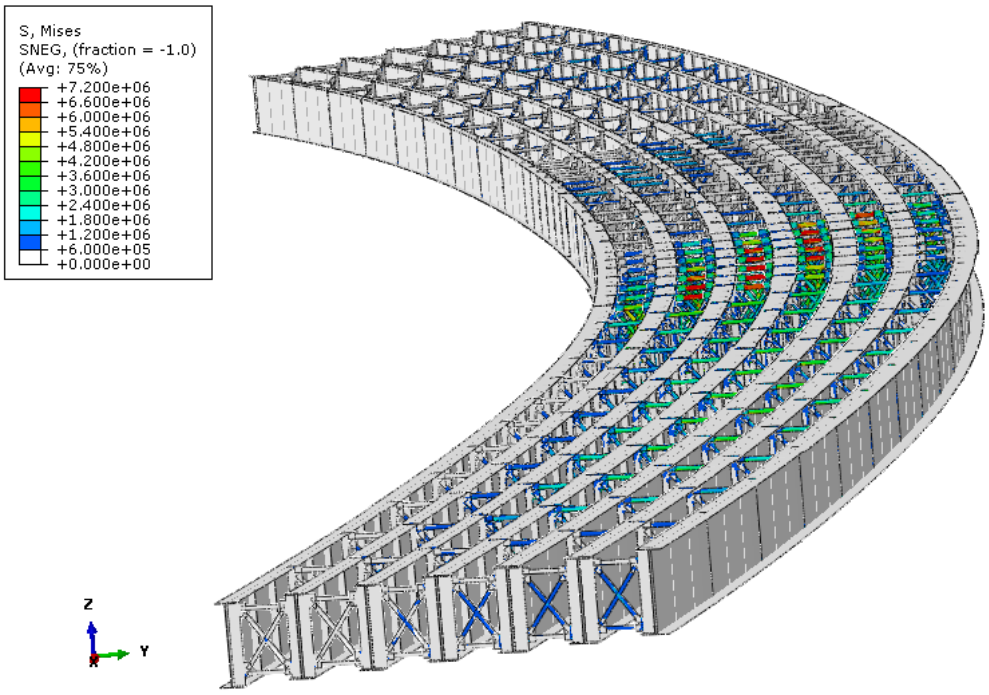

Figure 4-24. Stress distribution in the TDLF model following the application of initial stresses.

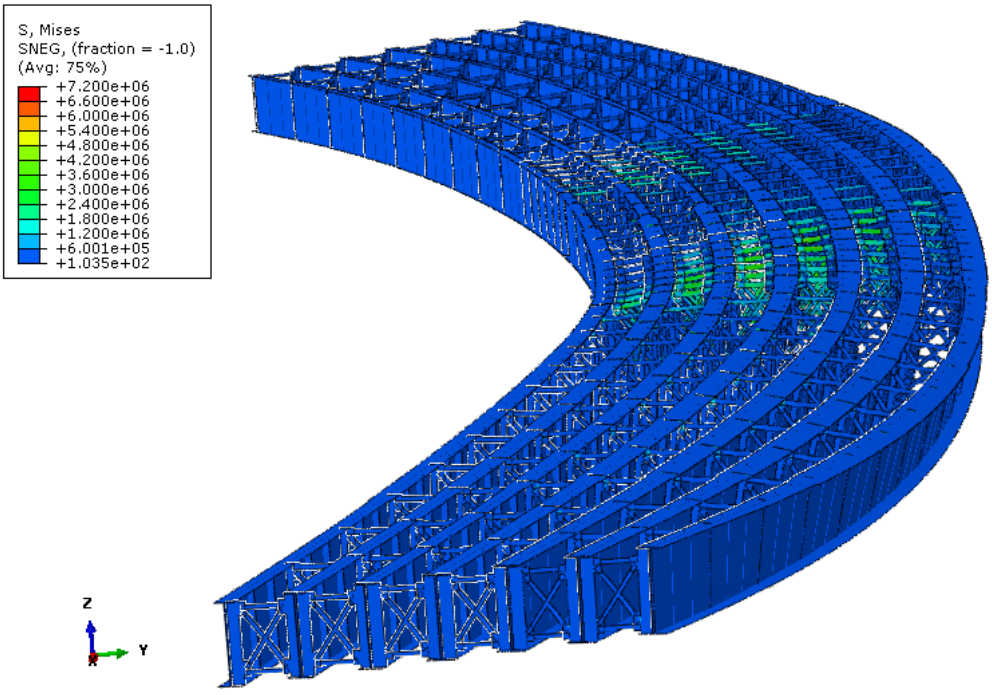

Figure 4-25. Stress distribution and deformed shape (50× magnified) of the TDLF model at its equilibrium condition after release.

4.9.6. Model SDLF

The Steel Dead Load Fit (SDLF) model also begins with the camber profile obtained from the C1 model (see Figure 3-4a). Initial stresses derived from the U2 analysis were applied to the cross-frames, reflecting the lack of fit produced when the bridge deforms under the steel dead load. This process introduces a controlled fabrication misalignment that aligns with the partially deflected geometry utilized in practice, wherein cross-frames are often erected to match the steel-only deformation profile. After the imposition of the initial stresses, the structure was released and attained an equilibrium configuration corresponding to the geometry shown in Figure 3-4c. Following this, the steel dead load (SDL) was applied, and the resulting stresses and deformations were exported for further utilization, as illustrated in Figure 3-4d. In the last phase, the total dead load (TDL) was implemented by including the concrete load onto the girders, and the corresponding stresses and deformations were exported (see Figure 3-4e).

This modeling framework enabled the study to isolate the effects of detailing-induced locked-in stresses while maintaining otherwise identical finite element characteristics. Consequently, any differences observed in cross-frame forces, girder layover, or stress distributions can be reliably ascribed to the detailed assumptions rather than to variances in geometry or material qualities. Table 4-9 presents the initial camber assignments and initial stress inputs employed in the numerical models for the NLF, SDLF, and TDLF detailing configurations.

Table 4-9. Summary of initial geometric and stress inputs for the three primary detailing models.

Model ID	Initial Camber from Model	Initial Stress form Model
NLF	C1	No Initial Stress
TDLF	C1	U1
SDLF	C1	U2

4.10. Post-Processing Analysis Procedure

To assess and contrast the efficacy of the three detailing approaches, a range of structural response parameters was derived from the numerical simulations. The metrics analyzed encompass vertical displacements of girders, girder layovers, major-axis bending stresses in the girders, lateral bending stresses in the flanges, and axial forces in the cross-frames. The quantities were evaluated for the no-load fit (NLF) scenario, as well as for the lack-of-fit consequences associated with the detailed techniques of Steel Dead Load Fit (SDLF) and Total Dead Load Fit (TDLF). More specifically, these quantities are obtained as follows:

- Vertical displacements of the girder were measured at the web-flange junction of the bottom flange nodes, indicating the total deflection response of the girders under applied loads.
- Girder layovers were assessed over the span by calculating the relative lateral (radial) displacement of the top flanges with relation to the bottom flanges, thus capturing cross-sectional rotational distortion.

- Major-axis bending stresses were assessed at the upper and lower flanges by obtaining stress values at the outer curvature of the flange tips, which correspond to the extreme fibers of the curved beam sections.
- Flange lateral bending stresses were ascertained from the stress differential between the flange tip and the neighboring web-flange junction, elucidating the out-of-plane flange bending effects.
- Cross-frame forces were derived from the axial stresses and associated axial forces in the top chords and bottom chords of the cross-frames.

This systematic post-processing paradigm offers a uniform foundation for evaluating bridge responses across various detailing methods and highlights the impact of dead load fit practices on both global and local structural behavior. The detailed results and analysis of the above quantities are shown in Chapter 5.

A local coordinate system was set up for each girder to accurately measure the bending stresses along the main axis and on the sides. This local system corresponds with the girder's shape, facilitating accurate extraction of stress components along the primary axes of the section while considering curvature and cross-sectional orientation. Figure 4-26 shows the local girder coordinate system aligned with the girder centerline (1-axis), along with the corresponding global coordinate system axes used for stress and force evaluation.

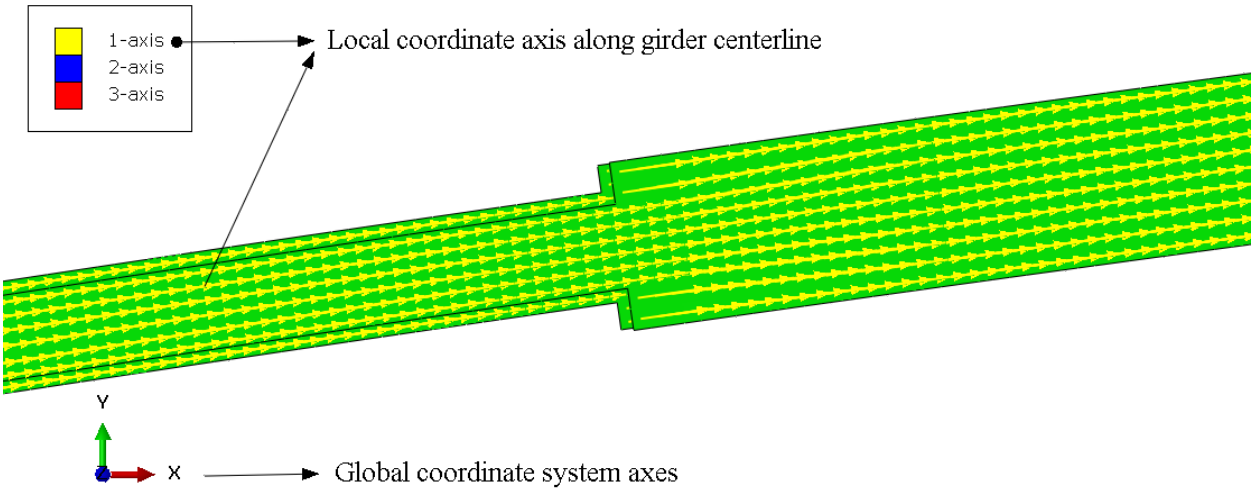

Figure 4-26. Local girder coordinate system aligned with the girder centerline and its relation to the global coordinate system axes.

CHAPTER 5: NUMERICAL RESULTS AND COMPARATIVE ANALYSIS OF DETAILING METHODS

5.1. Overview

AASHTO (2010) [23] emphasizes that engineers should account for potential locked-in stress effects resulting from detailing methods in horizontally curved I-girder bridges, irrespective of the presence of skewed supports; nevertheless, such effects are seldom integrated into current design practices. Engineers typically presume that girders can be positioned by cross-frames without explicitly accounting for the inherent lack of fit in their structural assessments. Although this simplification is convenient, it may fail to account for critical stress interactions. In some circumstances, the locked-in forces produced during construction may substantially affect girder layovers, vertical displacements, cross-frame forces, and both major-axis and flange lateral bending stresses. This chapter assesses the impact of locked-in forces resulting from cross-frame detailing on component-level behavior and the overall response of the bridge system. Comprehensive nonlinear finite element analysis is performed to evaluate various cross-frame detailing methods during construction. Section 5.2 presents the camber diagrams and vertical displacements of the girders. Section 5.3 demonstrates the cross-frame forces at the beginning and end of the analysis. Section 5.4 illustrates the girder layovers for various detailing. Section 5.5 investigates the major-axis and lateral bending stresses of the girders.

5.2. Camber and Vertical Displacements

In both straight and skewed bridges, the locked-in forces generated by SDLF and TDLF are typically small and exert an insignificant effect on the vertical displacements of the girders. This is mainly due to the limited interaction between individual girder twists and their vertical displacements in straight I-girder systems. Moreover, the girders exhibit considerable rigidity against major axis bending rotations due to the lack-of-fit related to SDLF and TDLF detailing methods, leading to only negligible extra vertical deformations.

The fluctuation in vertical displacements resulting from different detailing is minimal for both continuous straight and skewed bridges. This reduction is ascribed to the continuity effects throughout the spans and the use of continuous cross-frames, which mitigate the oscillatory flange movements and subsequently result in diminished locked-in vertical displacements.

Conversely, in horizontally curved bridges, the locked-in forces produced by SDLF and TDLF detailing methods can significantly affect girder vertical displacements. This phenomenon arises due to the significant interaction between major-axis bending and torsional behavior in curved I-girders. Consequently, these bridges may exhibit vertical deflection patterns that diverge from those anticipated during camber design, which is generally predicated on the No-Load Fit (NLF) condition. These discrepancies may result in deviations in the bridge cross-slope from the planned profile, potentially causing either underestimating or overestimating of the final deck elevations.

Based on section 4.10, vertical displacements of the girder were recorded at the web-flange junction of the bottom flange nodes, reflecting the overall deflection response of the girders under

applied loads. The locations of the bearings are shown in Figure 4-8 and they are depicted in the following figures using dashed gray lines.

Figures 5-1 and 5-*2* illustrate a comparison of the camber diagrams derived from the finite element model (FEM) with those from the design drawings for Girders A and G under conditions of steel, concrete, and total dead loads (refer to Figure 5-5). The FEM serves as the numerical reference model for the Corridor X–I65 bridge utilized in this study before imposing any locked-in stresses or deformations. The close match between the FEM-predicted cambers and the design cambers validates the precise modeling of continuous girder behavior and boundary conditions. Camber diagrams were produced by obtaining the vertical displacements of nodes situated at the junction of the girder web and bottom flange under reversed steel, concrete, and total dead load conditions.

A small mismatch was noted between the FEM results and the design cambers, mostly attributable to the differences in modeling methodology. This research developed a geometrically and materially nonlinear finite element model with 1,215,691 shell elements, ensuring great accuracy and dependability. The most significant discrepancy is observed in Girder A with a maximum variation of 1.7 inches under the total dead load. The discrepancies among the remaining girders are rather small.

The flanges of the girders were designed to reduce the differential displacement between girders caused by the curvature of the Corridor X bridge. The flanges of the outer girders are stronger than those of the inner girders. For example, at the midpoint between Bents 8 and 9, the bottom flange in Girder A is 42 in. wide and 3.75 in. thick (see Figure 4-3), while the bottom flange in Girder G at the same location is 36 in. wide and 2.75 in. thick. Yet, a differential deflection of approximately 17.07 in. still occurs at this location under the total dead load in the NLF model, as shown in Figure 5-4.

Figures 5-3 and 5-4 illustrate the vertical deflections of Girders A, D, and G under steel and total dead loads, respectively, for the different detailing methods. Deflection diagrams under dead load conditions were generated using the vertical displacements of nodes located at the intersection of the girder web and bottom flange. The deflections of Girder D, situated at the bridge's centerline, are nearly uniform across all detailing methods (NLF, SDLF, and TDLF). Nevertheless, Girders A and G demonstrate minor discrepancies in deflection under both steel and total dead load circumstances across the various detailing approaches. The most significant divergence is observed in Girder A, exhibiting a discrepancy of around 1.4 inches under the total dead load.

5.3. Cross-Frame Forces

Cross-frame members are recognized as the critical bracing elements for the stability of straight and curved steel bridges, and their internal forces are utilized for comparative assessment among the three design techniques. Cross-frames are essential in horizontally curved steel I-girder bridges, as they provide torsional rigidity and facilitate load distribution across neighboring girders. As previously mentioned, the initial stresses generated by SDLF and TDLF detailing methods can either increase or decrease the locked-in stresses in cross-frames, depending upon the detailed methodology and bridge design. According to the section 4.10, cross-frame forces were obtained from the axial stresses and corresponding axial forces in the upper and lower chords of the cross-frames. The initial forces in the TDLF and SDLF models were derived from their initial stresses, which were in turn obtained from Models U1 and U2 in Section 4.9.

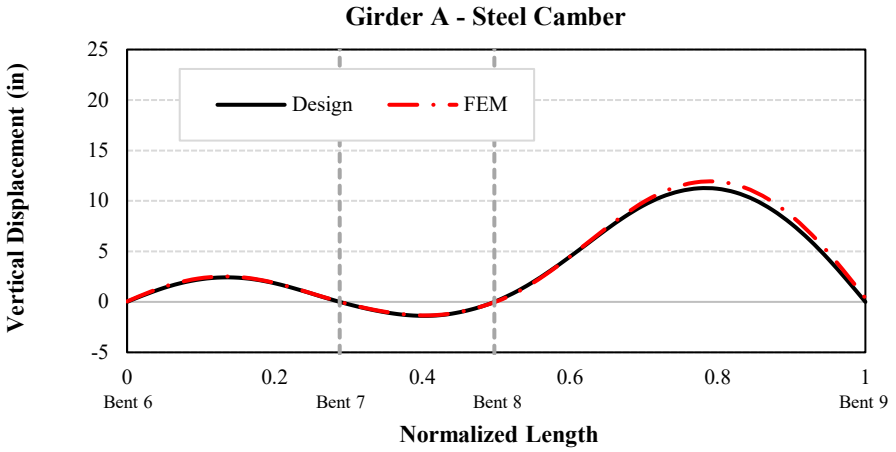

(a)

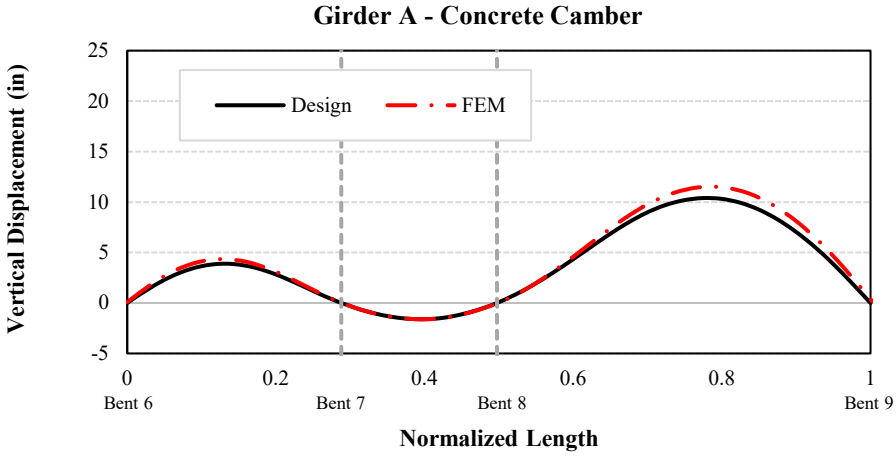

(b)

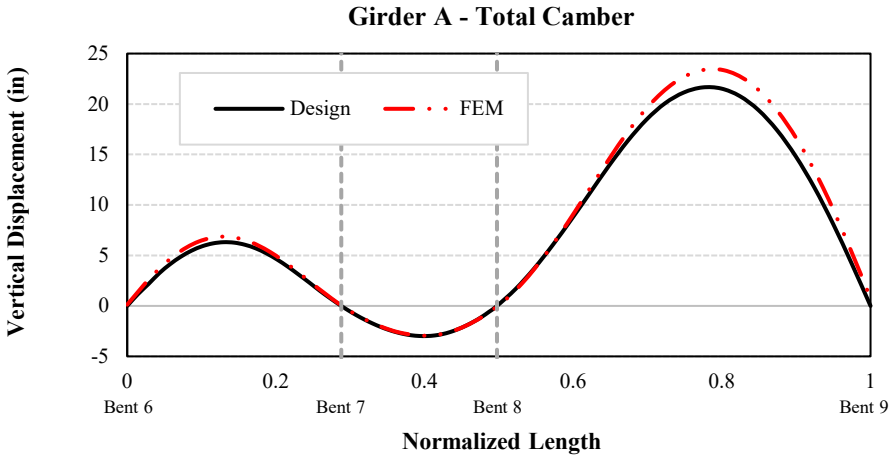

(c)

Figure 5-1. Comparison of (a) steel dead load, (b) concrete dead load, and (c) total dead load camber profiles from the FEM and the design drawings for Girder A.

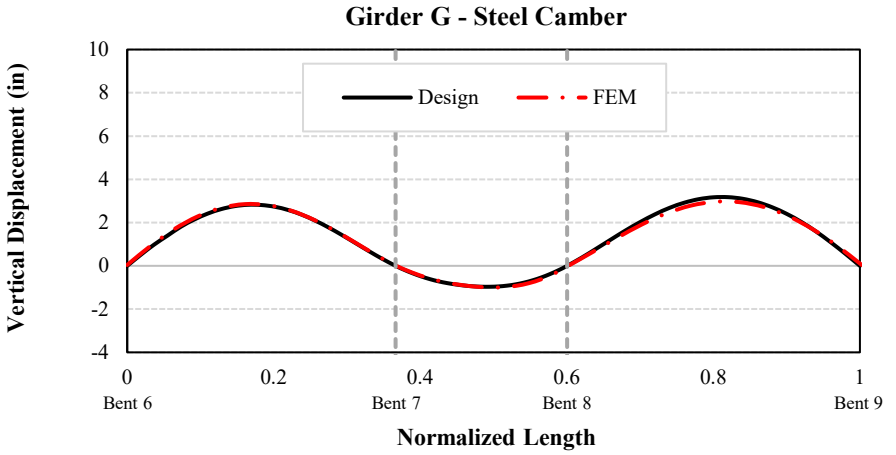

(a)

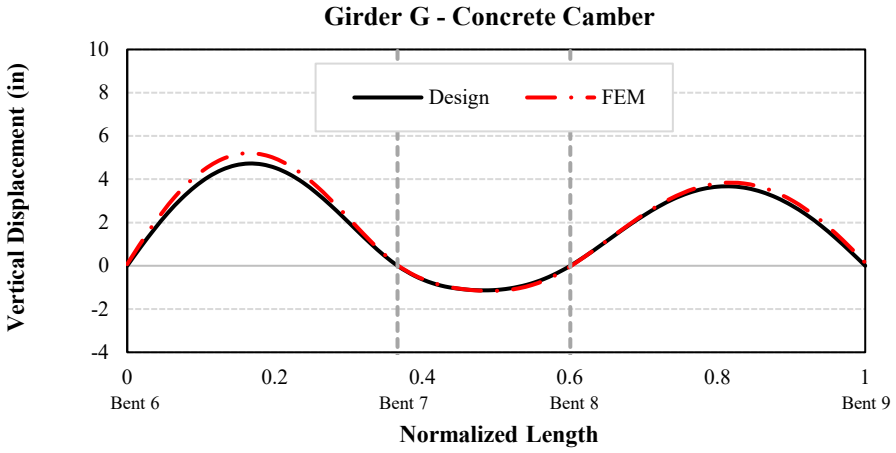

(b)

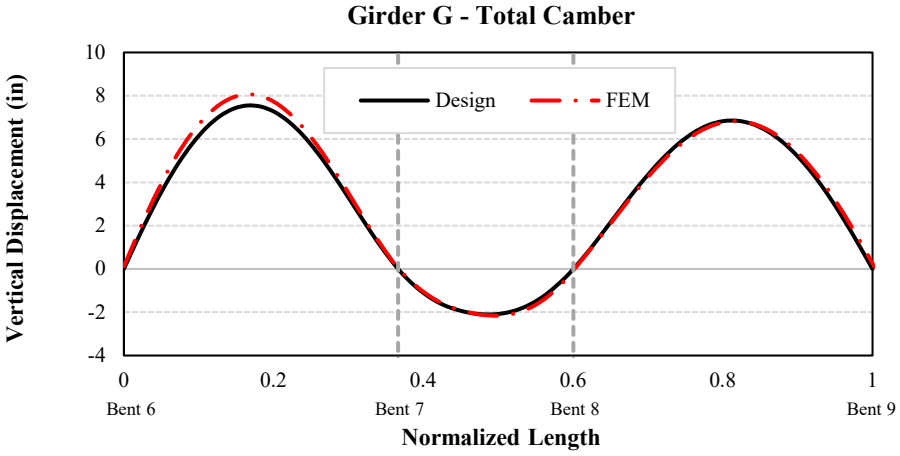

(c)

Figure 5-2. Comparison of (a) steel dead load, (b) concrete dead load, and (c) total dead load camber profiles from the FEM and the design drawings for Girder G.

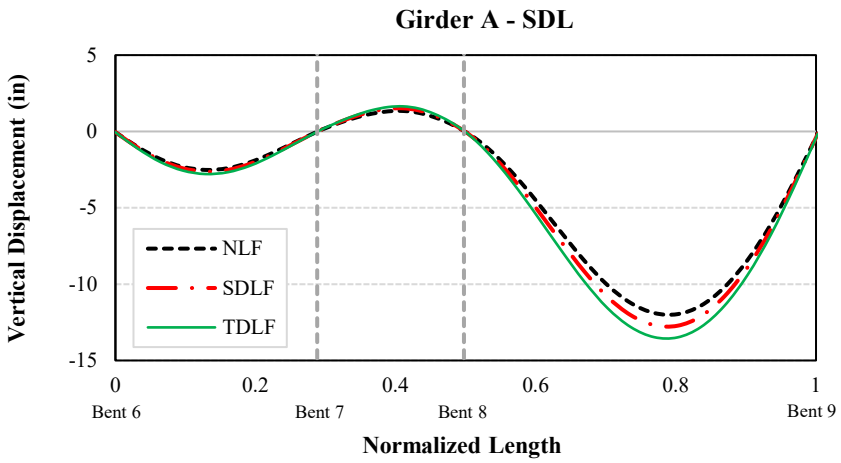

(a)

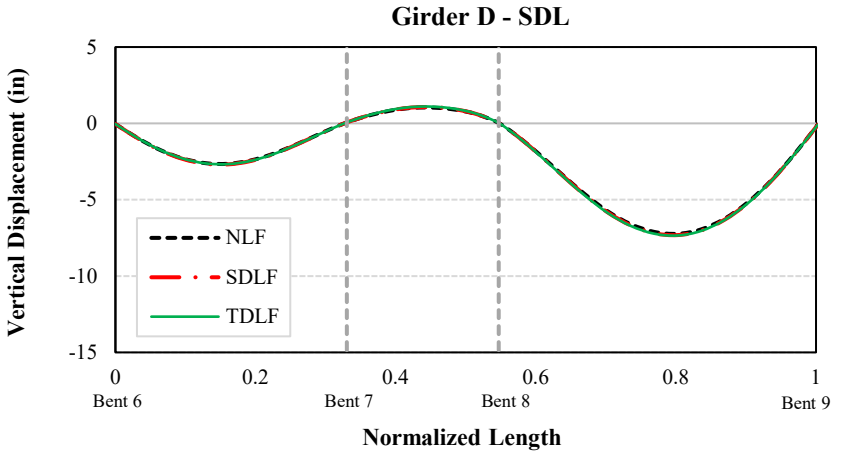

(b)

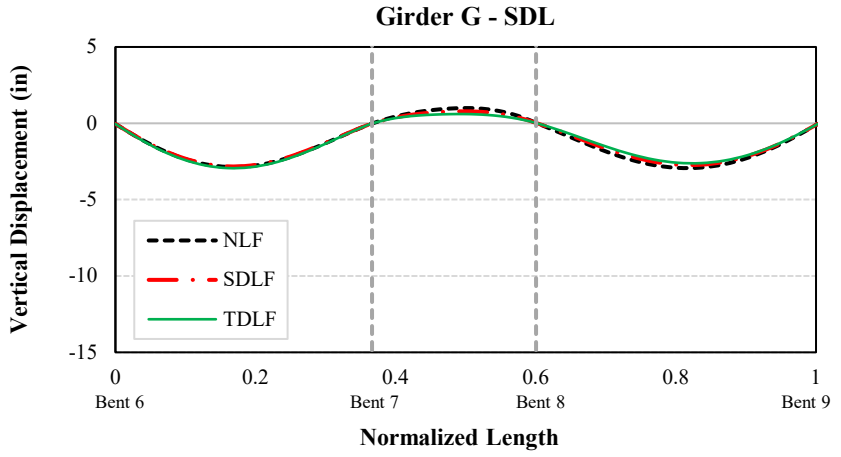

(c)

Figure 5-3. Deflection diagrams of Girders A, D, and G under steel dead load for various detailing methods.

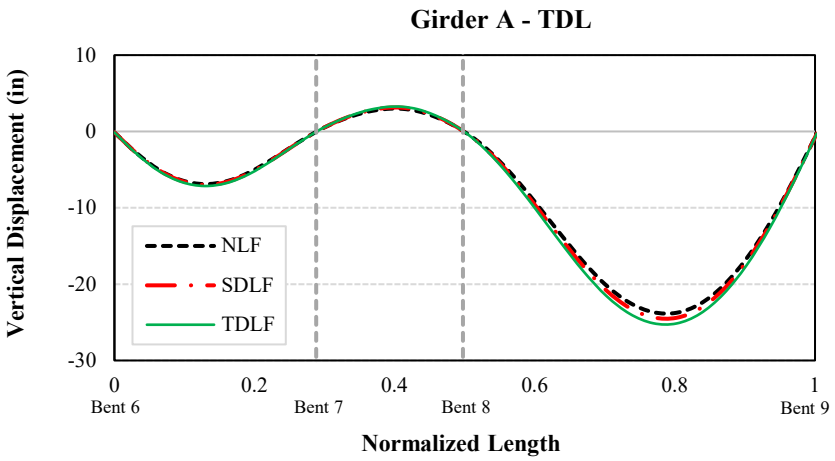

(a)

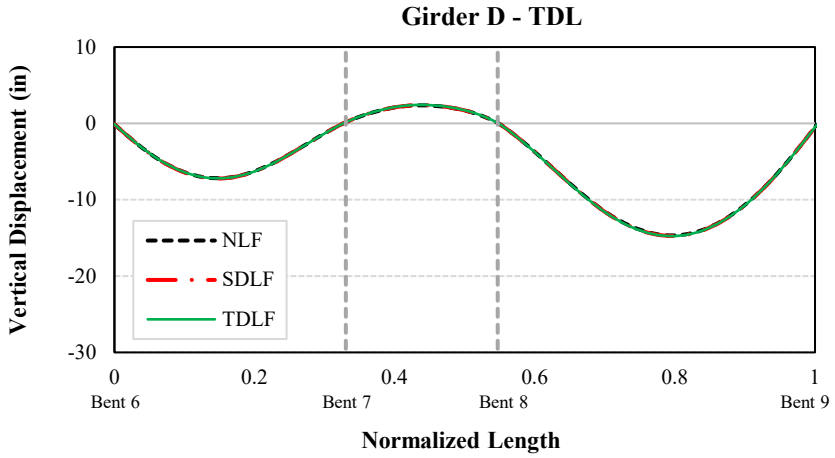

(b)

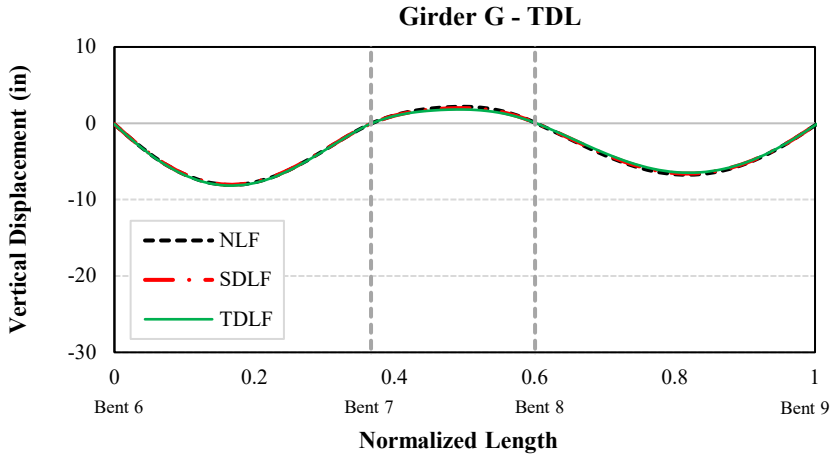

(c)

Figure 5-4. Deflection diagrams of Girders A, D, and G under total dead load for various detailing methods.

To evaluate this influence, three lines of cross-frames, totaling 36 cross-frames, were chosen throughout the bridge's length. Each line comprised 12 cross-frames, with their positions and identification numbers illustrated in Figure 5-5. Each cross-frame is identified by the expression XY–N, where X and Y denote the interconnected girders and N indicates the sequential position (1–12) along the span. AB–2 denotes cross-frame 2 positioned between Girders A and B.

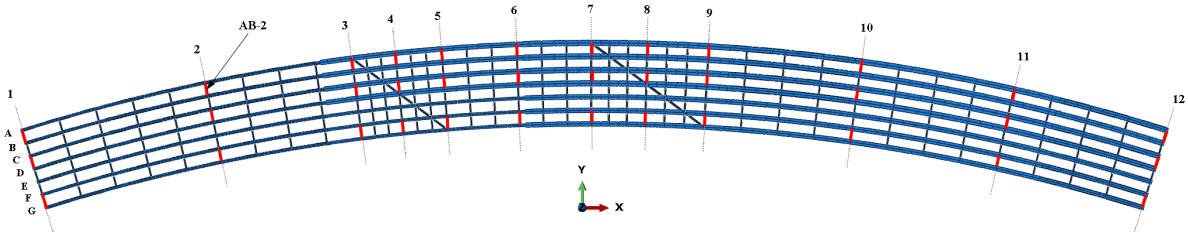

Figure 5-5. Cross-frame arrangement and identification scheme.

to Figure 5-11 present the cross-frame initial and locked-in forces obtained from different detailing techniques under various loading conditions. For each set, the first diagram depicts the initial forces, the second illustrates the locked-in forces under the steel dead load (SDL) condition, and the third exhibits the locked-in forces under the total dead load (TDL) condition.

The findings indicate that the TDLF method markedly decreases cross-frame locked-in forces under the final total dead load condition, particularly in components experiencing substantial locked-in force in NLF model near skewed Bent 8. Among the cross-frame components, the upper and lower chords exhibited considerably higher stress levels than the diagonals; therefore, they were selected for comparison. It should be noted that the initial forces in the NLF model are zero.

Figures 5-6 and 5-7 show the top and bottom chord forces of the cross-frames along line AB. The critical cross-frame is AB–7, which endures the highest forces in the NLF model. Under the steel dead load, the SDLF approach decreased the top and bottom chord forces by 42.1% and 48.9%, respectively, whereas the TDLF method achieved reductions of 89.7% and 93.4%. The total dead load reductions for the SDLF method were 23% and 23.7% for the top and bottom chord, respectively, and for the TDLF method were 48.1% and 50.7%. There is an exception in AB-3, where the TDLF approach slightly increased the forces under the steel dead load by 10.4 kips (top chord) and 15.2 kips (bottom chord).

Figures 5-8 and 5-9 show the corresponding results for line CD. The most critical cross-frame, CD–8, carries a force of 299.7 kips in the NLF model under the total dead load. Under the steel dead load, the SDLF method reduced the forces in this cross-frame by 45.2% and 43.8% in the top and bottom chords, respectively, whereas the TDLF method achieved reductions of 82.2% and 77.1%. Under the total dead load, the SDLF approach reduced forces by 19.2% for the top chord and 18.69% for the bottom chord, whereas the TDLF method attained reductions of 40.3% and 37.7%, respectively. This cross-frame exhibits the largest reduction in force among all examined cases, with decreases of 136.0 kips and 114.7 kips under the steel and total dead loads, respectively.

Figures 5-10 and 5-11 illustrate the locked-in forces on the top and bottom chords of the cross-frames along line FG. The critical cross-frame on this line, FG–9, bears the highest amount of

forces in the NLF model under the total dead load. The SDLF approach decreased the forces by 54% and 37.4% in the top and bottom chords, respectively, under the steel dead load, whereas the TDLF method accomplished reductions of 92.5% and 58%. The SDLF approach decreased forces by 26% for the top chord and 6.8% for the bottom chord under the total dead load, while the TDLF method achieved reductions of 51.5% and 19.4%, respectively. A local exception occurs at FG–5, where the TDLF method slightly increased the top and bottom chord forces by 7.2 kips and 15.7 kips, respectively, under the steel dead load.

Significant decreases in cross-frame forces are observed adjacent to the skewed supports, particularly near Bent 8, where these forces are the largest. In other words, the greater the locked-in cross-frame forces in the NLF model, the greater the reductions achieved when SDLF or TDLF methods are applied. Conversely, cross-frames positioned along the radial supports demonstrate little internal force, exhibiting no differences across the different detailing approaches. Similarly, cross-frames 2, 10, and 11, located far from the skewed bents, show minimal sensitivity to the detailing approach. Despite the common engineering assumption that cross-frames experience no force at their final location under the total dead load when utilizing the TDLF detailing approach, cross-frames may nonetheless endure considerable stress in practice.

Initial forces refer to the forces required during the construction phase to properly align and link the structural components, particularly the cross-frames, prior to the bridge attaining its self-equilibrium state. These forces arise due to the geometric constraints, fabrication tolerances, and pre-existing camber conditions before load application. In essence, they represent the effort required to "fit" the cross-frames across girders and guarantee that the structure is completely integrated in the designated configuration. Once the bridge is assembled and released under no-load conditions, these initial forces no longer act externally but remain as locked-in forces within the cross-frames, affecting the long-term locked-in force state of the system.

The TDLF approach, while the most successful in mitigating locked-in cross-frame stresses under both SDL and TDL, requires significantly greater initial forces to make proper connections. The peak initial forces in AB–7 cross-frame are 66.9 kips in the top chord and 60.6 kips in the bottom chord for the SDLF model, and for the TDLF model are 135.7 kips and 123 kips (see Figures 5-6a and 5-7a). For CD–8, the peak initial forces for SDLF model are 150.8 kips in the top chord and 153.4 kips in the bottom chord, respectively, while the corresponding forces in the TDLF model are 276.6 kips in the top chord and 268.0 kips in the bottom chord based on Figures 5-8a and 5-9a. Similarly according to Figures 5-10a and 5-11a, for FG–9, the values are 42.6 kips in the upper chord and 46.2 kips in the lower chord for the SDLF model, and 75.9 kips in the upper chord and 75.6 kips in the lower chord for the TDLF model.

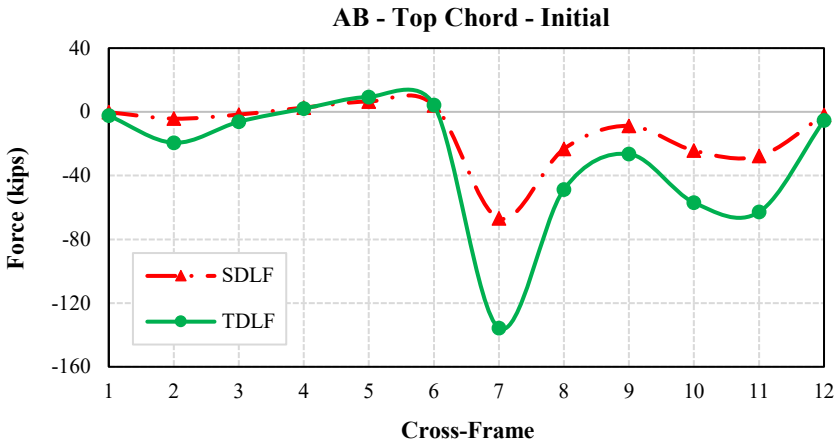

(a)

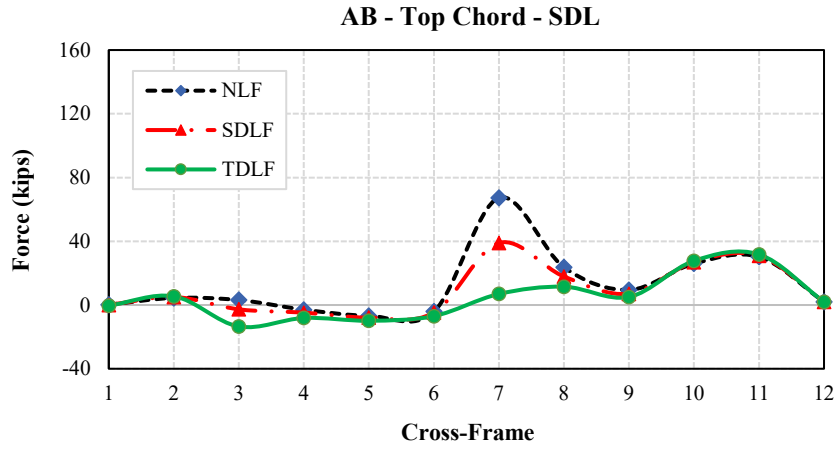

(b)

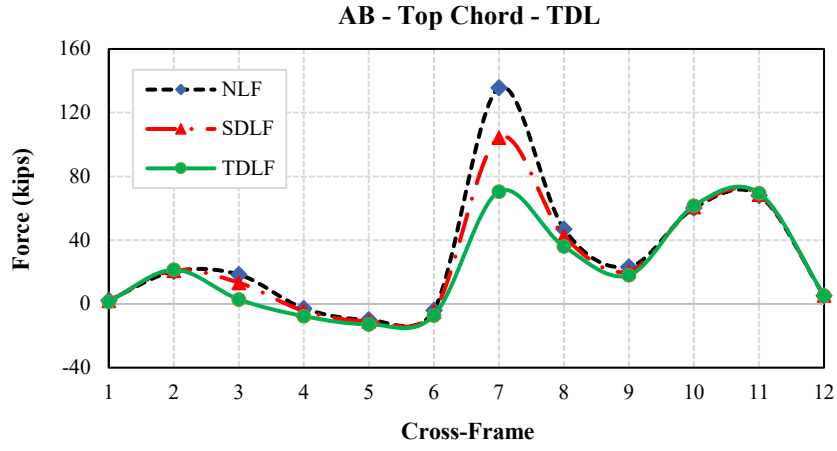

(c)

Figure 5-6. Comparison of top-chord cross-frame forces between Girders A and B under (a) initial force, (b) steel dead load, and (c) total dead load for different detailing methods.

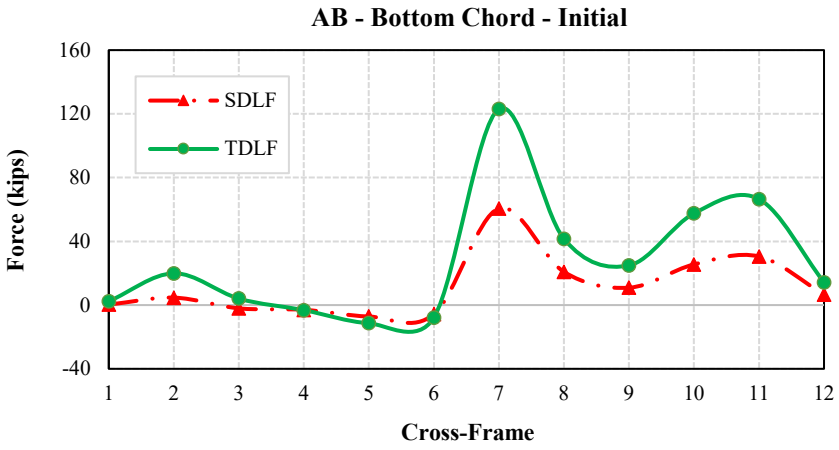

(a)

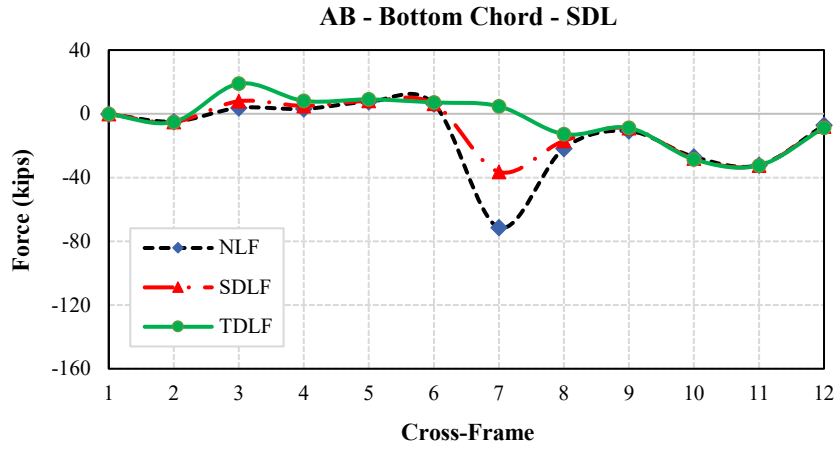

(b)

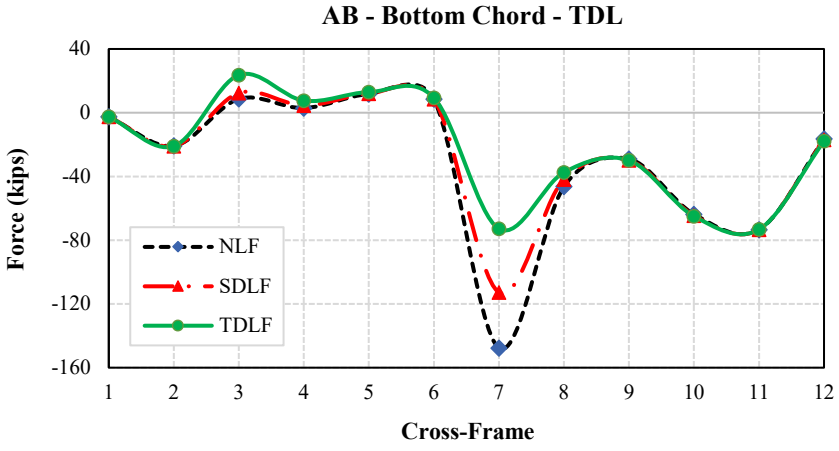

(c)

Figure 5-7. Comparison of bottom-chord cross-frame forces between Girders A and B under (a) initial force, (b) steel dead load, and (c) total dead load for different detailing methods.

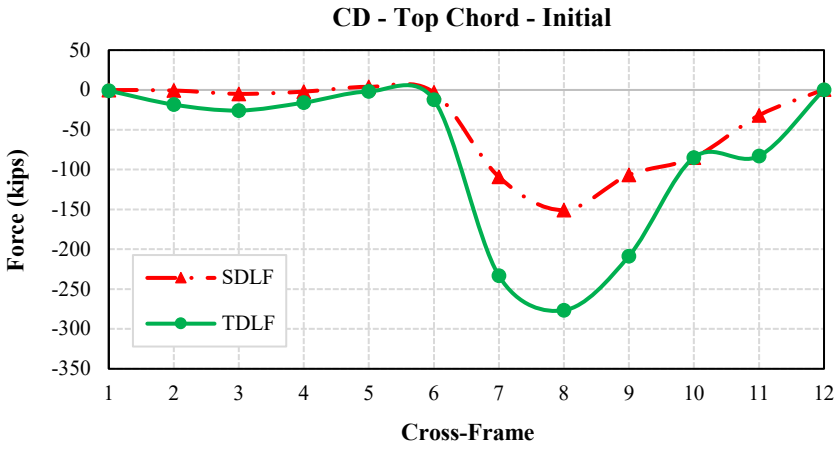

(a)

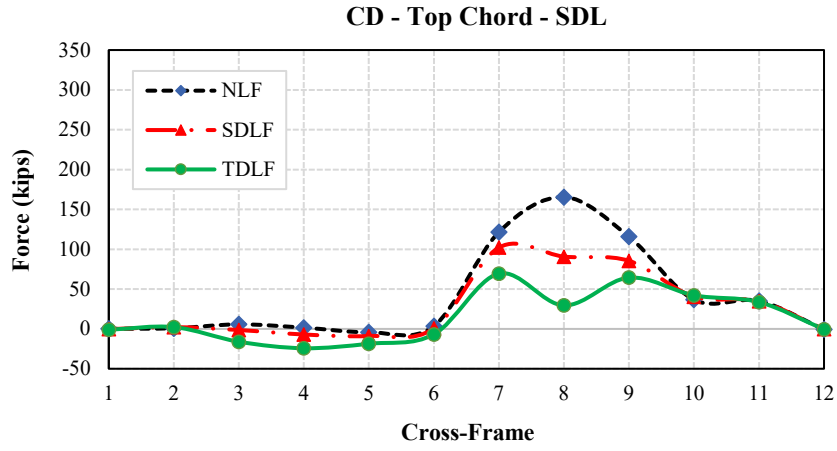

(b)

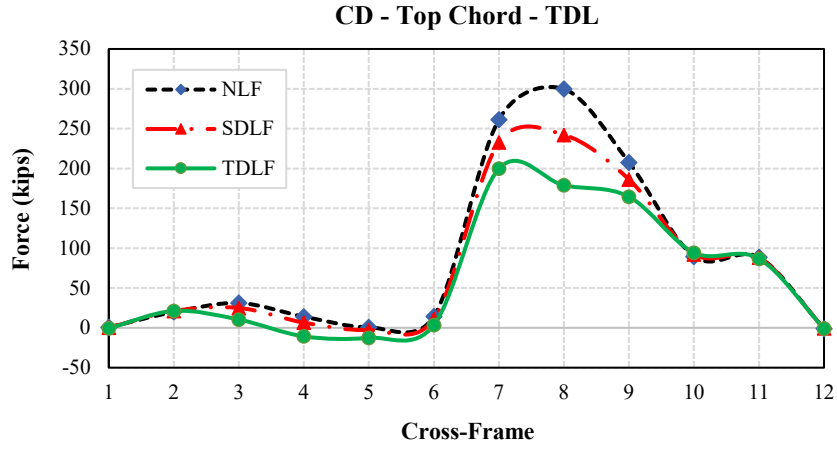

(c)

Figure 5-8. Comparison of top-chord cross-frame forces between girders C and D under (a) initial force, (b) steel dead load, and (c) total dead load for different detailing methods.

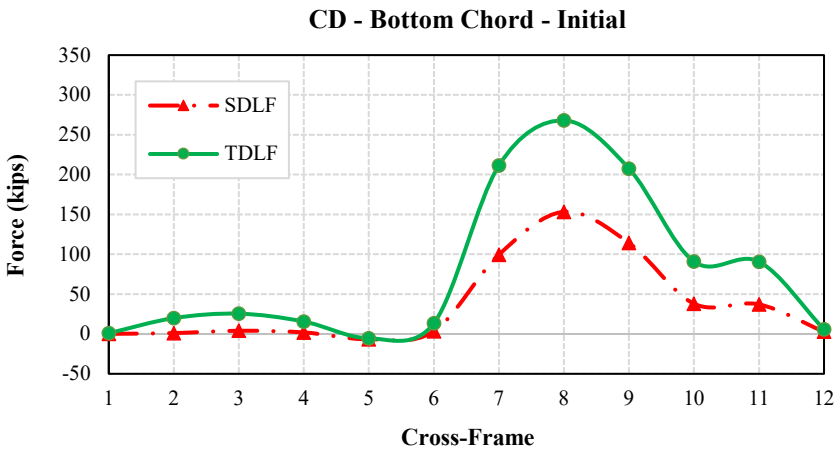

(a)

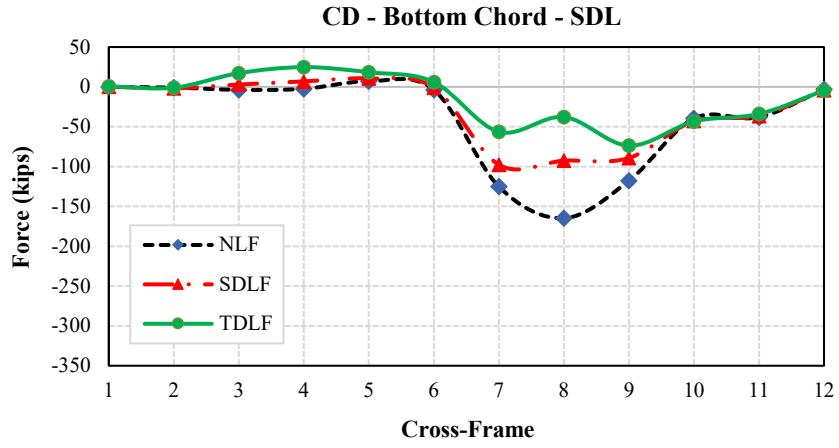

(b)

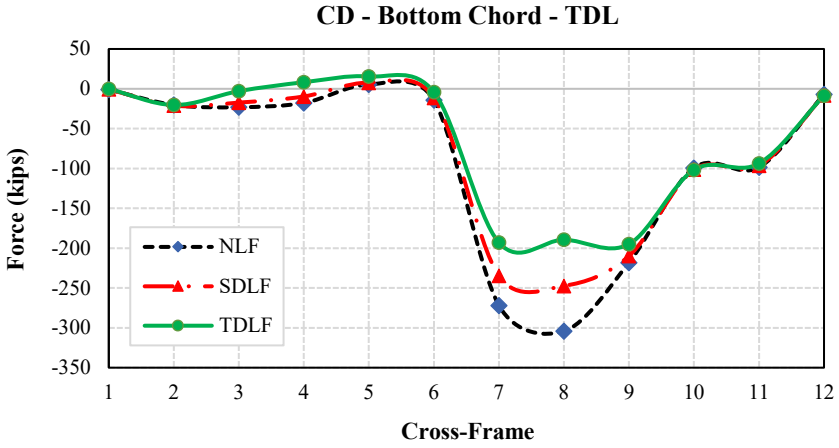

(c)

Figure 5-9. Comparison of bottom-chord cross-frame forces between Girders C and D under (a) initial force, (b) steel dead load, and (c) total dead load for different detailing methods.

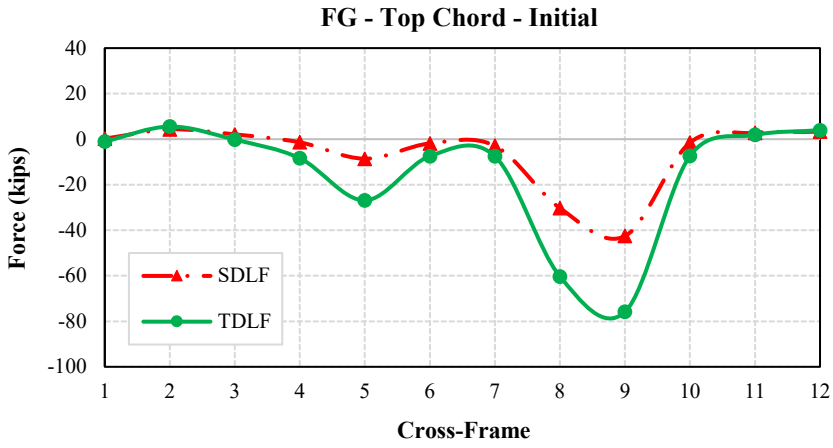

(a)

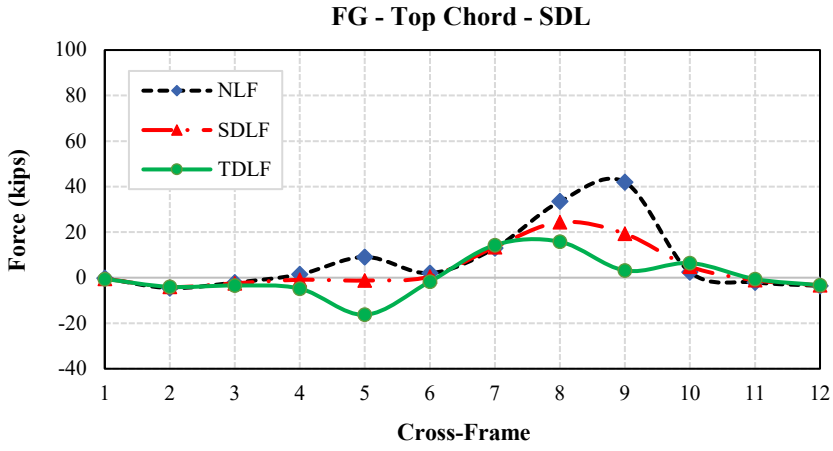

(b)

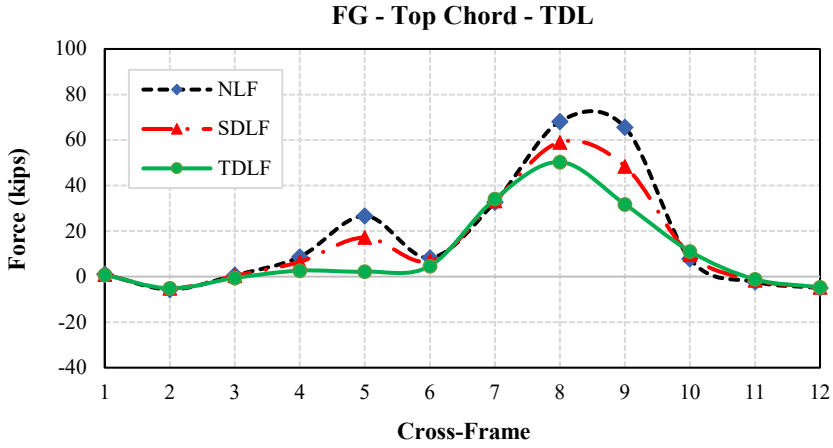

(c)

Figure 5-10. Comparison of top-chord cross-frame forces between Girders F and G under (a) initial force, (b) steel dead load, and (c) total dead load for different detailing methods.

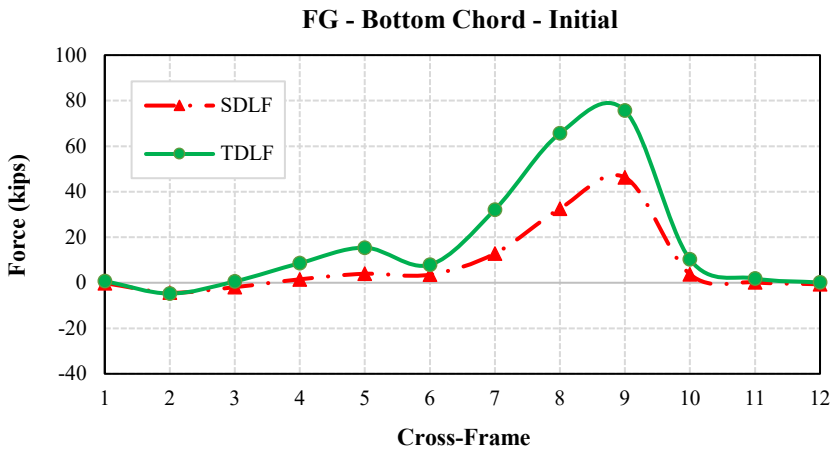

(a)

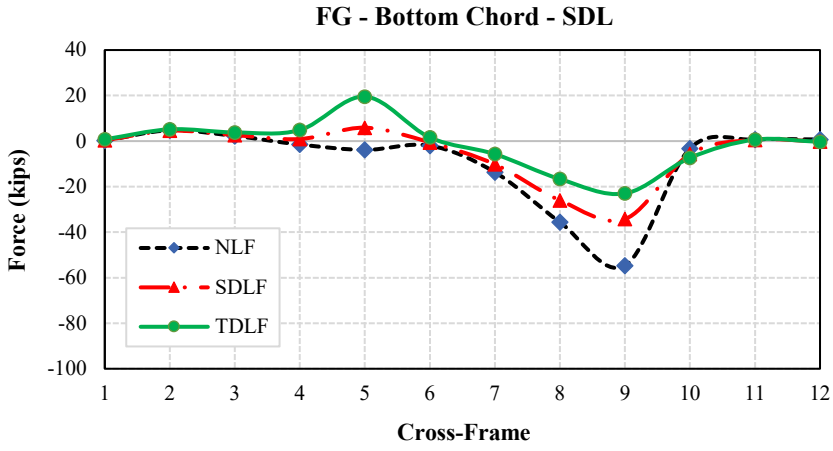

(b)

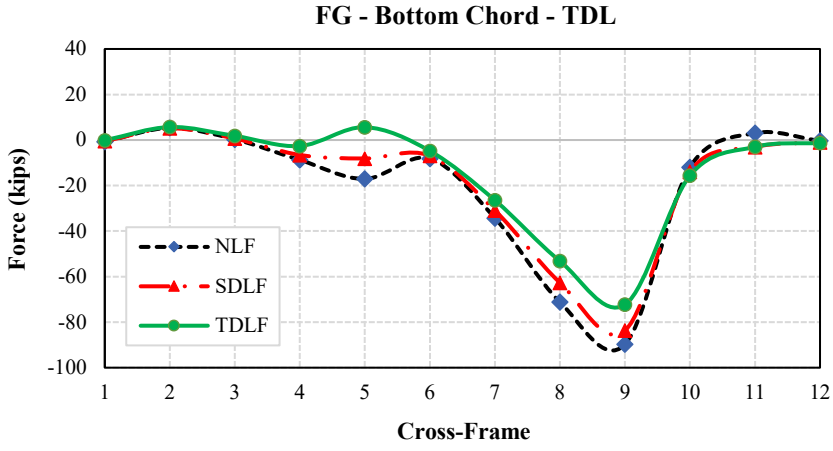

(c)

Figure 5-11. Comparison of bottom-chord cross-frame forces between Girders F and G under (a) initial force, (b) steel dead load, and (c) total dead load for different detailing methods.

5.4. Girder Layovers

In straight and skewed bridges, end layovers primarily result from the interaction between major axis bending rotations of the girder and torsional rotations at skewed bearing lines. Conversely, curved bridges with radial supports demonstrate a correlation between major axis bending deflections and torsional rotations resulting from curvature.

In curved bridges with skewed supports, torsional-bending coupling due to curvature occurs simultaneously with skew-induced rotations at the bearings. In continuous-span bridges, an extra interaction arises between spans. For instance, layovers formed in one span due to curvature may propagate onto adjacent spans through continuity effects, leading to secondary displacements even in straight spans. Likewise, barrier loads positioned along the fascia girders generally augment the outward layover of exterior girders while diminishing the inward layover of interior girders.

Cross-frames exhibit greater stiffness in their planes relative to the torsional stiffness of I-girders. This rigidity frequently results in the presumption that girders may be shifted into alignment with cross-frames, irrespective of any misalignment. This assumption is not always applicable. Twisting in curved girders is intricately linked to vertical deflections and major-axis bending rotations, complicating the forced fit and possibly increasing stress concentrations.

The primary aim of SDLF and TDLF detailing methods is to guarantee that girder webs attain vertical alignment under the specified dead load situation. This is achieved by utilizing the rigidity of cross-frames to counteract the torsional rotations caused by dead load effects. Steel Dead Load Fit (SDLF) approach involves detailing cross-frames to mitigate the rotations induced by the steel self-weight, hence maintaining the girder webs in a nearly vertical position under the steel dead load. The Total Dead Load Fit (TDLF) method considers the deflections resulting from the total dead load, encompassing both steel and concrete, by incorporating a computed lack-of-fit. When the girders are solely supported by their own weight, they incline in the contrary direction of the ultimate rotation. Upon the addition of the total dead load, they revert to a nearly vertical orientation. However, the compensatory layovers generated by SDLF or TDLF detailing do not entirely offset the real layovers induced by the dead loads. The mismatch principally stems from the fact that the torsional stress state caused by distributed dead loads cannot be entirely replicated by the discrete internal forces conveyed by the cross-frames in SDLF and TDLF detailing methods.

The difference between the stress state caused by lack-of-fit forces and that generated by dead load torsion results in secondary deformations inside the system. The camber profiles allocated to the girders frequently rely on oversimplified assumptions that may fail to effectively represent the three-dimensional interactions between the girders. These approximations tend to exacerbate the disparities between the stress state induced by dead load torsion and that produced by cross-frame misalignment. Under the designated dead load conditions, such effects generally lead to slight deviations from the theoretical vertical alignment. In complex bridge configurations (such as the ICCS bridge analyzed in this study) SDLF and TDLF detailing methods not only did not diminish layover but, in certain instances, marginally augmented it, particularly in the Outer Fascia Girder A; however, the magnitude of this increase was not significant. Based on section 3.6, the girder

layovers were evaluated by measuring the relative lateral (radial) displacement of the top flanges in reference to the bottom flanges, thereby quantifying cross-sectional rotational distortion.

Based on Section 2.5, the Corridor X—I-65 Bridge is an ICCS-type structure (continuous-span, curved, with skewed supports) consisting of three spans and four bents, with all bearings modeled as rotational. The locations of the bearings are shown in the following figures using dashed gray lines. Results indicate that the layovers at Bents 6 and 9 are approximately zero; however, nonzero layovers occur at Bents 7 and 8, with the three detailing methods producing very similar values. According to Figures 5-12 and 5-13, under the steel dead load (SDL), the layovers of Girders A, D, and G at Bent 7 are -0.28, -0.26, and -0.24 in., respectively, while at Bent 8 they are 0.39, 0.51, and 0.58 in. Furthermore, under the total dead load (TDL), the layovers of Girders A, D, and G at Bent 7 are -0.70, -0.63, and -0.59 in., respectively, and at Bent 8 they are 0.84, 1.00, and 1.17 in.

The maximum layover occurs at the midpoint of span 3, between Bents 8 and 9, across all girders under total dead load. Girder A exhibited the largest layover, measuring 1.96, 2.34, and 2.76 in. for the NLF, SDLF, and TDLF techniques, respectively, under the steel dead load, and 3.81, 4.16, and 4.58 in. under the total dead load. This location also shows the greatest differences in layovers among the three detailing methods. In contrast, the corresponding differences in other girders (e.g., Girders D and G) are not significant.

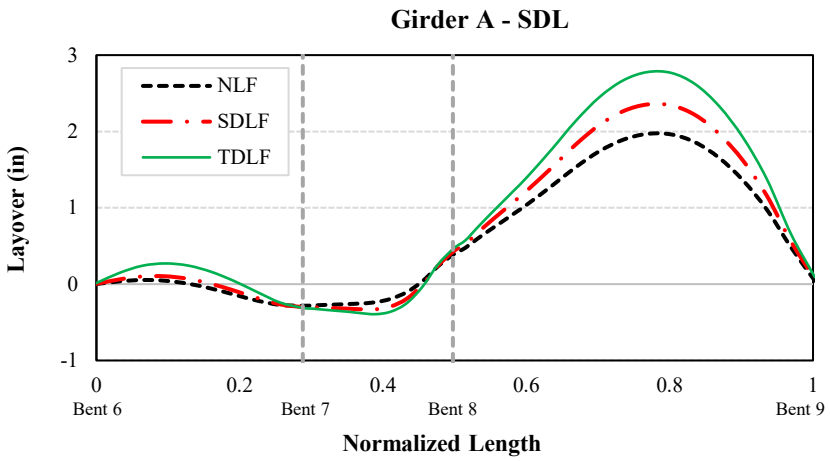

(a)

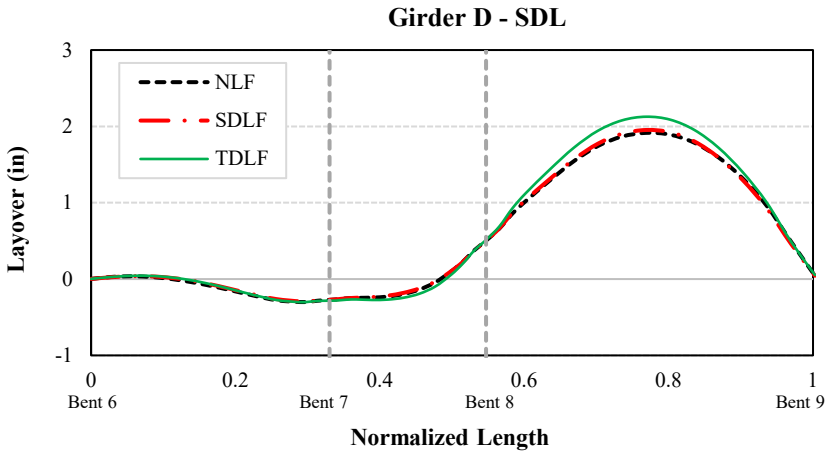

(b)

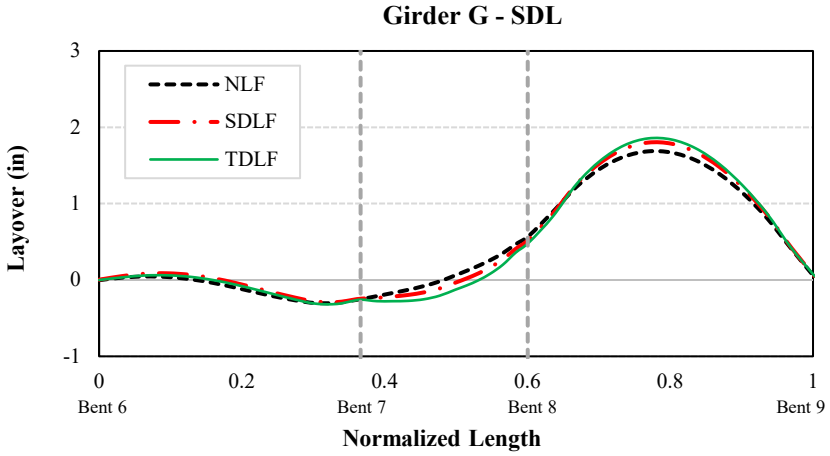

(c)

Figure 5-12. Comparison of girder layover diagrams for Girders A, D, and G under steel dead load conditions.

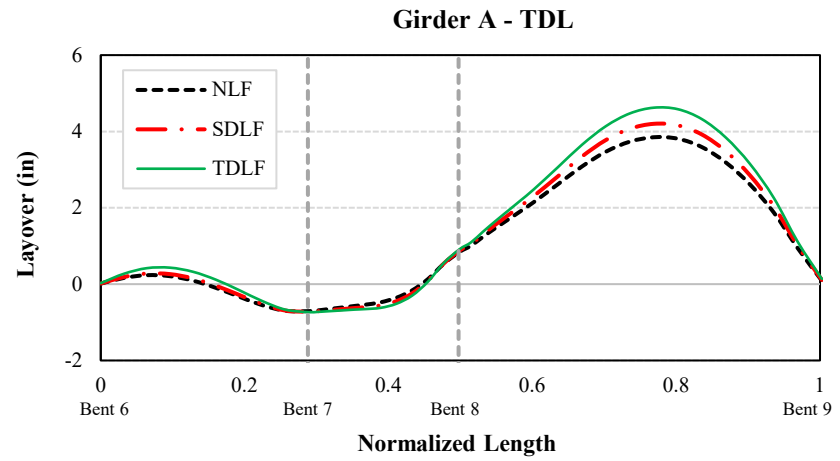

(a)

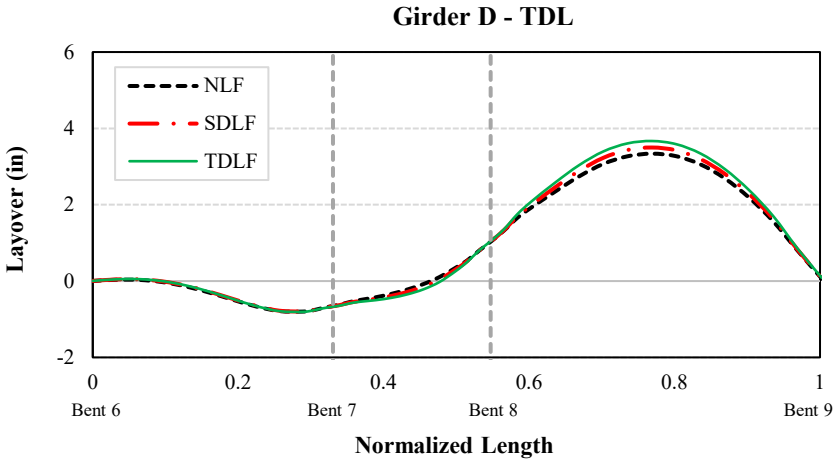

(b)

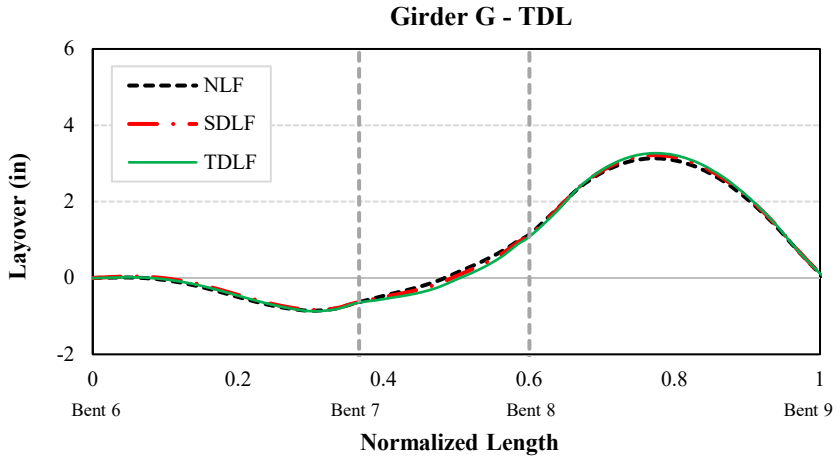

(c)

Figure 5-13. Comparison of girder layover diagrams for girders A, D, and G under total dead load conditions.

5.5. Girder Stresses

Figures 5-14 to 5-17 illustrate the major-axis bending stresses in the upper and lower flanges of Girders A and G under the steel dead load (SDL) and total dead load (TDL) scenarios. Under the steel dead load, the stresses are approximately half of those observed under the total dead load. The peak major-axis bending stress in Girder A is observed near Bent No. 8, attaining 26.14 ksi under the total dead load condition. The locations of the bearings are shown in the following figures using dashed gray lines.

The various detailing procedures yield minimal differences in the major-axis bending stresses of the girders. According to section 4.10, major-axis bending stresses were evaluated at the top and bottom flanges by measuring stress levels at the outside curvature of the flange tips, corresponding to the extreme fibers of the curved beam sections. Furthermore, the lateral bending stresses of the flange were determined by analyzing the stress difference between the flange tip and the web-flange junction, clarifying the out-of-plane bending effects of the flange.

The variations in flange lateral bending stresses across the different detailing procedures are negligible. At the obtuse corners, relatively large lateral forces are transmitted into the fascia girders through the chords of the first two intermediate cross-frames located near the bearing lines. This interaction generates localized “spikes” in flange lateral bending stresses near the girder ends. Under total dead load, these lateral bending stresses remain substantial in Girder A regardless of the detailing approach, with the most pronounced effects again occurring near Bent No. 8.

Figures 5-18 to 5-21 illustrate the lateral bending stresses in the upper and lower flanges of Girders A and G under the SDL and TDL conditions. The lateral bending stresses in fascia girders predominantly arise from eccentric loads on overhang brackets. Consequently, they cannot be mitigated through cross-frame detailing adjustments. The findings indicate that the SDLF and TDLF detailing methods exert no substantial impact on the major axis and lateral bending behavior of the girders.

In conclusion, the cross-frame locked-in force effects resulting from SDLF and TDLF detailing methods have a small influence on the girder stresses, deflections, and layover behavior of the Corridor X—I-65 bridge, which adopts an ICCS configuration. Nonetheless, SDLF and TDLF detailing methods significantly decrease cross-frame forces, especially in crucial areas adjacent to the skewed bearings.

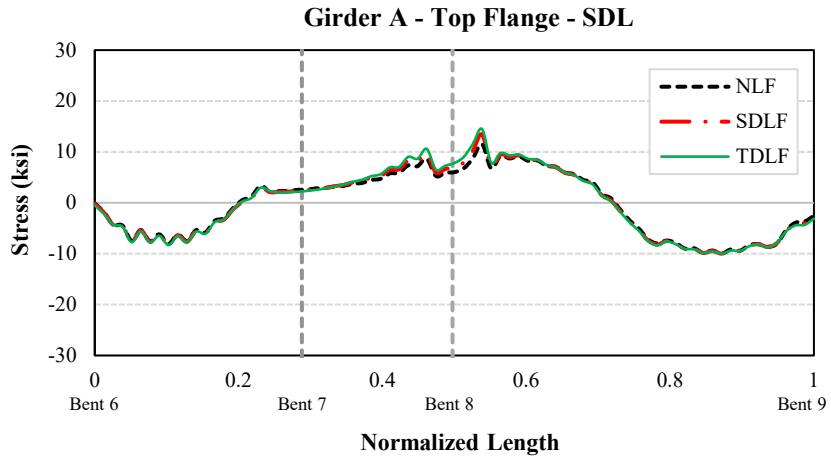

(a)

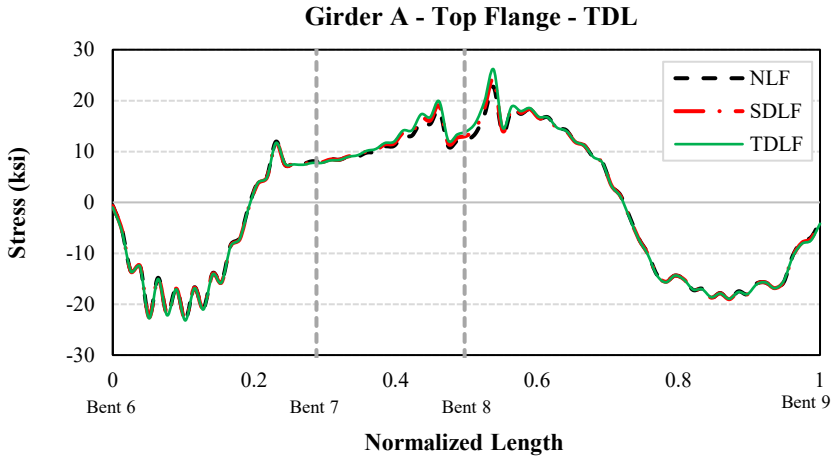

(b)

Figure 5-14. Major-axis bending stress in the top flange of Girder A under (a) steel dead load and (b) total dead load.

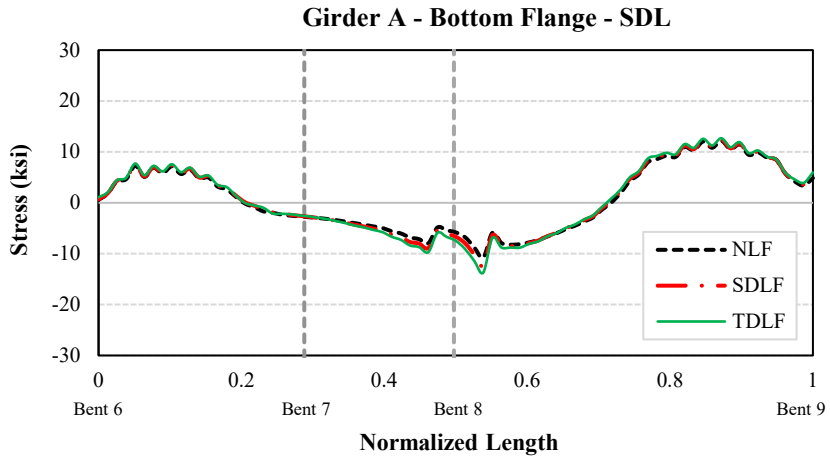

(a)

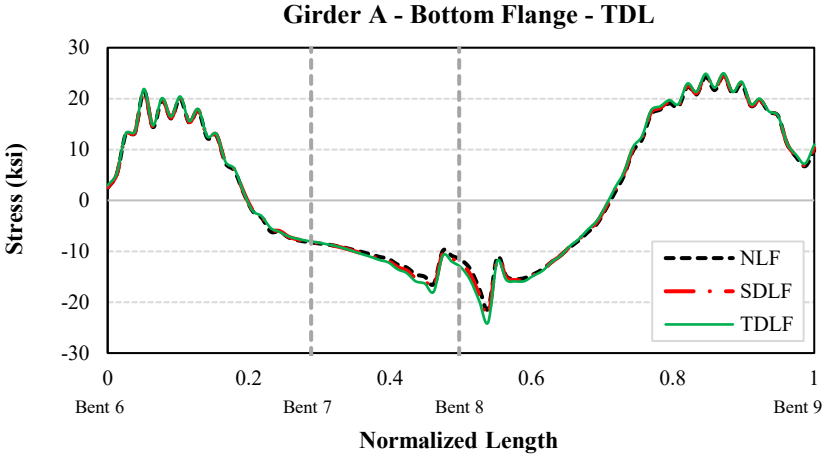

(b)

Figure 5-15. Major-axis bending stress in the bottom flange of Girder A under (a) steel dead load and (b) total dead load.

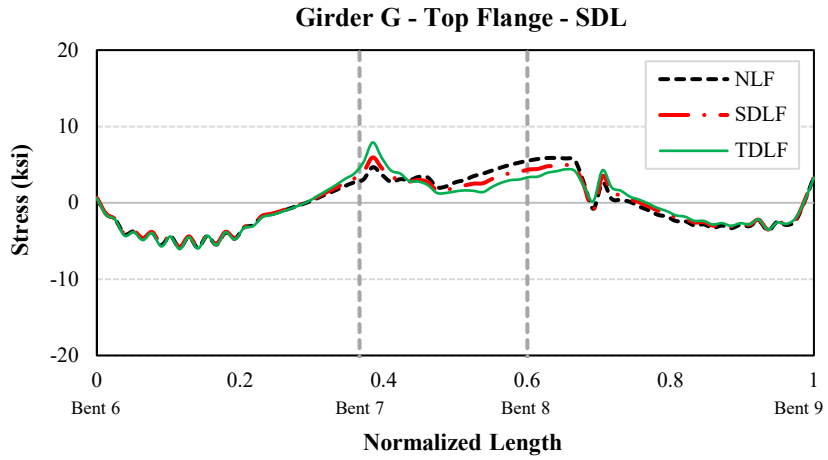

(a)

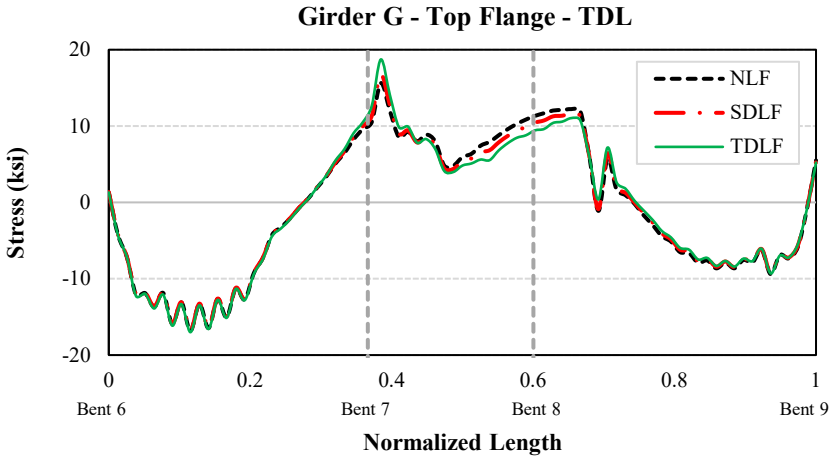

(b)

Figure 5-16. Major-axis bending stress in the top flange of Girder G under (a) steel dead load and (b) total dead load.

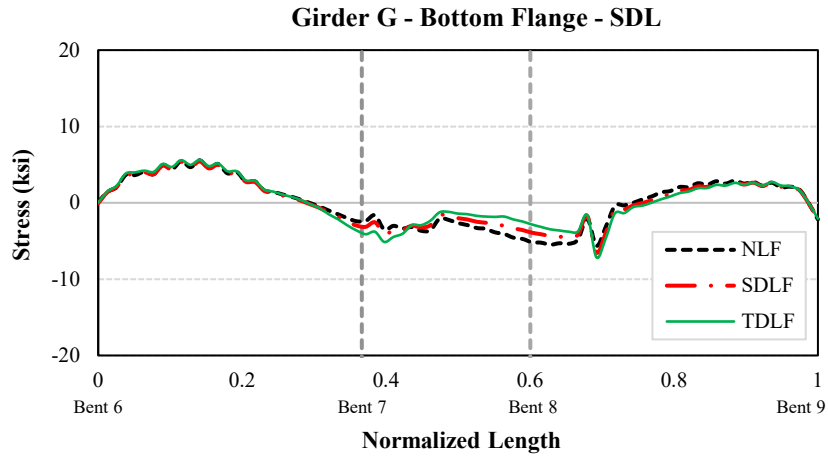

(a)

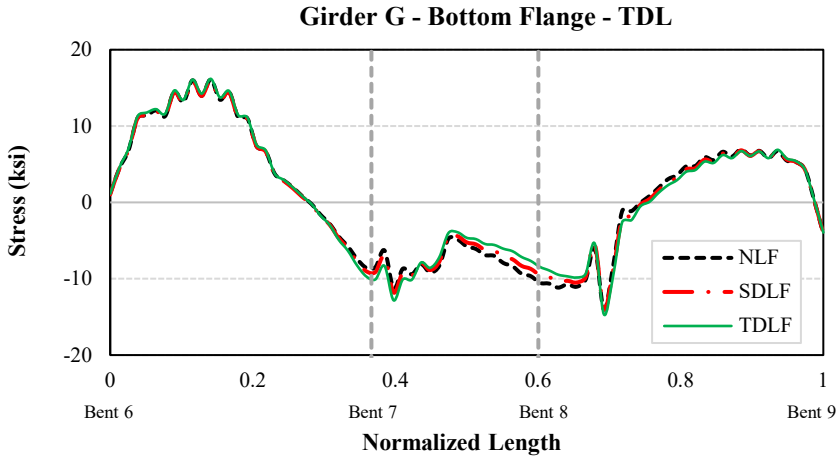

(b)

Figure 5-17. Major-axis bending stress in the bottom flange of Girder G under (a) steel dead load and (b) total dead load.

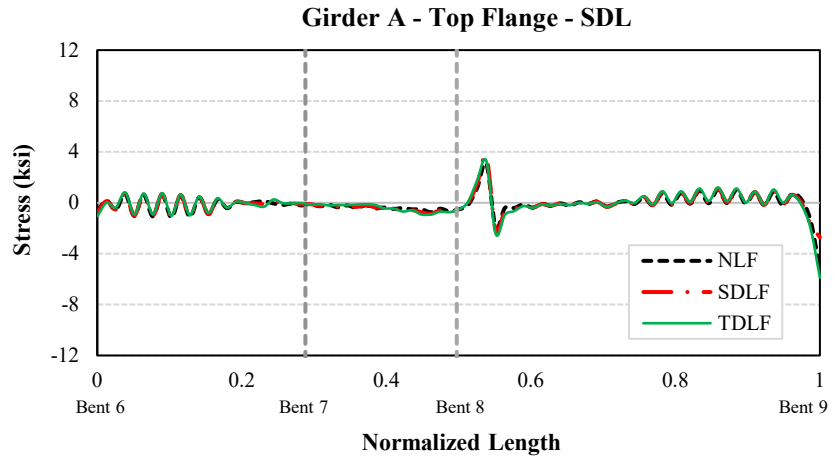

(a)

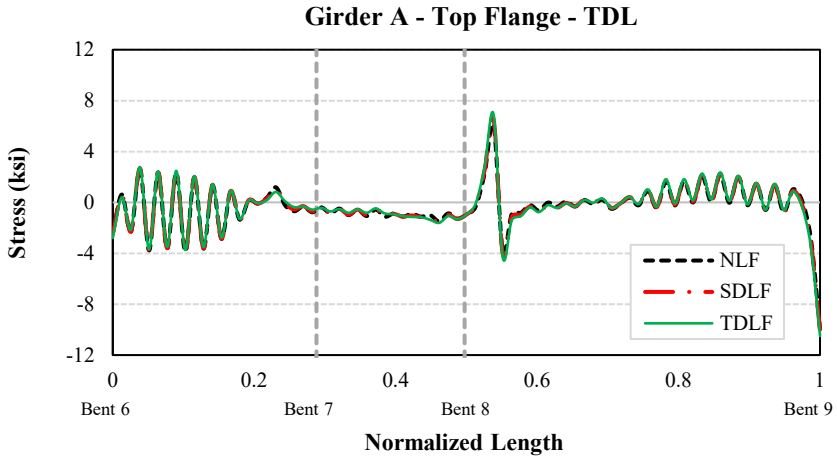

(b)

Figure 5-18. Lateral bending stress in the top flange of girder A under (a) steel dead load and (b) total dead load.

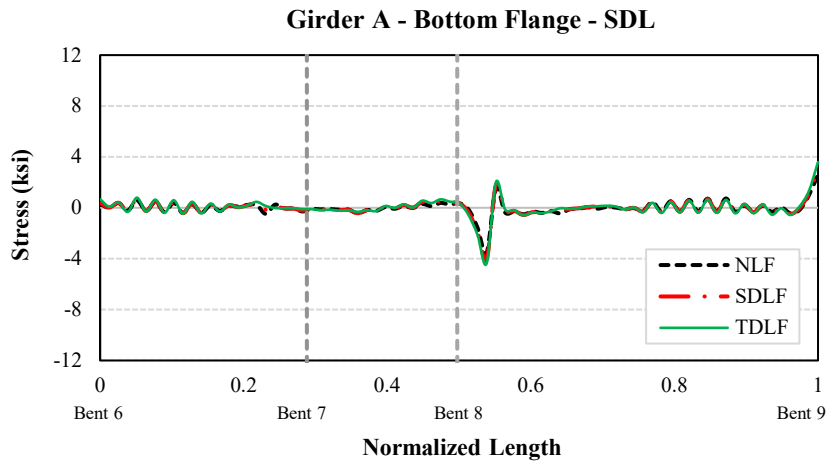

(a)

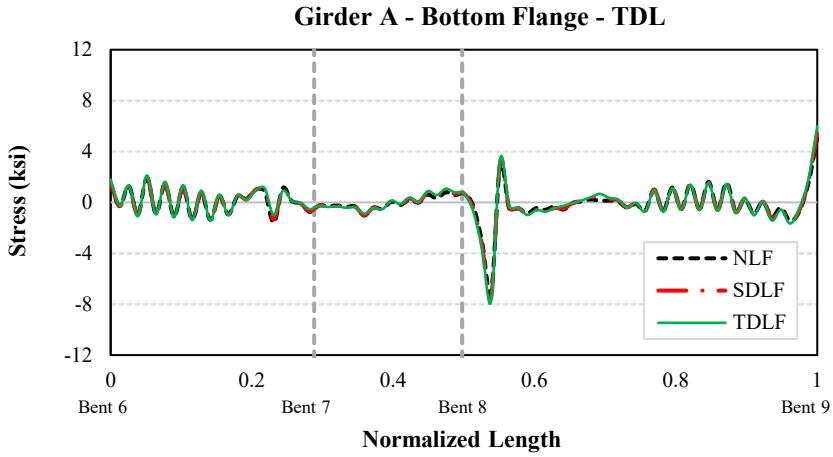

(b)

Figure 5-19. Lateral bending stress in the bottom flange of Girder A under (a) steel dead load and (b) total dead load.

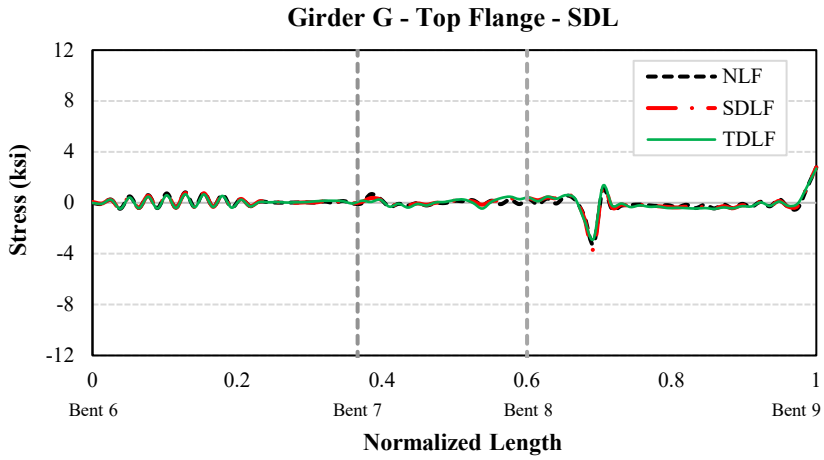

(a)

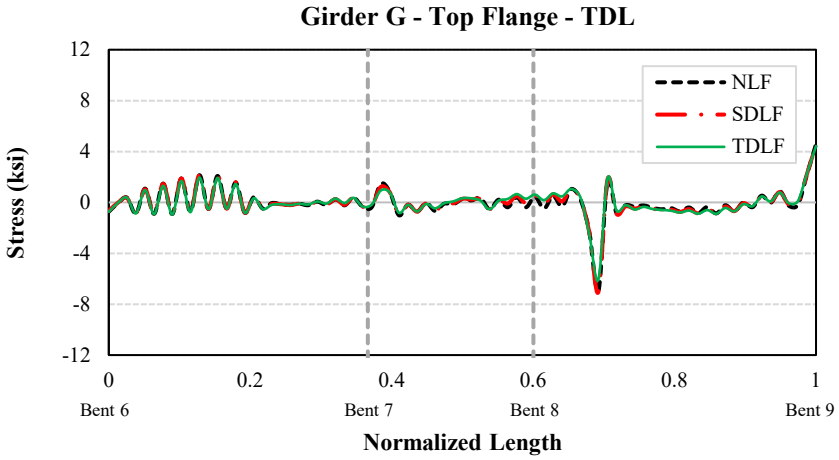

(b)

Figure 5-20. Lateral bending stress in the top flange of Girder G under (a) steel dead load and (b) total dead load.

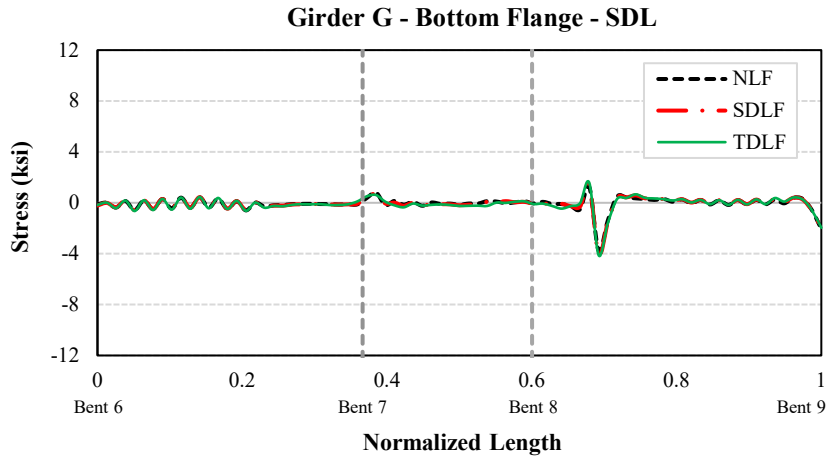

(a)

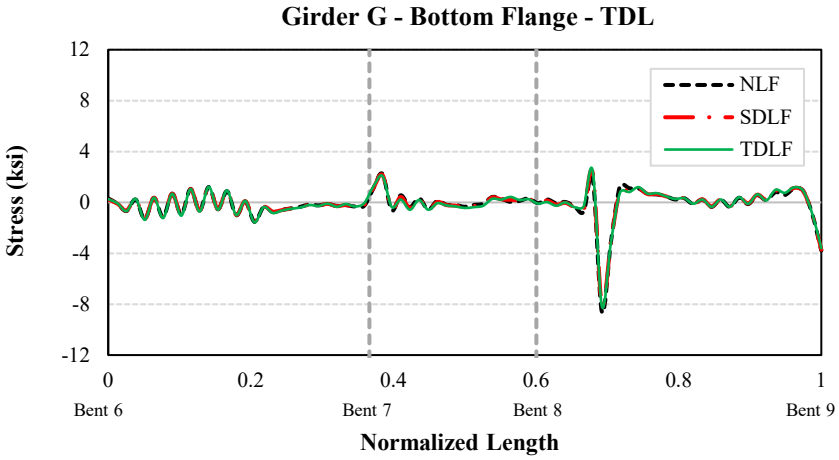

(b)

Figure 5-21. Lateral bending stress in the bottom flange of Girder G under (a) steel dead load and (b) total dead load.

CHAPTER 6: CONCLUSIONS

6.1. Overview

This research systematically assessed the influence of three cross-frame detailing methods, namely No-Load Fit (NLF), Steel Dead Load Fit (SDLF), and Total Dead Load Fit (TDLF), as discussed in Chapter 3, on the structural behavior of horizontally curved and skewed steel I-girder bridges. Through a detailed finite-element modeling framework developed in Abaqus and verified against design and experimental benchmarks in Chapter 4, the study provided a comparison of vertical displacements, cross-frame forces, girder layovers, and girder stress distributions under different dead load conditions. The analyses revealed distinct behavioral patterns for each detailing method and demonstrated clear interdependence between the bridge geometry, cross-frame interaction, and the formation of locked-in stresses. The numerical results in Chapter 5 revealed that the selection of detailing method produced distinguishable yet moderate effects on the global response of the Corridor X–I-65 curved and skewed I-girder bridge. The principal findings are summarized as follows:

6.2. Global Deflections and Camber Profiles

According to section 5.2, the overall vertical deflections of the girders under steel and total dead loads were nearly identical for all three detailing methods, indicating that different fitting designs do not significantly influence global girder deflection or camber accuracy in the Corridor X—I-65 bridges. Furthermore, the finite-element (FE) model results closely matched the design camber diagrams, confirming the adequacy of the FE model.

6.3. Cross-Frame Forces

Cross-frame forces were highly sensitive to the selected detailing method based on the results obtained in section 5.3. Among the three approaches, the TDLF configuration produced the lowest internal forces under both steel and total dead load conditions, followed by the SDLF method, whereas the NLF model exhibited the largest cross-frame forces and the most pronounced unbalanced stress patterns near the skewed bents. Compared with NLF, the maximum reduction in cross-frame forces achieved by TDLF method was 93.4 % under the steel dead load and 51.5 % under the total dead load. Similarly, the maximum reduction achieved by SDLF method was 54 % under the steel dead load and 26 % under the total dead load. This reduction was more significant in cross-frames experiencing higher initial forces and less pronounced in those with smaller force magnitudes. Nevertheless, the TDLF method required greater initial installation forces during erection due to the larger lack-of-fit introduced during construction; in some cases, the initial force demand reached about 153.4 kips for SDLF and 276.6 kips for TDLF.

6.4. Girder Layover

Girder layovers result from the intricate interaction of major-axis bending, torsional rotations, and curvature effects, particularly in curved and skewed bridges. While SDLF and TDLF detailing techniques strive to maintain vertical girder alignment under dead load by compensating for

torsional rotations, the resulting layovers do not perfectly counterbalance those observed in the Corridor X—I-65 bridge according to section 5.4. Among the examined methods, TDLF yielded the most significant outward layovers, especially in the fascia girder, reaching up to 4.6 in. under total dead load; however, the differences among NLF, SDLF, and TDLF were limited to less than 1 in., indicating that geometric rotation was effectively controlled by the bridge's overall stiffness and cross-frame configuration. Overall, curvature–skew coupling and cross-frame stiffness play key roles in governing girder rotation and alignment behavior.

6.5. Girder Stress Distribution

The variations in flange lateral bending stresses across the different detailing procedures are negligible based on section 5.5. Furthermore, the lateral bending stresses in fascia girders predominantly arise from eccentric loads on overhang brackets. Therefore, they cannot be alleviated by modifications to cross-frame detailing adjustments. The results demonstrate that the SDLF and TDLF detailing methods have no significant effect on the major axis and lateral bending behavior of the girders in the Corridor X—I-65.

6.6. Practical Evaluation of Detailing Methods

As previously stated, practicing engineers generally do not explicitly consider locked-in forces and their corresponding locked-in stresses in design. Nonetheless, the findings of Section 5.3 indicate that these forces may be substantial in specific important regions, especially adjacent to skewed supports. Locked-in forces in cross-frames diminish the ability for supplementary load effects and elevate the demands on members and connections. The members experience significant stress before live loads are applied, resulting in a substantial portion of their resistance being used on dead-load-related locked-in effects. This condition may lead some members to approach yielding or even local buckling when subjected to live loads and secondary effects. In addition, bolts, welds, and gusset plates are subjected to repeated live load cycles superimposed on stresses caused by locked-in forces; over the bridge's operational lifespan, this combination can potentially accelerate fatigue damage, especially at welded gusset corners, cope regions, and welded attachments.

The analysis results indicate that SDLF and TDLF detailing methods primarily influence the magnitude of locked-in cross-frame forces and initial stresses, while having minimal effect on global deflections, layover, and overall girder stress levels. Among the evaluated approaches, the Total Dead Load Fit (TDLF) method yielded the smallest cross-frame locked-in forces for under both steel and total dead loads; nevertheless, it necessitated significantly greater initial forces during construction. The Steel Dead Load Fit (SDLF) method exhibited a more balanced behavior, moderately reducing cross-frame forces but still demanding considerable initial installation forces. In contrast, although the No-Load Fit (NLF) method generated greater locked-in stresses in the Corridor X—I-65 bridge, its initial force at construction is theoretically zero. The above findings are generated based on the selected Corridor X—I-65 bridge studied herein; therefore, some findings, particularly the quantitative ones, may not be directly applicable to all bridge configurations.

6.7. Recommendations for Future Research

The findings of this study provide a foundation for future analytical and experimental work aimed at improving the design and detailing of curved and skewed steel I-girder bridges. To enhance and substantiate the insights derived from this research, the following recommendations are suggested:

- **Extend the current numerical framework to other bridge configurations:** Future investigations should apply the same finite-element modeling and comparative methodology used in this study to other bridge types introduced in Chapter 2 such as ISSS, ICSS, ICCR, and ISCS systems, to determine the most effective detailing approach for each configuration. This will aid in formulating generalized criteria for choosing the suitable detailing method according to bridge geometry, curvature index, and skew index.
- **Broaden the investigation to further ICCS bridges:** According to Table 2-1, the Galleria Bridge exhibits the same ICCS bridge classification as the Corridor X–I-65 Bridge, although possesses a higher curvature index and a lower skew index. In addition, the state of Alabama has many more similar ICCS bridges. Conducting the similar numerical assessment on these bridges would be able to provide generalizable results and can lead to valuable recommendations for future ALDOT practices on choices of cross-frame fitting details, by considering the impacts of various factors such as bridge geometry, support (bent) locations, etc., on the structural performance and long-term safety in ICCS systems.
- **Evaluation of cross-frame modeling strategies in numerical analysis:** As outlined in Section 4.6, simplified cross-frame representations using truss or beam elements, which are commonly employed by engineers, are considered unreliable. Truss elements overestimate stiffness by disregarding out-of-plane bending, whereas beam elements underestimate stiffness due to geometric simplifications and the exclusion of gusset plates and stiffeners. These limitations highlight the imperative of using shell elements to accurately capture the authentic stiffness, load transfer, and deformation characteristics of cross-frames in curved and skewed steel I-girder bridges. Subsequent numerical investigations should further quantify the differences among these modeling approaches, particularly for bridges with higher curvature and skew indices, to establish clear modeling protocols for design and research applications.
- **Conduct large-scale experimental validation:** Physical testing using full-scale or scaled bridge mock-ups should be performed to measure initial force development during erection and the evolution of locked-in stresses within cross-frames. These trials would yield essential data for validating finite-element predictions and enhancing assumptions on material nonlinearity, connection rigidity, and geometric tolerances.
- **Experimentally characterize cross-frame performance:** Subsequent research ought to build from the experimental benchmarking presented in Section 4.8, wherein cross-frame stiffness was validated through full-scale testing. Further tests on single- and multi-member cross-frame assemblies are required to accurately estimate stiffness, connection eccentricities, and out-of-plane deformation under realistic boundary conditions. This data will enhance the calibration of finite-element models, especially for gusset-plate flexibility, welded connections, and three-dimensional deformation modes, aiding in the formulation of more reliable brace sizing and detailing standards for ICCS bridges.

REFERENCES

[1] B. Haseli, G. Nouri, M. M. Taromi, M. Bahari, E. Adili, and A. Keyghobadi, "Effect of skew angle on seismic response of irregular concrete bridges with horizontal curve," *KSCE J Civ Eng*, vol. 28, no. 6, pp. 2329–2343, June 2024, doi: 10.1007/s12205-024-1464-y.

[2] J. Seo and D. G. Linzell, "Use of response surface metamodels to generate system level fragilities for existing curved steel bridges," *Engineering Structures*, vol. 52, pp. 642–653, July 2013, doi: 10.1016/j.engstruct.2013.03.023.

[3] A. Kalantari and M. Amjadian, "An approximate method for dynamic analysis of skewed highway bridges with continuous rigid deck," *Engineering Structures*, vol. 32, no. 9, pp. 2850–2860, Sept. 2010, doi: 10.1016/j.engstruct.2010.05.004.

[4] T. Wilson, H. Mahmoud, and S. Chen, "Seismic performance of skewed and curved reinforced concrete bridges in mountainous states," *Engineering Structures*, vol. 70, pp. 158–167, July 2014, doi: 10.1016/j.engstruct.2014.03.039.

[5] J. Seo and D. G. Linzell, "Horizontally curved steel bridge seismic vulnerability assessment," *Engineering Structures*, vol. 34, pp. 21–32, Jan. 2012, doi: 10.1016/j.engstruct.2011.09.008.

[6] D. Linzell, D. Hall, and D. White, "Historical perspective on horizontally curved I-girder bridge design in the United States," *Journal of Bridge Engineering*, vol. 9, no. 3, pp. 218–229, May 2004.

[7] P. Kaviani, F. Zareian, and E. Taciroglu, "Seismic behavior of reinforced concrete bridges with skew-angled seat-type abutments," *Engineering Structures*, vol. 45, pp. 137–150, Dec. 2012, doi: 10.1016/j.engstruct.2012.06.013.

[8] D. H. Hall, M. A. Grubb, and C. H. Yoo, "Improved design specifications for horizontally curved steel girder highway bridges," NCHRP Project 12–38, Aug. 1998.

[9] R. D. Medlock, *NCHRP 603, Practices for steel bridge fabrication and erection tolerances*. Washington, DC: National Academies Press, 2023. doi: 10.17226/27096.

[10] A. N. Gergess and R. Sen, "Cambering structural steel I-girders using cold bending," *Journal of Constructional Steel Research*, vol. 64, no. 4, pp. 407–417, Apr. 2008, doi: 10.1016/j.jcsr.2007.10.001.

[11] Y. Wu, Y. Zhu, X. Chen, and S. Wan, "Automatic welding of corrugated steel webs on composite box girder with corrugated steel webs," *Advances in Civil Engineering*, vol. 2024, no. 1, p. 5289340, 2024, doi: 10.1155/2024/5289340.

[12] K. Kawashima, "Damage of bridges due to the 2011 Great East Japan Earthquake," *Journal of JAEE*, vol. 12, p. 4_319-4_338, 2012, doi: 10.5610/jaee.12.4_319.

[13] M. Amjadian and A. K. Agrawal, "Rigid-body motion of horizontally curved bridges subjected to earthquake-induced pounding," *Journal of Bridge Engineering*, vol. 21, no. 12, Dec. 2016, doi: https://doi.org/10.1061/(ASCE)BE.1943-5592.0000962.

[14] S. J. Fatemi, A. H. Sheikh, and M. S. M. Ali, "Development and application of an analytical model for horizontally curved bridge decks," *Advances in Structural Engineering*, vol. 18, no. 1, pp. 107–117, Jan. 2015, doi: 10.1260/1369-4332.18.1.107.

[15] S. Movaghati and A. E. Abdelnaby, "Advancements in fragility analysis using numerical calibration methods for a horizontally curved RC bridge," *Engineering Structures*, vol. 125, pp. 236–243, Oct. 2016, doi: 10.1016/j.engstruct.2016.07.017.

[16] H. C. Gomez, P. J. Fanning, M. Q. Feng, and S. Lee, “Testing and long-term monitoring of a curved concrete box girder bridge,” *Engineering Structures*, vol. 33, no. 10, pp. 2861–2869, Oct. 2011, doi: 10.1016/j.engstruct.2011.05.026.
[17] D. W. White *et al.*, *Guidelines for analysis methods and construction engineering of curved and skewed steel girder bridges*. Washington, D.C.: Transportation Research Board, 2012. doi: 10.17226/22729.
[18] *AASHTO LRFD Bridge Design Specifications (2010)*, 5th ed. Washington, DC 20001: American Association of State Highway and Transportation Officials, 2010.
[19] T. A. Sanchez Grunauer, “Influence of bracing systems on the behavior of curved and skewed steel I-girder bridges during construction,” Text, Georgia Institute of Technology, GA, 2011.
[20] J. H. Gull and A. Azizinamini, “Steel plate girder diaphragm and cross bracing loads,” Florida International University, BDK80 977-20, May 2014.
[21] A. D. Battistini, S. M. Donahue, W. H. Wang, T. A. Helwig, M. D. Engelhardt, and K. H. Frank, “Stiffness and forces of x-type, k-type, and z-type cross-frames in steel i-girder bridges,” presented at the Proceedings of the annual stability conference, structural stability research council, St. Louis, Missouri, Apr. 2013, pp. 344–357.
[22] B. Shafei, B. Phares, A. Kulkarni, and W. Shi, “Determination of the forces in X-frames in curved girder bridges,” 16–594, Apr. 2021.
[23] *AASHTO LRFD Bridge Design Specifications (2020)*, 9th ed. Washington, DC 20004: American Association of State Highway and Transportation Officials, 2020.
[24] A. E. Abdelnaby *et al.*, “Numerical and hybrid analysis of a curved bridge and methods of numerical model calibration,” *Engineering Structures*, vol. 70, pp. 234–245, July 2014, doi: 10.1016/j.engstruct.2014.04.009.
[25] C. Ozgur, “Influence of cross-frame detailing on curved and skewed steel I-girder bridges,” Georgia Institute of Technology, GA, 2011.
[26] A. D. Battistini, W. Wang, T. A. Helwig, M. D. Engelhardt, and K. H. Frank, “Stiffness Behavior of Cross Frames in Steel Bridge Systems,” *Journal of Bridge Engineering*, vol. 21, no. 6, p. 04016024, June 2016, doi: 10.1061/(ASCE)BE.1943-5592.0000883.
[27] D. Liu and R. Magnolia, “End forces on crossframes in horizontally curved steel I-girder bridges,” *Practice Periodical on Structural Design and Construction*, vol. 15, no. 1, 2010, doi: https://doi.org/10.1061/(ASCE)SC.1943-5576.0000018.
[28] J. Seo and D. G. Linzell, “Probabilistic vulnerability scenarios for horizontally curved steel I-girder bridges under earthquake loads,” *Journal of the Transportation Research Board*, pp. 206–211, 2010, doi: 10.3141/2202-24.
[29] H. Ma, “Analytical and experimental study of horizontally curved steel bridge girders with tubular top flanges,” Lehigh University, 2015.
[30] “Abaqus analysis user’s manual.” Dassault Systèmes, 2016.
[31] *Abaqus 2025 documentation*. Dassault Systèmes, Providence, RI.
[32] D. White, *Steel bridge design handbook*, vol. 4. U.S. Department of Transportation, 2015.